QQO-12398.1-E

⑫

B.S.

SURFACE ROUGHNESS EFFECTS ON THE

HYPERSONIC TURBULENT BOUNDARY LAYER

by

Toshi Kubota and Dale E. Berg

June, 1977

Final Report

DDC
RECEIVED
JUL 27 1977
E

CALIFORNIA INSTITUTE OF TECHNOLOGY

REPORT DOCUMENTATION PAGE		READ INSTRUCTIONS BEFORE COMPLETING FORM
1. REPORT NUMBER	2. GOVT ACCESSION NO.	3. RECIPIENT'S CATALOG NUMBER
4. TITLE (and Subtitle) Surface Roughness Effects on the Hypersonic Turbulent Boundary Layer		5. TYPE OF REPORT & PERIOD COVERED Final Report 1 Feb. 1974-31 Jan. 1976
		6. PERFORMING ORG. REPORT NUMBER
7. AUTHOR(s) Toshi Kubota and Dale E. Berg		8. CONTRACT OR GRANT NUMBER(s) DAHC04-74-C-0009
9. PERFORMING ORGANIZATION NAME AND ADDRESS California Institute of Technology 1201 E. California Blvd. Pasadena, CA 91125		10. PROGRAM ELEMENT, PROJECT, TASK AREA & WORK UNIT NUMBERS
11. CONTROLLING OFFICE NAME AND ADDRESS U. S. Army Research Office Post Office Box 12211 Research Triangle Park, NC 27709		12. REPORT DATE June 1977
		13. NUMBER OF PAGES 113
14. MONITORING AGENCY NAME & ADDRESS(if different from Controlling Office) 115 p.		15. SECURITY CLASS. (of this report) Unclassified
		15a. DECLASSIFICATION/DOWNGRADING SCHEDULE NA

16. DISTRIBUTION STATEMENT (of this Report)

ARO

17. DISTRIBUTION STATEMENT (of the abstract entered in Block 20, if different from Report)

12398.1E

18. SUPPLEMENTARY NOTES

The findings in this report are not to be construed as an official Department of the Army position, unless so designated by other authorized documents

19. KEY WORDS (Continue on reverse side if necessary and identify by block number)

hypersonic flow, supersonic flow, turbulent boundary layer, roughness effects, skin friction measurement, turbulence measurement, hot wire

20. ABSTRACT (Continue on reverse side if necessary and identify by block number)

An experimental investigation of the response of a hypersonic turbulent boudary layer to a step change in surface roughness has been performed. The boundary layer on a flat nozzle wall of a Mach 6 wind tunnel was subjected to abrupt changes in surface roughness and its adjustment to the new surface conditions was examined. Both mean and fluctuating flow properties were acquired for smooth-to-rough and rough-to-smooth surface configurations.

DD FORM 1 JAN 73 1473   EDITION OF 1 NOV 65 IS OBSOLETE

071 550

i

Part of the work reported herein was conducted under
SANDIA Contract 63-2327, 04-8804.

ABSTRACT

An experimental investigation of the response of a hypersonic turbulent boundary layer to a step change in surface roughness has been performed. The boundary layer on a flat nozzle wall of a Mach 6 wind tunnel was subjected to abrupt changes in surface roughness and its adjustment to the new surface conditions was examined. Both mean and fluctuating flow properties were acquired for smooth-to-rough and rough-to-smooth surface configurations.

The boundary layer was found to respond gradually and to attain new equilibrium profiles, for both the mean and the fluctuating properties, some 10 to 25δ downstream of the step change. Mean flow self-similarity was the first to establish itself, followed by the mass flux fluctuations, followed in turn by the total temperature fluctuations.

Use of a modified Van Driest transformation resulted in good correlation of smooth and rough wall data in the form of the incompressible law of the wall. This is true even in the nonequilibrium vicinity of the step for small roughness heights.

The present data are found to correlate well with previously published roughness effect data from low and high speed flows when the roughnesses are characterized by an equivalent sand grain roughness height.

Existing correlations based on low speed data were found to be unsuccessful in predicting the effect of this roughness on the skin friction and velocity profile. The indiscriminate use of low speed

roughness effects correlations to predict the effects of roughness on supersonic and hypersonic flows must therefore be regarded as a procedure subject to gross errors.

Significant pressure and temperature history effects were observed throughout the boundary layer. The existence of these effects was found to create a nozzle wall boundary layer whose properties were far different than those in a boundary layer on a flat plate in the freestream, raising questions about the validity of simulating the flat plate boundary layer with the nozzle wall boundary layer.

TABLE OF CONTENTS

Title   Page

v

Table of Contents (Cont'd)

LIST OF SYMBOLS

A   constant (Eqs. 4, 6 and 7)

a_1 $1 + \frac{\gamma-1}{2} M^2$

C   constant in the law of the wall (Eqs. 1 and 5); hot-wire sensitivity coefficient

C_f skin friction coefficient

C_{f_0} smooth wall skin friction coefficient

c   specific heat

D   constant in the law of the wall (Eqs. 2, 5 and 8)

H δ^*/θ - shape factor

$\dot{H}$ $\frac{100}{\delta^*} \int \frac{\rho u}{\rho_e u_e} (1 - T_t/T_{t_e}) dy$ - enthalpy flux coefficient

k   roughness height; thermal conductivity

k_s equivalent sand grain roughness (Eqs. 9 and 11)

k^+ $k u_\tau/\nu_w$

k_s^+ $k_s u_\tau/\nu_w$

ℓ wavelength of roughness (Fig. 5); hot wire length; characteristic length in Reynolds number of roughness

ℓn natural logarithm

$\dot{m}$ ρu, mass flux

p   pressure (static unless noted otherwise)

Pr $\mu c_p/k$, Prandtl number

q   heat flux

$R_{\dot{m}T_t}$ $\overline{\dot{m}' T_t'} / \left(\sqrt{\overline{\dot{m}'^2}} \sqrt{\overline{T_t'^2}} \right)$

r   recovery factor (Eq. 7)

List of Symbols (Cont'd)

Re $\quad \rho u \ell/\mu \quad$ Reynolds number

T $\quad$ temperature (static unless otherwise noted)

u $\quad$ streamwise component of velocity

$u_\tau \quad \sqrt{\dfrac{\overline{\tau_w}}{\rho_w}}$, friction velocity

$u^* \quad$ Van Driest transformed velocity (Eq. 4)

$\Delta u \quad$ change in velocity due to wall roughness

v $\quad$ component of velocity normal to the wall

w $\quad$ wake function (Eq. 5)

x $\quad$ streamwise coordinate, distance from the throat

y $\quad$ normal to the wall; displacement of balance beam (Eq. 5)

$y^+ \quad y\, u_\tau/\nu_w$

$y_0 \quad$ effective origin for rough surface

$\gamma \quad c_p/c_v$, ratio of specific heats

$\delta \quad$ boundary layer thickness

$\delta^* \quad \displaystyle\int_0^\delta (1 - \dfrac{\rho u}{\rho_e u_e})dy$ - displacement thickness

$\kappa \quad$ Karman constant in the law of the wall

$\lambda \quad \ell/k$ - roughness wavelength-to-height ratio

$\mu \quad$ fluid viscosity

$\nu \quad \mu/\rho$, kinematic viscosity

$\overline{\pi} \quad$ wake strength parameter in the law of the wall (Eq. 5)

$\rho \quad$ fluid density (static unless otherwise noted)

$\tau \quad$ shear stress; nondimensional temperature

List of Symbols (Cont'd)

$\theta \qquad \int_0^\delta \dfrac{\rho}{\rho_e} \dfrac{u}{u_e} \left(1 - \dfrac{u}{u_e}\right) dy$ - momentum thickness

Superscripts

$'$ fluctuation quantity

$-$ time average or nondimensional quantity

Subscripts

aw   adiabatic wall

e   boundary layer edge conditions

ℓ local value

t   total conditions

w   wall or wire property

∞ free stream conditions

LIST OF TABLES

LIST OF FIGURES

xi

List of Figures (Cont'd)

INTRODUCTION

The effect of surface roughness on the characteristics of flow over a surface has long been of interest, especially to those people who are involved in the design of vehicles which operate in or on the water or within the atmosphere. It is well known that the presence of surface roughness can significantly alter the drag and heat transfer characteristics of a surface and can even cause considerable modification of the flow-field about a body, compared to the smooth wall case. Quantitative knowledge of these roughness effects, and insight into the physical phenomena which give rise to these effects is essential for the realistic design of new vehicles, regardless of their speed range or medium of operation. Without such knowledge, vehicle performance cannot be adequately predicted and considerable overdesign is mandatory to insure that the vehicle will satisfy the design criteria. Ship hulls, aircraft, reentry vehicles, and the space shuttle are but a few areas in which the design is influenced heavily by the knowledge or lack of knowledge of roughness effects.

One of the earliest extensive studies of roughness effects was that of Nikuradse,[1] in which the effects of Reynolds number and relative roughness heights were investigated. This work was carried out using dense sand grain roughness in pipe flow. He discovered that for Reynolds number based on roughness height below a certain critical value, the roughness had no discernible effect on the flow, i.e., the surface was "hydraulically smooth." For roughness Reynolds numbers above this critical value and below a second critical value, the effect of the wall roughness on the boundary layer properties

was dependent on flow Reynolds number and roughness density, k/d (k is the roughness height, and d is some characteristic length of the flow, such as the pipe diameter for Nikuradse's work). These flows were termed "transitional." Flows with roughness Reynolds numbers above the second critical value were found to depend only on the roughness density and were termed "fully rough."

Moore,[2] in 1951, investigated a zero pressure gradient boundary layer over a roughness consisting of square bars placed normal to the flow with a ratio of pitch to height of 4. Moore found that a similarity defect law correlated his boundary layer profiles, and the law was identical with the smooth-wall law, provided the origin for measuring y and δ (the boundary layer thickness) was located some distance below the crest of the roughness elements.

Hama,[3] in 1954, conducted an extensive investigation which showed that the Clauser[4] form of the logarithmic velocity distribution for rough wall flows

$$\frac{u}{u_\tau} = \frac{1}{\kappa} \ell n \left(\frac{y u_\tau}{\nu}\right) + C - \frac{\Delta u}{u_\tau} \tag{1}$$

where

$$u_\tau \qquad = \sqrt{\tau_w / \rho_w}$$

κ and C = universal constants

τ_w = wall shear stress

ρ_w = fluid density at the wall

$\frac{\Delta u}{u_\tau}$ = a roughness function which is zero for smooth walls and which depends on the roughness Reynolds number

and the Clauser[4] form of the roughness function for fully rough flows

$$\frac{\Delta u}{u_\tau} = \frac{1}{\kappa} \ell n \left(\frac{k u_\tau}{\nu} \right) + D \tag{2}$$

are both universal for a given roughness geometry in pipe, channel, and zero pressure gradient boundary layer flow. The constant D is found to depend upon the free stream pressure gradient.

More recently, the work of Betterman,[5] Morris,[6] Liu et al.,[7] and Perry et al.[8] have included the effects on the constant D of the element density. Perry and Joubert[9] have investigated the effect of an adverse pressure gradient on the roughness function. All of these works were for either a sand grain roughness[1,3] or a transverse square bar type of roughness,[2,4-9] while Streeter and Chu,[10] Sams,[11] Ambrose,[12] and Corrsin and Kistler,[13] have investigated different types of roughnesses.

Antonia and Luxton,[14] Liu et al.,[15] and Logan and Jones[16] are among those who have studied the turbulent properties of incompressible fluid flow over rough surfaces. They have found that the velocity fluctuation magnitudes in the outer part of the rough wall boundary layer are significantly higher than those on the smooth wall. The fluctuation profiles were also found to assume a self preserving shape.

Using the information obtained in these investigations, Van Driest[17] has constructed a mathematical model of incompressible fluid flow over a rough wall which has met with considerable success when used to compute the mean properties of such a flow.

Dvorak[18] utilizes the correlation of Betterman, [5] extends it to other roughness densities, and incorporates the universal rough surface law of the wall into a procedure for computing incompressible rough wall turbulent boundary layer profiles.

Considerably less progress has been made in determining the effects of surface roughness on compressible turbulent boundary layers. One of the first investigations was that of Goddard[19] who studied the effects of sand grain roughness at Mach numbers of 2 to 4.5. Wade[20] at about the same time determined the effects of "screw thread" roughness at Mach number 2.5. Fenter,[21] Young,[22] Shutts and Fenter,[23] Mann,[24] Reda,[25] and Monta et al.[26] have also investigated this phenomenon at Mach numbers varying from 2 to 5.

With the added phenomenon of compressibility, it is no longer possible to directly correlate the boundary layer profiles in the law-of-the-wall form as was done for incompressible flow. Even compressible smooth wall turbulent boundary layers, at different Mach numbers or wall-to-stagnation temperature ratios, cannot be directly correlated by the law of the wall. Several transform methods[27-37] have been proposed, based on either theoretical analysis or experimental data. These methods are designed to transform compressible velocity profile data into an "equivalent" incompressible form which can then be correlated by the incompressible law of the wall.

Spalding and Chi,[34] Hopkins et al.,[38] Miles and Kim,[39] and Hopkins and Inouye[40] have compared several of the theories with available data and conclude that while some of them work

quite well for a wide variety of data, many of them perform adequately only for data which were acquired under certain conditions such as limited Mach number range, limited wall temperature range, etc. Since only the immediate wall region of the compressible turbulent boundary layer is affected by the presence of wall roughness, it seems likely that the smooth wall transform methods will work for the rough wall case as well, and Fenter,[21] Young,[22] and Reda[25] have verified this.

Dvorak[41] and Chen[42] have developed computational procedures based on a combination of empirical laws and theoretical equations which purport to predict the compressible rough wall boundary layer development in a pressure gradient. The agreement with the limited amount of data is quite good, but Dvorak specifically deplores the availability of suitable test data.

The earliest comprehensive investigation of the fluctuating properties of the compressible turbulent boundary layer was performed by Kistler[43]. He found that in the Mach number range of 1.7 to 4.7, the mass flow and total temperature fluctuation intensities increased throughout the boundary layer with increasing Mach number. The velocity fluctuation profile was observed to be generally similar in shape to low speed fluctuation profiles. Subsequent to Kistler's work, Owen and Horstman[44] and Laderman and Demetriades,[45, 46] have investigated smooth wall turbulent boundary layer flows at Mach numbers of 7, 8, and 9 with adiabatic and cold walls. Laderman and Demetriades[46] conclude that the fluctuation intensity is strongly dependent on the wall temperature

to stagnation temperature ratio.

An investigation of the response of a hypersonic turbulent boundary layer to a step change in roughness was seen as serving several purposes; it would provide information on the distance required to achieve equilibrium rough wall flow in hypersonic flow-- essential for future roughness work; it would yield information on the equilibrium rough wall boundary layer flow downstream of the transition region, creating additional test data for the existing computational procedure; and it would serve as a preliminary step for possible later investigations of a turbulence production dominated region of flow, designed to gain further understanding of the mechanisms involved in turbulence. In addition, comparison of the data with the existing low speed results of Antonia and Luxton[14] would reveal the Mach number dependence of the boundary layer response to sudden perturbations.

A detailed account of the present investigation is presented in Ref. 77.

DESCRIPTION OF THE EXPERIMENT

Facility

This work was performed in Leg II of the Graduate Aeronautical Laboratories, California Institute of Technology (GALCIT) hypersonic wind tunnel. The tunnel is a closed circuit, continuously operating facility utilizing heated air as the test gas. Leg II has a two dimensional, flexible nozzle which may be contoured to produce Mach numbers in the range of 6 to 9. The side walls of the tunnel diverge to compensate for boundary layer growth in the flow direction. For this work, a half nozzle configuration was contoured to produce a nominal free stream Mach number of 6.0. This resulted in a total test section height of approximately 2.8 inches, with an inviscid core approximately 0.8 inches in height by 5.0 inches in width.

The nominal tunnel operating conditions for this work were chosen to give the highest possible Reynolds number consistent with good quality flow and safety conditions. These conditions were $p_t = 228$ psia and $T_t = 770^\circ R$ which resulted in a free stream Reynolds number.

Experimental Apparatus

The bottom flexible nozzle wall of the tunnel was removed and replaced by an assembly consisting of a permanent 0.625 inch thick steel plate (base plate) upon which removable surface plates 0.35 inch thick were mounted. The base plate itself was 48.8 inches long and the removable surface element length was 46.3 inches.

Four sets of surface plates were fabricated, one of which was left smooth to serve as a reference condition, while the others were machined to different surface roughness.

The surface roughness chosen for this study was a transverse square bar type as illustrated in Figure 1. This configuration was chosen because it has been extensively studied in low speed flow (Moore, [2] Antonia and Luxton, [14] Perry, Schofield and Joubert, [8] Betterman [5]) and it may be readily characterized by a height and a wavelength. The wavelength to height ratio used was 4, and the grooves were recessed into the surface, leaving the top of the roughness elements level with the smooth wall upstream of the roughness. Roughness heights of 0.0125, 0.0250 and 0.050 inch were used, which, using the data of Betterman, [5] correspond to incompressible sand grain roughness heights of 0.04, 0.09, and 0.18 inch yielding non-dimensional roughness values $k_s^+ (= \frac{k_s u_\tau}{\nu_w})$ of approximately 18, 40 and 85.

To reduce the heat loss from the flat plate to the room, a continuous flow of low speed (< 40 ft/sec) heated air was maintained in a channel formed by the base plate and the tunnel side walls.

Instrumentation

The mean flow properties of the boundary layer were computed from data acquired during Pitot pressure and total temperature surveys. A limited amount of static pressire data was obtained, the main concern being the verificiation of the standard assumption of constant static pressure across the boundary layer. Direct measurements of wall temperature and pressure were made via instrumentation in the tunnel wall, while the wall shear stress was determined using a skin friction balance which could be installed at either of two axial locations. A constant current hot wire anemometer was used to obtain fluctuation

data from which the turbulent properties of the boundary layer could be deduced.

Pitot pressures were measured using a Statham pressure transducer (PA-208TC-10-350, 0-10 psia). Static pressures were measured using a Datametric electronic barometer, type 1014A. Pitot pressure readings are estimated to be accurate to within ± 1%.

The total temperature probe was based on the design of Behrens[47] and consisted of a micarta body and wedge shaped micarta supports 0.5 inch apart.

Two traverse mechanisms were used in this experiment. One traverse was window mounted and permitted cross stream as well as vertical and axial movement, while the other was a top mounted unit which utilized a more rigid support system for the axial moving sting and permitted only axial and vertical movement. Both mechanisms were located at the aft end of the test section ($\approx$ 52 inches from the throat). Estimates of the probe position (with respect to the flat plate) accuracy under tunnel operating conditions vary from ± 0.002 inch at the aft end of the test section to ± 0.005 inch at the maximum probe extension of 28 inches.

The smooth surface plate sections were instrumented with static pressure taps and thermocouples. The taps consisted of a 0.067 inch diameter hole drilled from the back surface of the surface plate to within 0.025 inch of the front surface with a 0.014 diameter inch hole through the surface. These static pressure readings are estimated to be accurate to within ± 1 mm silicone oil (0.0013 psi) or ± 1% or less of the minimum wall pressure sensed. The outputs of all of the surface

thermocouples were monitored on a self balancing strip chart recorder, and the accuracy of the thermocouples based on calibration was ± 1°F.

Provisions were made for mounting a skin friction balance at two axial locations, 27.9 and 47.9 inches from the throat. The surface elements of the balance could be interchanged in the same manner as the rest of the flat plate surface sections. Roughness elements for the balance were machined to match the various plate roughnesses with no interruption or discontinuity. The roughness heights were such that an integral number of roughness wavelengths would be present on the balance element (1, 2, and 4λ for k = 0.050, 0.025, and 0.125 inch, respectively).

The balance itself was a floating element, null return instrument based on the design of Coles.[48] Installation of the instrument in the flat plate was accomplished by means of 16 leveling screws located near the outer edge of the balance table which were alternately tapped into the table and into the base plate. Discontinuity in surface level between the balance table surface and the surrounding plate surface was held to less than 0.0001 inch for the smooth flat plate and less than 0.0002 inch for the rough plates.

The hot wire anemometer system used in this experiment was a Shapiro-Edwards constant current set with a half power frequency of 320 KHz.[49]

Experimental Procedure

The nozzle contour was set with the smooth surface to provide uniform Mach 6 flow in the test section, and this contour was not altered when different surfaces were used. A nominal contour was calculated using a method of characteristics computer program and correcting

for the boundary layer displacement thickness. This contour was then adjusted (while the tunnel was running at operating conditions) to minimize freestream Mach number variations in the test section. The centerline axial Mach distribution achieved in this manner is shown in Figure 2.

The surface plate lengths were such that the leading edge of the third plate from the throat was located at x = 25.4 - several boundary thicknesses downstream of the intersection of the test rhombus with the wall. All step changes in surface roughness occurred at this location. For the smooth surface to rough surface configurations, the surface of the two aft surface plates consisted of the roughness illustrated in Figure 1 with one of three roughness heights (k = 0.0125, 0.025 and 0.050 inch). Preliminary results of the smooth-to-rough wall investigation revealed that an axial distance of some 8 inches (10δ or $20\delta^{*}$) was sufficient for the disturbed boundary layer to reach a new mean flow equilibrium state over the rough wall. Based on this information, the rough-to-smooth wall step change model was configured with a smooth plate immediately downstream of the throat, followed by rough surface (k = 0.050 inch) second plate, with the use of two smooth surface plates downstream of x = 25.4 inches completing the surface plate set. The length of the rough wall section was 11.5 inches - considerably more than the length found necessary for the attainment of new mean flow equilibrium profiles in the absence of an axial pressure gradient. The choice of k = 0.050 inch for the roughness height was predicated on the fact that preliminary calculations indicated it would be in the fully rough regime, while the other

roughness heights would fall into the transitionally rough region.

The low speed channel below the flat plate was instrumented with two thermocouples on the lower side of the base plates on the plate centerline, two on the lower side of the base plate adjacent to a side wall, and two in the low speed flow, two inches below the base plate. With the tunnel at operating conditions the low speed heater temperature was adjusted so that the temperatures indicated by the two thermocouples on the low speed side of the base plate were the same as those indicated by their respective surface thermocouples. The thermocouple readings were monitored over a period of several hours and were found to remain constant.

The thermocouples near the side walls indicated temperatures within 2°F of those on the tunnel centerline, indicating negligible heat loss to the side walls. There was a somewhat more severe axial temperature gradient near the aft of the test section. This gradient was due to the presence of the support structure for the aft end of the flat plate and could not be eliminated. The influence of this slight gradient on the plate temperature is considered to have been negligible as evidenced by the very long section of constant plate temperature shown in Figure 3.

A simple calculation based on the tunnel stagnation temperature indicates that a recovery temperature of 695°R would be expected. As shown in Figure 3, the flat plate temperature

was 618°R, considerably below the anticipated value. The reason for this discrepancy is not fully understood, but it is believed to be due to a combination of heat loss from the uninsulated upper nozzle wall, and the influence of throat cooling far upstream. This will be discussed further in the Results and Discussion section, below.

Prior to the acquisition of any data the flat plate was brought up to within 2-3°F of its equilibrium temperature over its entire length. The temperature distribution on the plate surface would normally level out and reach equilibrium conditions some 45 minutes to 1 hour after tunnel startup.

DATA REDUCTION

Pressure Data

The free stream Mach number was computed from the free stream total pressure to stagnation pressure ratio assuming an isentropic expansion from the throat to the final flow conditions. The static pressure corresponding to this Mach number and stagnation pressure was then computed (using isentropic, perfect gas relations) and assumed to be constant across the boundary layer (a static pressure traverse established the validity of this approximation). The local measured Pitot pressure, corrected for Reynolds number effects using the results of Ramaswamy,[51] was used in conjunction with this static pressure to compute the local Mach number from the Rayleigh Pitot formula.

Total Temperature Data

The local total temperature was determined using the theory of Behrens.[47] Due to the probe construction, it was not possible to acquire data within 0.030 inch of the wall, so a linear variation of total temperature between the last measured data point and the wall temperature was assumed. Adiabatic, perfect gas relations were used to compute the local static temperature.

Hot Wire Data

Quantitative information on the fluctuating flow properties was obtained from the hot wire measurements utilizing the techniques developed by Kovasznay,[51] Morkovin,[52] Kistler,[43] Laufer,[53] and Gran.[49] The reduction of both mean and fluctuating flow hot wire data, including the end loss correction, is given in a condensed form by Gran.[49]

RESULTS AND DISCUSSION

Profile Data

Mean flow Pitot pressure and total temperature data were
obtained throughout the boundary layer at least every two inches
axially throughout the test section. Near the step change in roughness,
profile data were obtained at one inch axial spacings.

Smooth Wall

Comparison of the smooth wall velocity profiles as presented
in Figure 4 reveals that the smooth plate boundary layer is very
nearly self preserving downstream of $x = 25.4$. A small amount of
adjustment in the shape is seen to occur between $x = 25.4$ and $x = 29.4$,
followed by very nearly identical profiles downstream to $x = 35.4$.
However, the velocity profile suddenly becomes more "full" near the
wall at $x = 27.4$. Although no data downstream of $x = 37.4$ are pre-
sented on the overlay plot, the profile data remain self-similar down-
stream to $x = 47.4$. The velocity profiles for all the step change con-
figurations exhibit similar behavior in the vicinity of $x = 37.4$.
Comparable perturbations are present in the density data. The profile
integral data (to be discussed later) in Figures 8, 9, 10 and 11 also
exhibit sudden shifts in level in the vicinity of $x = 37.4$.

An examination of the typical freestream Pitot pressure distri-
bution (Fig. 2) offers some insight into the cause of these anomalies.
Small pressure peaks are seen to be centered in the freestream
($y = 1.1$ inches) near $x = 33$ and $x = 48$. This spacing is compatible
with the existence of a weak pressure wave which is reflected off the

upper nozzle wall such that it intersects the lower wall boundary layer near x = 33, reaches the wall near x ≈ 40 and reflects back into the freestream near x = 47. Static pressure from widely dispersed smooth plate boundary layer surveys indicate that such a pressure wave does exist, although it is weak--maximum pressure variation across the boundary layer was observed to be some 7% at axial location 33.4.

Since all the data were reduced assuming $\frac{dp}{dy} = 0$, a question arises as to whether the observed effects of the pressure wave are real or due to the method of data reduction. Reduction of the smooth plate profile data at x = 33.4 and 39.4 utilizing the measured static pressure distributions produced velocity and density profiles which were very similar between the two locations. The effect of the wave was observed to be a slightly fuller velocity profile close to the wall at x = 33.4 as compared to x = 39.4. The effect of this wave on the profile integral data will be discussed in a later section. Thus, even though the pressure variation across the boundary layer was small, the assumption $\frac{dp}{dy} \approx 0$ is the major cause of the non self-similar boundary layer profiles. The presence of the pressure wave does affect the profiles, but only slightly. Use of the measured static pressure data was precluded by the limited amount obtained (some four axial locations, all on the smooth plate), so the constant pressure assumption was utilized to produce the data reported here.

Comparison of the profile data for the various configurations was predicated on the fact that although strictly similar profiles could not be attained for an extended axial distance due to the pressure wave, the effect of this wave on the profile should be independent of configuration.

Roughness Effects

The step change configuration profile data are presented in Figures 5, 6 and 7. A cursory examination of the profile data reveals that the step change in roughness does, as expected, introduce significant changes into the various profiles and results in new equilibrium or self-similar profiles some distance downstream.

The development of the disturbed boundary layer may readily be observed from overlays of profile data at progressively greater distance downstream of the throat (Figs. 5, 6 and 7). The smooth-to-rough wall development as seen in these figures is representative of all the smooth-to-rough configurations. An increase or decrease in roughness size simply causes a corresponding increase or decrease in the magnitude of the observed effects. The influence of the step change in roughness is seen to spread rapidly across the entire layer, causing progressively larger changes as the layer continues downstream, until a new equilibrium profile is assumed.

Analysis of the smooth-to-rough configuration profiles reveals that, for all quantities presented, the attainment of a new equilibrium profile is accomplished in approximately the same axial distance, regardless of the roughness height. The new profiles are definitely established 33 inches downstream of the throat, corresponding to some 10 boundary layer thicknesses (δ) or 20 displacement thicknesses (δ^*) downstream of the step change.

The boundary layer appears to take a slightly greater distance to adjust to the rough-to-smooth step change, but even in this case the new equilibrium profile is definitely established 37 inches downstream of the throat, some 14δ or $26\delta^*$ downstream of the step change. Thus, although the boundary layer adjusts to the rough-to-smooth step change somewhat more slowly than to the smooth-to-rough step change, the difference in distance involved is only some 30% in terms of δ^*, or 40% in terms of δ.

Jacobs[54] performed his low speed work in fully developed channel flow on a two-dimensional roughness comprised of transverse rectangular bars. He found that the rough-to-smooth surface change resulted in a new equilibrium state within 17 channel half heights, while the rough-to-smooth change took some 25 channel half heights, an increase of 50%. Antonia and Luxton,[14,55] working with the same type of roughness as used here in a low-speed boundary layer, found that less than 20 boundary layer thicknesses were required for the flow over the smooth-to-rough step to adapt to the change, while after 16 boundary layer thicknesses the profiles were "far from

self preserving" for the flow over the rough-to-smooth step.
The present data, when δ^* is regarded as the thickness of the compressible boundary layer, are consistent with the results of both investigations.

Comparison of the profile data for the smooth wall case and the rough-to-smooth step change case (as presented in Figure 7) reveals that although the flow over the step change does attain new equilibrium profiles, they are not the same as the profiles for the smooth wall. The velocity, density and Mach number profiles for the rough-to-smooth configuration are found to be considerably less full throughout the boundary layer than the corresponding smooth plate configuration profiles. Much smaller differences are noticeable in the total temperature data. Thus the presence of the rough wall seems to give rise to some non-reversible changes in the boundary layer flow.

Rotta[56] and Bertram and Neal,[57] have suggested that non-equilibrium or upstream history effects may account for the differences observed in nozzle wall and flat plate boundary layers.

Feller,[58] Voisinet, et al.,[59] Sturek[60] and Bushnell, et al.[61] have investigated the effects of upstream conditions on the boundary layer. Their findings indicate that the properties of the nozzle-wall boundary layers are indeed very sensitive to changes in the upstream wall temperature and freestream pressure gradients. The effect of the upstream favorable pressure gradient was found by Bushnell, et al. to result in increased fullness of the velocity profile while not significantly affecting the total temperature profile. They

quote the data of Feller and Jones in the Langley Mach 6 high Reynolds number tunnel as revealing a tendency to relax from the characteristic tunnel wall quadratic total temperature-velocity variation to the usual flat plate linear relationship some 60 boundary layer thicknesses downstream of the nozzle exit. If the data of Feller and Jones could be applied to this work, this relaxation tendency would become evident some three feet downstream of the end of the test section.

If the subjection of the boundary layer to the rough wall section followed by the readjustment to smooth wall conditions produced a large enough perturbation to destroy or significantly decrease these upstream pressure and temperature effects, the anticipated result would be a somewhat less full velocity profile and a more nearly Crocco Temperature-velocity variation. The observed velocity profile difference supports such a hypothesis, as do the temperature-velocity relationships presented in Figure 12.

Profile Integral Data

$$\delta^* = \int_0^\delta (1 - \frac{\rho u}{\rho_e u_e})dy$$

$$\theta = \int_0^\delta \frac{\rho u}{\rho_e u_e}(1 - \frac{u}{u_e})dy$$

$$H = \delta^*/\theta$$

$$\dot{H} = \frac{100}{\delta^*}\int_0^\delta \frac{\rho u}{\rho_e u_e}(1 - T_t/T_{t_e})dy$$

These data are tabulated in Table II and presented graphically in Figures 8, 9, 10 and 11.

As discussed earlier, the flow in the test section where these measurements were obtained was characterized by a freestream Mach number of $6.02 \pm 1\%$ where the variations in the Mach number were found to be caused by the presence of a weak pressure wave. The effect of this wave on the profile data was discussed earlier with respect to the consequences of utilizing the assumption $\frac{dp}{dy} = 0$ for the boundary layer reduction. The effect of this assumption on the integral data is illustrated in Figures 8, 9, 10 and 11 where the summary parameters resulting from the use of the measured static pressure profile at two axial locations on the smooth wall are plotted.

The $\frac{dp}{dy} = 0$ assumption is observed to be the major reason for the anomalous behavior of the momentum thickness near $x = 35$. This assumption, however, has little effect on the displacement thickness and enthalpy flux, implying that their sudden shift in level in the vicinity of $x = 33 \to 37$ is due to the presence of the weak pressure wave in the test section.

The momentum integral equation for a two dimensional, zero pressure gradient flow such as this may be written

$$\frac{d\theta}{dx} = \frac{\tau_w}{\rho_e u_e^2} = \frac{C_f}{2}$$

The skin friction was directly measured (through use of the skin friction balance) for three configurations (smooth plate and smooth-to-rough wall with $k = 0.025$ and 0.050 inch) at $x = 27.9$ and 47.9. These data are included in Table II. The data at $x = 47.9$ were used in the above equation to determine the anticipated streamwise variation of θ for the various configurations. Lines with the appropriate slopes are faired

through the data downstream of x = 37 (where the presence of the pressure wave has little effect on the data) in Figure 9. The actual streamwise variation of θ is seen to be in good agreement with the calculated value for all configurations.

Examination of the data in Figures 8-11 with the effect of the wave on the data in the vicinity of x = 33-37 in mind reveals no sudden changes due to the existence of a step change in roughness. The parameters are observed to adjust gradually to the change and to approach new equilibrium behavior in the vicinity of x = 37, just as the mean flow profiles do.

Transformation and Correlation

As mentioned in the introduction, there exists a multitude of transformation techniques for casting compressible velocity profile data into an equivalent incompressible form, but several recent papers including Lewis, et al.,[62] Keener and Hopkins,[32] and Kemp and Owen[63] have found that the Van Driest I[29] method accomplishes this task as well as any of the others, and perhaps better than most. This occurs in spite of the fact that it was one of the earliest developed, is based on a less firm "theoretical" foundation, and is simpler to use than most.

Briefly, the Van Driest I transformation starts with the assumption of a Crocco temperature distribution through the boundary layer, i.e.

$$\frac{T_t - T_w}{T_{t_e} - T_w} = \frac{u}{u_e}$$

and uses the Prandtl mixing length theory to determine the Reynolds stress in the flow. The result is a transformation of the compressible velocity, u, into an "incompressible" velocity u^* via the equation

$$\frac{u^*}{u_e} = \frac{1}{A} \sin^{-1} \frac{2A^2(u/u_e) - B}{(B^2 + 4A^2)^{\frac{1}{2}}} + \frac{1}{A} \sin^{-1} \frac{B}{(B^2 + 4A^2)^{\frac{1}{2}}} \tag{3}$$

where A and B are parameters that depend on the temperature distribution.

Van Driest deduced that this velocity would be correlated by

$$\frac{u^*}{u_\tau} = \frac{1}{\kappa} \ln \frac{y u_\tau}{\nu_w} + F$$

where

$$u_\tau = \sqrt{\tau_w / \rho_w}$$

κ $=$ 0.4 - Karman's constant

ν_w $=$ kinematic viscosity at the wall temperature

F $=$ constant dependent only on the boundary conditions (i.e. freestream pressure gradient and wall conditions)

The similarity of this equation and the law of the wall immediately suggests the use of the law of the wall to correlate the transformed velocities. The form of the law of the wall to be used in this work is[64]

$$u^+ = \frac{1}{\kappa} \ln y^+ + C + \frac{\overline{\pi}}{\kappa} w(y/\delta) - \frac{\Delta u}{u_\tau} \tag{4}$$

where

$$u^+ \quad = \quad u^*/u_\tau$$

$$y^+ \quad = \quad \frac{y \, u_\tau}{\nu_w}$$

$$C \quad = \quad 5.0 \text{ - universal constant}$$

$$\overline{\pi} \quad = \quad \text{wake strength parameter dependent on the free-stream pressure gradient}$$

$$w(y/\delta) \quad = \quad 2 \sin^2 \left(\frac{\pi y}{2\delta}\right) \text{ - "wake function" suggested by Coles}[64]$$

$$\frac{\Delta u}{u_\tau} \quad = \quad \text{Clauser's}[65] \text{ rough wall velocity defect}$$

$$= \quad \frac{1}{\kappa} \ell n \frac{k \, u_\tau}{\nu_w} + D$$

$$D \quad = \quad \text{a constant dependent only on the wall conditions}$$

As stated above, the Van Driest transformation is based on the assumption of a Crocco temperature profile. The temperature profile most often used to estimate temperature distributions in boundary layers are one due to Crocco and another given in Walz.[66] Comparison of these formulae with the experimental data for two sample cases is made in Figure 12 where it is evident that while the trend of the temperature-velocity relation is represented by both profiles, neither is a good approximation. Also shown is a least squares quadratic curve fit to the data for each case.

Since the Crocco distribution is such a poor fit to the data, doubt is cast on the validity of the transformation for the velocity data. It is readily verified, however, that the Van Driest transformation may be altered to utilize the coefficients of the curve fit to

the actual data in evaluating A and B in equation (3). Both the Crocco
and empirical temperature distributions were used in an attempt to
correlate the data. The transformation of the velocity data via the
"modified" van Driest relationship resulted in a better correlation
(in the sense that the deduced skin friction was closer to the measured
value) for the smooth plate data at $x = 47$. This procedure yielded a
skin friction within 1% of the measured value while the use of the
standard Van Driest transformation resulted in a skin friction value
some 8% lower. The modified form of the transformation has been
used exclusively in the results discussed below.

Figure 13 presents the results of two correlations, both at
$x = 47.4$ inches from the throat. The correlation of the smooth wall
data was computed, as indicated earlier, assuming $\Delta u/u_\tau = 0$ while
the rough wall correlation was based on the measured skin friction at
that location. A comparison of Coles' wake function with the actual
data is made in Figure 14. In both figures the fit of the data is seen
to be excellent.

Correlation Results

The various parameters resulting from the curvefits are
presented in Table II with graphical presententation made in Figures
15, 16 and 17. A cursory examination of these figures reveals the
existence of sudden shifts in the parameter values at axial locations
of 33 to 39 inches from the throat. This is the same region in which
changes occurred in the profile shapes and the integral properties,
indicating that these anomalies are also due to the previously

discussed pressure wave and data reduction techniques.

The wake strength parameter $\bar{\pi}$ (Fig. 15) is observed to vary betessn 1.1 and 1.6 fpr all configurations. This is significantly larger than the value of 0.61 advanced by Coles[64] as being the representative value for the incompressible, smooth, flat plate equilibrium boundary layer. Once again, the effect of the $\frac{dp}{dy} = 0$ assumption in data reduction was investigated and found to be the cause of the large change in level between $x = 33$ and $x = 39$ (Fig. 15). As stated above, only the wake strength parameters for the smooth wall case and those at $x = 25.4$ and 47.4 for the step change configurations were computed from the curvefit. All others were estimated from these values, as discussed in the Transformation and Correlation section.

The existence of such a large $\bar{\pi}$ parameter is in contrast to the results of Keener and Hopkins[32] at Mach 7 ($\bar{\pi} = 0.4$) and those of Lewis, et al.[62] at Mach 4 ($\bar{\pi} = 0.6$). The data of Reda, et al.[67] at Mach 2.9 yields $\bar{\pi} = 1.2$, while those of Owen, et al.[44] at Mach 7 yield $\bar{\pi} = 0.8$. Laderman and Demetriades[45] at Mach 9 report $\bar{\pi} = 1.4$. In all cases the Van Driest transformation was used to cast the velocity data into an "incompressible" form for use in the correlation. Only Keener and Hopkins have investigated the effect on the transformation of using a fit of the actual data in place of the usual

Crocco distribution. They concluded, as did the author above, that the use of the measured temperature velocity relationship resulted in better correlation results and a somewhat higher value for $\bar{\pi}$, compared to the results achieved utilizing the Crocco distribution.

The correlation skin friction results are presented in Figure 16, along with the measured skin friction. The measured skin friction at $x = 47.9$ for the two smooth-to-rough wall configurations was used to determine $\bar{\pi}$ in the correlation, so any disagreement of the computed and measured values would be indicative of problems in the correlation procedure. The skin friction measurements at $x = 27.9$ for the step change configuration and at $x = 47.9$ for the smooth plate, however, were not used as inputs to the correlation. The excellent agreement of the computed skin friction with the measured values for the smooth plate and $k = 0.025$ inch step-change configurations is conclusive evidence that the correlation procedure is valid and that it may be used in a non-equilibrium region with great success. Disagreement of the computed skin friction with that measured at $x = 27.9$ for the $k = 0.050$ inch smooth-to-rough step configuration and the behavior of the computed skin friction in the vicinity of the step indicate that the perturbation of the flow due to the large roughness height is too large for the

correlation to be successful. The rough-to-smooth results, on the other hand, indicate a very smooth and relatively rapid transition to the downstream values. Although no measured values are available for comparison, these trends indicate that the correlation is applicable for this configuration, even though the roughness height is the same as that in the smooth-to-rough step where the correlation was found to be invalid.

The roughness induced velocity shift data in Figure 17 ($\frac{\Delta u}{u_\tau}$ is from equation (3) above) tend to support these conclusions, although the scatter in the $k = 0.0125$ inch smooth-to-rough configuration would, by itself, give rise to doubts about the applicability of the correlation in this case. In the light of its suitability for the $k = 0.025$ inch configuration, however, this scatter is attributed to the use of the same $\bar{\pi}(x)$ distribution for $k = 0.0125$ inch as was determined for the $k = 0.025$ inch configuration. The significant increase in the value of $\frac{\Delta u}{u_\tau}$ immediately downstream of the step for the $k = 0.050$ inch smooth-to-rough case corresponds to either a significant decrease in τ_w (as seen in Fig. 16) or a significant increase in the velocity across the boundary layer. Neither of these effects would be expected and neither is observed for the other con-figurations, thus substantiating doubts about the correlation's validity in the step region for this roughness. The rough-to-smooth velocity defect, however, is observed to adjust gradually

to the smooth wall conditions, pausing at a somewhat low value in the vicinity of $x = 37 \rightarrow 41$ before attaining its smooth wall value of 0.

The examination of the curvefit results to this point has thus yielded the following results:

1. The assumed form of the law-of-the-wall correlates the equilibrium smooth data very well, judging by the accuracy with which the skin friction was computed.

2. The correlation is applicable in the non-equilibrium flow region immediately downstream of a step change in roughness, provided the change is not too large (what constitutes "large" cannot be deduced on the basis of these results).

3. The boundary layer adjusts gradually to the step change, assuming the properties appropriate to the new wall condition only a considerable distance downstream (the same location as that at which new equilibrium profiles are observed). This is in contrast to the finding of Antonia and Luxton[14] (for a smooth-to-rough step change) that adjustment to the rough wall condition is made within three or four boundary layer thicknesses following an initial overshoot to a level above that finally attained. Antonia and Luxton's[55] results for a rough-to-smooth change are consistent with those found here, i.e. τ_w changes gradually to the value appriate for the smooth wall.

Quantitative Roughness Effects

One convenient method of describing any given roughness is to determine its "equivalent sand grain" roughness, which is defined as the height of Nikuradse's sand grain roughness which would be required to produce the same velocity defect. The subject roughness, however, must be "fully rough," i.e. it must have a large enough roughness Reynolds number that the law of the wall may be expressed in the form

$$u^+ = \frac{1}{\kappa} \ell n \, y/k + \frac{2\overline{\pi}}{\kappa} \sin^2 (\frac{\pi y}{2\delta}) + D \tag{5}$$

Dvorak[41] presents tentative criteria for the upper limit of the transitionally smooth regime which indicate that the critical roughness Reynolds number for this particular roughness is $k^+ (= \frac{k u_\tau}{\nu_w}) = 30$. Thus the $k = 0.050$ inch roughness ($k^+ = 33.8$ from measurements) would be considered "fully rough," while the $k = 0.0125$ inch and $k = 0.025$ inch roughness heights ($k^+ = 7.1$ and 14.9, respectively) would fall into the transitionally rough regime.

For the fully rough regime, the results of Nikuradse for incompressible pipe flow (where there is no "wake" function) may be represented by[1,68]

$$u^+ = \frac{1}{\kappa} \ell n \, y/k_s + 8.5$$
$$= \frac{1}{\kappa} \ell n \, y^+ - \frac{1}{\kappa} \ell n \, k_s^+ + 8.5 \tag{6}$$

where k_s is the sand grain roughness height. The smooth wall results of Nikuradse are correlated by

$$u^+ = \frac{1}{\kappa} \ell n \, y^+ + 5.5$$

Equation (6) may be rewritten as

$$u^+ = \frac{1}{\kappa} \ln y^+ + 5.5 - \frac{\Delta u}{u_\tau}$$

where

$$\frac{\Delta u}{u_\tau} = \frac{1}{\kappa} \ln k_s^+ - 3.0 \tag{7}$$

which yields

$$k_s^+ = e^{\kappa(3 + \frac{\Delta u}{u_\tau})} \tag{8}$$

As before, the effect of compressibility is to require the use of ν_w in place of ν.

The application of equation (8) to the velocity defect of the $k = 0.050$ inch roughness from Figure 33 ($\frac{\Delta u}{u_\tau} = 6.5$) yields $k_s^+ = 44.7$ or, since $k^+ = 33.8$, $k_s/k = 1.3$. Returning for a moment to the low speed correlation results of Dvorak and Betterman (and extended by Simpson[69] and Dirling[70] to other geometries with good results), the effect of the square bar roughness with $\ell/k = \lambda$ (wavelength-to-height ratio) < 4.7 is found to be

$$\frac{\Delta u}{u_\tau} = \frac{1}{\kappa} \ln k^+ + 17.35 (0.705 \ln \lambda - 1) \tag{9}$$

which yields, for $k^+ = 33.8$, $\lambda = 4$

$$\frac{\Delta u}{u_\tau} = 8.4$$

The validity of this equation is limited to the fully rough regime ($k_s^+ \geqslant 70$); however, $k_s^+ = 45$ is close enough to this regime that no large errors are introduced ($\frac{\Delta u}{u_\tau}$ varies little from the fully rough relation-- see Fig. 18. This is significantly higher than the observed value (Fig. 17) of 6.5--some 30% higher. The use of equation (8) with $\frac{\Delta u}{u_\tau} = 8.4$ yields $k_s/k = 2.8$--more than double the actual value of 1.3

calculated above. These results illustrate quite graphically the inability of the low speed correlation results of Dvorak, Betterman, Simpson and Dirling to correlate the present hypersonic data.

The current data are presented, along with previously published data, in Figures 18 and 19. Use of the equivalent sand grain roughness Reynolds number in the abscissa effects the collapse of data for several roughness configurations and Mach numbers ranging from 0 to 6 into a single, well defined curve in both cases. The sand grain roughness, unless otherwise noted, was computed for each set of data by choosing a value of $\frac{k \, u_\tau}{\nu_w}$ in the fully rough regime and utilizing the associated value of $\frac{\Delta u}{u_\tau}$ in equation 8 above. This value of k_s was then used to plot all data points for that configuration.

When presented in this manner, a single curve is sufficient to describe the data in Figure 18. For $k_s^+ > 70$ the appropriate equation is $\frac{\Delta u}{u_\tau} = \frac{1}{\kappa} \ln k_s^+ - 3.0$. An equation of the form suggested by Dvorak may be used to describe the trend of the data in the transitionally rough regime. Such an equation is presented in Figure 18. The velocity defect and its first derivative were specified to vanish at $k_s^+ = 3.5$ and to match the fully rough values at $k_s^+ = 70$.

The data in Figure 19 are adequately represented by the equation

$$\frac{C_f}{C_{f_0}} = 0.39(\ln k_s^+ - 2.3) + 1.0$$

Thus, once the effective sand grain roughness is known, the effect of surface roughness on the skin friction and velocity defect may readily be determined. The only problem that remains is the determination of the equivalent roughness, which is basically what is accomplished

by the correlations of Dirling and the others mentioned previously.
However, these correlations were found to be inapplicable for these
flow conditions. A brief discussion of the flow over the type of
roughness is in order.

The data of Liu, et al. [7] were obtained on transverse square
bar roughness with a wavelength of 4 in low speed water flow, and
their results indicate an equivalent roughness of $k_s = 2 \rightarrow 2.5k$, fairly
close to the value of $k_s = 2.7$ for the work of Betterman. The results
of Betterman indicate that for λ in the vicinity of 4, the effectiveness
is extremely sensitive to small changes. The visualization work of
Liu, et al. revealed that in the vicinity of $\lambda = 4$, the character of the
flow in the cavity between the roughness elements changes radically.
For λ considerably less than 4, the flow completely bridges the cavity
(the "d" type flow of Perry, et al. [8]), creating an "open" cavity,
while for λ much larger than 4, the flow reattaches to the cavity floor,
creating two distinct separation regions within the cavity (a "closed"
cavity). The transition from one type of cavity to the other occurs
for λ somewhere in the range of 2 to 8. This explains the sudden
shift in slope of the correlation results of Dirling as presented in
Figure 20 from Mills and Courtney [71]). As λ increases from 2, the
vortex structure within the cavity is stretched and pressure communi-
cation between the upstream and downstream faces is decreased,
resulting in increased pressure drag. The maximum drag is reached
very near the value of λ at which reattachment occurs, for then the
pressure drag on the faces has reached the maximum and any increase
in spacing simply produces less force per unit length, and, therefore,

less drag per unit length. The slope change occurs at a value of λ slightly above 4, corresponding to the change between open and closed cavity flow.

Charwat, et al. [72] have investigated higher speed flow over two dimensional transverse notches and conclude that for supersonic flow over large cavities, closed cavity flow exists for $\lambda > 12$ and open cavity flow exists for $\lambda < 10$. The observation of a crossover point near $\lambda = 4$ for subsonic flow is also made, supporting the conclusions of Liu, et al.

In conclusion, the data acquired in this work for equilibrium rough wall flow show good agreement with previously published data, when correlated with respect to Reynolds number based on the equivalent sand grain roughness height. The equivalent roughness, however, is found to be significantly altered from that for identical roughness in low speed flow. These data support the claim advanced by Mills and Courtney, [71] and others that once the equivalent sand grain roughness is determined, the effect of a given roughness on the skin friction and velocity may readily be determined (i.e. Figs. 18 and 19). The determination of equivalent sand grain roughness, however, is not a trivial matter, as demonstrated by the results of this work. In particular, the extrapolation of any low speed correlation for equivalent sand grain roughness, such as that of Dirling, [70] to higher speed flows must be viewed as highly susceptible to very large errors.

Fluctuation Data

Preliminary analysis of the data during the acquisition phase of this work indicated that the data were of reasonable magnitude and

and possessed the anticipated profile shape. Later complete reduction and extensive analysis revealed that some of the data were obviously in error, but it was not possible to repeat the measurements. As a result, fluctuation data for some of the wall configurations at some axial locations were discarded and are not included in this discussion.

The fluctuation magnitudes, as discussed herein, contain rather large error bands--probably $\pm$ 10-20% on a point by point basis. However, when considered in conjunction with data at other points throughout the boundary layer, very definite trends which do not depend on the magnitude accuracy are observed. In addition, the consistency of the observed magnitudes lends considerable credit to their validity.

Fluctuation data are presented as mass flux fluctuations $\left(\sqrt{\overline{\dot{m}'^2}}/\dot{m}_\ell\right)$, total temperature fluctuations $\left(\sqrt{\overline{T_t'^2}}/T_{t_\ell}\right)$, and the associated correlation coefficient, $R_{mT_t} = \overline{\dot{m}'T_t'}/\left(\sqrt{\overline{\dot{m}'^2}}\sqrt{\overline{T_t'^2}}\right)$ for all wall configurations in Figures 21, 22, and 23. No smooth wall data were obtained at $x = 24.4$, and where data for a particular configuration have been omitted, the data were found to be in error.

Here, as for the mean flow data, the profiles at various axial locations were compared to determine where the profiles ceased to show discernible change. The boundary layer downstream of this location was then defined as an equilibrium or self preserving layer. In the case of the mean flow data, the number of axial locations and the high resolution of the data yielded

fairly definitive results. For the fluctuation data, however, data were obtained at far fewer axial stations and the data scatter was much greater. As a result, the axial location at which the profiles become self similar is far more difficult to locate. Data considerably downstream of the test section would be required to verify that equilibrium profiles actually are established.

Smooth Wall

The smooth wall configuration serves as a reference for determining the roughness induced effects, and as such, will be discussed first. Examination of the mass flux ($\dot{m}$) and total temperature (T_t) fluctuation profiles reveals that both profiles become "fuller" as the axial distance increases from 27.4 to 39.4 inches from the throat and then remain essentially constant downstream to $x = 45.4$. Thus, although the mean flow profiles, as discussed above, indicate that mean flow equilibrium on the smooth wall is achieved near the upstream end of the test rhombus, the fluctuation properties do not achieve a self similar or equilibrium state until some distance downstream, between $x = 33$ and $x = 39$, some 14 to 20 inches (18 to 25δ) downstream of the test section boundary. It appears that the fluctuation levels characteristic of the smooth wall are suppressed in the favorable pressure gradient flow created by the nozzle and gradually relax to an equilibrium profile once free of the large gradient. The data of Rose[73] indicate that the fluctuation magnitude in a compressible flow is significantly affected by pressure gradients, with a favorable gradient causing a decrease in magnitude.

Comparison of the smooth wall data with that obtained by Kistler,[43] Laderman and Demetriades[75] and Owen et al.[76] is made in Figure 24 (replotted from Owen, et al.). The present data are observed to agree quite well with the $M = 1.72$ results of Kistler, in opposition to his findings that all the quantities increase with Mach number in the Mach number range of 1.7 to 4.7. Although Owen, et al. attribute the differences between Kistler's results and their own to heat transfer effects, the present data do not substantiate such a claim, for in spite of the present adiabatic nozzle wall, the data do not agree with the trends established by Kistler's results.

Smooth-to-Rough Transition

Examination of the smooth-to-rough wall configuration data (Figs. 21, 22, and 23) reveals that self-similar shapes (within the accuracy of the data) are attained for the $\dot{m}$ fluctuation profiles upstream of $x = 39$ inches for all roughness sizes. Equilibrium profiles for the T_t fluctuations are attained somewhat later, between $x = 39.4$ and $x = 45.4$, as verified by the available $x = 51.4$ data. Following the smooth-to-rough wall step change, then, a definite pattern is noted--the mean flow data are the first to attain new equilibrium profiles, followed by the mass flux fluctuation data, followed in turn by the total temperature fluctuation data. This progression is a consequence of the manner in which the roughness interacts with the boundary layer to produce the mass flux and total temperature fluctuations. The roughness actually induces velocity fluctuations which interact with the mean flow to result in mass flux fluctuations which in turn interact with the mean flow and velocity fluctuations to create total temperature

fluctuations. Thus, before the fluctuations can reach equilibrium levels, the mean flow must be in equilibrium, and since a finite amount of time is required for $\dot{m}$ fluctuations to respond to a change in mean flow conditions, there will be a time (and distance) lag prior to the establishment of $\dot{m}$ equilibrium profiles. In the same manner, the T_t fluctuations are dependent upon the interaction of the mean flow and $\dot{m}$ fluctuations, and so will reach equilibrium even later in time and further downstream.

Roughness effects (the increase in fluctuation levels with respect to those over a smooth wall) are readily apparent at $x = 27.4$, remain about constant in the inner half of the profile but increase in the outer section at $x = 33.4$, and then decrease somewhat at $x = 45.4$. The actual rough wall fluctuation magnitudes, on the other hand, develop to a self similar shape prior to $x = 39.4$. The apparent decrease in the effect of roughness (smaller amount of increase due to the roughness), then, is due not to a decrease in the rough wall fluctuation levels, but to an increase in the smooth wall levels. As discussed previously, the presence of the rough wall significantly alters the upstream history effects of the mean flow, and this, in conjunction with its increased turbulence production, leads to an earlier attainment of equilibrium. Of particular interest in the stream- wise development downstream of the step is the fact that the $\dot{m}$ fluc- tuation level at the wall appears to first decrease upon transition to a rough wall, and then increase along with the rest of the boundary layer. The total temperature data indicate no such decrease.

Careful examination of the data reveals further insights into the manner in which the various roughness heights affect the turbulent flow structure. Turning first to the $\dot{m}$ fluctuations, consider Figure 21 in which these data are presented for all configurations. The general features of the profiles downstream of x = 27.4 are all similar, but those at x = 39.4 illustrate the trends as well as any and will be used for purposes of illustration. The largest effect is seen to be caused by the k = 0.0125 inch rough wall configuration which also exhibits a conspicuous maximum some $y/\delta^* = 0.8$ away from the wall as opposed to the more ambiguous maximum exhibited by the other configurations located at distances of $y/\delta^* = 0.5$ for the smooth wall and k = 0.050 inch rough wall and $y/\delta^* = 0.8$ for the k = 0.025 inch rough wall. The shape of the k = 0.0125 inch rough wall $\dot{m}$ profile is significantly different from that of the other configurations throughout the inner half of the boundary layer. It not only has a more definite maximum, in general, as noted above, but it also decreases in magnitude very rapidly as the wall is approached-- so rapidly, in fact, that near the wall it actually falls below the smooth wall profile. The magnitude also decreases rapidly as the freestream flow is approached.

The k = 0.025 inch rough wall profile data also exhibit a peak magnitude well out in the boundary layer, as indicated above. This maximum, however, is usually less pronounced than that for the k = 0.0125 inch data, with the magnitude decreasing less rapidly as the wall is approached, achieving a value somewhat higher than the smooth wall configuration profile adjacent to the wall. Consideration

of the profile between the maximum magnitude and the freestream reveals that the magnitude drops off less rapidly than the $k = 0.0125$ inch profile as the freestream is approached and is larger than that of the small roughness from $y/\delta^* = 1.2$ to the freestream at $y/\delta^* = 2.0$.

Consider now the $k = 0.050$ inch rough wall data; it is observed that its maximum occurs much nearer the wall, in the vicinity of $y/\delta^* = 0.5$, the magnitude being very comparable to that of the $k = 0.025$ inch data. In fact, the behavior of the profile between this maximum magnitude point and the wall is virtually identical to that of the $k = 0.025$ inch profile. Going toward the freestream flow, the magnitude first drops below that of the smaller roughness configurations, and then assumes virtually the same value as the $k = 0.0125$ inch data from $y/\delta^* = 1.2$ to the freestream.

Thus, although the data for actual fluctuation magnitudes may be subject to considerable error, the effect of roughness size is definitely discernible. The effect of a small roughness $\left(\dfrac{ku_\tau}{\nu_w} \approx 7 \right)$ is an increase in the $\dot{m}$ fluctuation levels throughout the boundary layer except in the immediate vicinity of the wall, where a slight decrease may occur. A very definite maximum magnitude peak is established well displaced toward the freestream compared to the smooth wall peak, with the roughness effect decreasing significantly as the freestream is approached, but not disappearing. An increase in the roughness height causes an increase in the fluctuation level relative to the magnitude peak throughout the boundary layer, with no change in peak location. As the roughness size continues to increase, the location of the magnitude peak approaches that of the smooth wall

magnitude peak and the fluctuation level between this peak and the freestream decreases somewhat but remains above the smooth wall level. In all cases the rough wall freestream fluctuation levels are about double the smooth wall freestream levels. The increased levels throughout the flow are due to the high level of velocity fluctuation production on the rough walls.

Turning now to the total temperature fluctuation data presented in Figure 22, it is apparent that significant roughness effects are present at x = 27.4 and increase in the outer portion of the boundary layer prior to x = 33.4, then decrease somewhat throughout the boundary layer between x = 33.4 and x = 39.4. Subsequent to x = 39.4, little change occurs. No definite roughness size effects are discernible in the data. In contrast to the $\dot{m}$ fluctuation data, the peak magnitude occurs at the same location for all the rough walls as for the smooth wall.

The mass flux-total temperature correlation function is presented in Figure 23. A rather consistent profile is seen to exist at all stations for all the surface conditions. The correlation function starts off with a small negative value near the wall, rapidly becomes positive, then decreases to a minimum near $y/\delta^* = 1.0$ before increasing again and approaching a freestream value of about 0.5-0.7. The smooth wall deviates from this pattern near the freestream to assume a negative value near -0.5 which is close to the value of -0.7 found by Owen, et al.[76] at M = 7 for a non-adiabatic boundary layer. The profile shape is also similar, although these correlation

functions are significantly smaller throughout the body of the boundary layer.

The k = 0. 050 inch rough wall data generally are very similar to the smooth wall data, except near the boundary layer edge, while the smaller roughnesses maintain somewhat different profiles, just as for the $\dot{m}$ fluctuation profiles.

Rough-to-Smooth Transition

Only the rough-to-smooth step change fluctuation data presented in Figures 21-23 remain to be analyzed. Both the $\dot{m}$ and T_t fluctuation profiles at x = 24. 4 are observed to be generally similar to those for the k = 0.050 inch smooth-to-rough configuration at x = 39 (fully developed or self similar rough wall flow). The profiles are, however, concentrated much closer to the wall, probably the result of the strong favorable pressure gradient in the nozzle. As indicated earlier, such a gradient tends to suppress fluctuation magnitudes somewhat. The correlation functions for the two configurations are very similar.

By x = 27, some 3δ downstream of the step change in roughness, the character of both fluctuation profiles has changed considerably, decreasing in magnitude at the wall and increasing in magnitude toward the freestream. This growing in the freestream direction accompanied by development of magnitude peaks near $y/\delta^* = 0.5$ is a reflection of the adjustment to a zero pressure gradient freestream, while the change in wall level is a reaction to the shift from the rough to the smooth wall. The correlation function is also seen to respond to the

absence of the favorable pressure gradient by expanding in the free-stream direction.

The profiles continue to adjust to the changes in both the freestream and wall conditions downstream of $x = 27.4$. A gradual increase in level on the freestream side of the profiles is observed, accompanied by a shift of the maximum amplitude peak in the same direction. Both profiles appear to be close to equilibrium at $x = 39.4$, but continue to change in the vicinity of the freestream between $x = 39.4$ and $x = 45.4$. A self similar profile for the $\dot{m}$ fluctuations appears to be established at $x = 45.4$, but the T_t profile shows evidence of continued evolvement on the freestream side. Throughout this adjustment to new surface conditions, the correlation coefficient remains essentially unchanged downstream of $x = 27.4$.

The large magnitude of the $\dot{m}$ fluctuations (larger than the $k = 0.050$ inch smooth-to-rough configuration) is due to the location of the rough plate in the nozzle. The same roughness height was used for both configurations, but the rough-to-smooth arrangement placed the upstream end of the plate in a much thinner boundary layer ($\delta^* \approx 0.2$ inch versus $\delta^* \approx 0.4$ inch for the smooth-to-rough step change). The effective roughness height was thus much greater, well within the fully rough regime, as opposed to the downstream location where it was at the very lower limit of that regime. The turbulence production caused by the roughness would therefore be considerably larger for the rough-to-smooth model. In addition, the presence of this large roughness in the strong pressure gradient section of the nozzle would significantly perturb the mean flow and exert a larger

effect on the upstream boundary history than would a similar plate in the zero pressure gradient test section.

The rough-to-smooth configuration fluctuation data are also presented in Figure 24. It is obvious that the history effects are very important and no meaningful comparison of nozzle wall data may be attempted in the absence of more detailed knowledge of these effects.

In summary, the fluctuating flow properties were found to respond to changes in the wall roughness somewhat more slowly than did the mean flow properties. This phenomenon is due to the mechanism by which the fluctuating properties are actually influenced by the surface condition. Definite roughness size effects are present in the $\dot{m}$ fluctuation data for flow over a rough wall, but none were observed for the T_t fluctuation data. Comparison of the rough-to-smooth step change data with the smooth wall data revealed upstream history effects, just as mean flow data did earlier.

CONCLUSIONS

An experimental investigation of the response of the hypersonic turbulent boundary layer to a step change in surface roughness has been performed in Leg II of the GALCIT Hypersonic Wind Tunnel. The subject boundary layer developed on the flat nozzle wall adjacent to Mach 6 freestream flow. Both mean and fluctuating flow data were acquired for several smooth-to-rouch surface step changes and a single rough-to-smooth surface step change. Use of a transverse square bar type of roughness facilitated direct comparisons with low speed data. Analysis of the data from this program has yielded the following conclusions:

1. The establishment of new equilibrium mean and fluctuating flow profiles downstream of a step change in surface roughness is accomplished in nearly the same distance (in terms of boundary layer thicknesses) as in the incompressible case. The step change smooth-to-rough configuration boundary layer attains new mean flow self similar profiles some 10δ or $20\delta^*$ downstream of the step, while the fluctuation profiles reach this state some 14-16δ or 28-$32\delta^*$ downstream of the step. These distances are independent of roughness height for roughnesses in the transitionally rough regime ($\frac{k_s u_\tau}{\nu_w} < 70$). The step roughness change rough-to-smooth configuration produced a somewhat slower adjustment of the boundary layer, some 14δ or $26\ \delta^*$ for mean flow equilibrium and some 20-25δ or 40-$50\ \delta^*$ for fluctuation equilibrium.

2. The hypersonic smooth and rough wall equilibrium profile velocity data, subsequent to a modified Van Driest transformation to "equivalent incompressible" form, are well correlated by the incompressible composite law of the wall. The use of a virtual origin for the effective surface is necessary to achieve good results for the flow over the surface roughness configurations, just as for incompressible flows. The modified form of the Van Driest transformation used incorporated a least squares quadratic curve fit to the measured temperature data in place of the standard Crocco temperature profile.

3. The above correlation is also found to be applicable in the highly non-equilibrium flow region immediately downstream of the step change in roughness, provided the roughness is not too large. A roughness height of 0.050 inch ($k_s^+ = 45$) for the smooth-to-rough step surface change was found to be too large in this sense, but the same height used in the rough-to-smooth step change configuration was not.

4. The effects of surface roughness on equilibrium or self-preserving boundary layers were found to exhibit excellent agreement with previously published data, when correlated versus equivalent sand grain roughness. When viewed in this manner, with the equivalent sand grain roughness a unique parameter for a given type of roughness in a given freestream velocity, the effect of a change in roughness height on the skin friction and nondimensional velocity (u/u_τ) profiles is found to be a universal function.

5. Existing procedures (based on incompressible data) for calculating the equivalent sand grain roughness of a given roughness configuration were found to be inapplicable in the present case, due

to velocity induced changes in the flow over the roughness. In light of this finding, the extrapolation of any low speed roughness correlation to higher velocities must be viewed very critically with the knowledge that any results of such a procedure are very susceptible to gross errors. A concentrated effort to determine the effects of compressibility and velocity on such correlations is definitely needed.

6. The investigation of the rough-to-smooth step change configuration revealed the existence of very significant pressure and temperature history effects throughout the boundary layer. The existence of these effects affords an explanation of apparent inconsistency of data obtained on wind tunnel nozzle walls with that obtained on flat plates supported in the tunnel freestream. The presence of the rough surface on the nozzle wall within the expansion region was sufficient to alter the history effects, but was not able to eliminate them. The unknown nature and extent of such history effects casts serious doubts on the validity of simulating boundary layers on freestream surfaces by use of nozzle wall boundary layers. Considerably more research is needed in this area to delineate the extent of these history effects and investigate the possibility of destroying them.

REFERENCES

1. Nikuradse, J. "Strömungsgeretze in rauken Rohren." VDI
   Forshungsheft no. 361, 1933. Translated as NACA TM 1292,
   1950.

2. Moore, W. F. "An Experimental Investigation of the Boundary
   Layer Development Along a Rough Surface. Ph. D. dissertation,
   State Univ. of Iowa, 1951.

3. Hama, F. R. "Boundary Layer Characteristics for Smooth and
   Rough Surfaces." Trans. Soc. Naval Arch. Mar. Engrs., Vol.
   62, pp. 333-358.

4. Clauser, F. H. "Turbulent Boundary Layers in Adverse Pres-
   sure Gradients," J. Aero. Sci., Vol. 21, pp. 91-108, 1954.

5. Betterman, D. "Contribution a l'Etude de la Convection Force
   Turbulente le long de Plaques Ruguenses," Int. J. Heat Mass
   Transfer, Vol. 9, pp. 153-164, 1966.

6. Morris, H. M., Jr. "Flow in Rough Conduits." Trans. ASCE,
   Vol. 120, pp. 373-397, 1955.

7. Liu, C. K., Kline, S. J. and Johnston, J. P. "An Experimental
   Study of Turbulent Boundary Layers on Rough Walls," Rept.
   MD-15, Stanford University Dept. of Mechanical Engineering,
   1966.

8. Perry, A. E., Schofield, W. H., and Joubert, P. N. "Rough Wall
   Turbulent Boundary Layers," J. Fluid Mech., Vol. 37, Part 2,
   pp. 383-413, 1969.

9. Perry, A. E. and Joubert, P. N. "Rough Wall Boundary Layers
   in Adverse Pressure Gradients," J. Fluid Mech., Vol. 17,
   pp. 193-211, 1963.

References (continued)

10. Streeter, V. and Chu, H. "Fluid Flow and Heat Transfer in Artificially Roughened Pipes," Final Report Project 4918, Armour Research Foundation, 1949.

11. Sams, E. W. "Experimental Investigations of Average Heat Transfer and Friction Coefficients for Air Flowing in Circular Tubes Having Square-threads Type Roughness," NACA Res. Mem. RME S2017.

12. Ambrose, H. H. "The Effect of Surface Roughness on Velocity Distribution and Boundary Resistance," University of Tennessee, Dept. of Civil Engineering Contract N/r 811(03). Office of Naval Research, Department of the Navy, 1956.

13. Corrsin, S. and Kistler, A. L. "Free Stream Boundaries of Turbulent Flows," NASA-1244, Jan. 1954.

14. Antonia, R. A. and Luxton, R. E. "The Response of a Turbulent Boundary Layer to a Step Change in Surface Roughness. Part 1. Smooth to Rough," J. Fluid Mech., Vol. 48, Part 4, pp. 721-761, 1971.

15. Liu, C. Y., Sandborn, V. A. and Tieleman, H. W. "Turbulent Spectral Data in Large-Scale Turbulent Boundary Layers, Developed over Different Types of Boundary Roughness," Colorado State University, Research Memo No. 10, N68-29202, 1967.

16. Logan, E. Jr. and Jones, J. B. "Flow in a Pipe Following an Abrupt Increase in Surface Roughness," Trans. of ASME, J. Basic Eng., pp. 35-40, March 1963.

References (continued)

17. Van Driest, E. R. "On Turbulent Flow Near a Wall," J. Aero. Sci., Vol. 23, No. 11, pp. 1007-1011. Nov. 1956.

18. Dvorak, F. A. "Calculation of Turbulent Boundary Layers on Rough Surfaces in Pressure Gradient," AIAA J. Vol. 7, No. 9, pp. 1752-1759, Sept. 1969.

19. Goddard, F. E. Jr. "Effect of Uniformly Distributed Roughness on Turbulent Skin-Friction Drag of Supersonic Speeds," J. Aeron. Sci. Vol. 26, No. 1, pp. 1-15, Jan. 1959.

20. Wade, J. H. T. "An Experimental Investigation of the Effect of Surface Roughness on the Drag of a Cone-Cylinder Model at a Mach Number of 2.48," Rept. 34, Institute of Aerophysics, Univ. of Toronto, Toronto, Canada, Sept. 1955.

21. Fenter, F. W. "The Turbulent Boundary Layer on Uniformly Rough Surfaces of Supersonic Speeds," DRL-437. Defense Research Laboratory, University of Texas, Austin, Texas, Jan. 1960.

22. Young, F. L. "Experimental Investigation of the Effects of Surface Roughness on Compressible Turbulent Boundary Layer Skin Friction and Heat Transfer," DRL-532, Defense Research Laboratory, University of Texas, Austin, Texas, May 1965.

23. Shutts, W. H. and Fenter, F. W. "Turbulent Boundary Layer and Skin Friction Measurements on an Artificially Roughened, Thermally Insulated Plate at Supersonic Speeds," DRL-366, Defense Research Laboratory, University of Texas, Austin, Texas, August 1955.

References (continued)

24. Mann, H. W. "Experimental Study of the Compressible Turbulent Boundary Layer Skin Friction and Heat Transfer in the Fully Rough Regime," DRL-554 Defense Research Laboratory, University of Texas, Austin, Texas, Aug. 1967.

25. Reda, D. C. "Compressible Turbulent Skin Friction on Rough and Rough/Wavy Walls in Adiabatic Flow," NOLTR 74-34, NAVAL Ordnance Laboratory, February 1974.

26. Monta, W. J., Czarnecki, K. R. and Deveikis, W. D. "Drag Due to Two-Dimensional Roughness in a Turbulent Boundary Layer at Mach 3 with and without Heat Transfer," NASA TN D-4746, Sept. 1968.

27. Baronti, P. O. and Libby, P. A. "Velocity Profiles in Turbulent Compressible Boundary Layers," AIAA J, Vol. 4, No. 2, pp. 193-202, Feb. 1966.

28. Coles, D. "The Turbulent Boundary Layer in a Compressible Fluid," The Physics of Fluids, Vol. 7, No. 9, pp. 1403-1423, Sept. 1964.

29. Van Driest, E. R. "Turbulent Boundary Layer in Compressible Fluids," J. Aeron. Sci., Vol. 18, No. 3, pp. 145-160, March 1951.

30. Van Driest, E. R. "Problem of Aerodynamic Heating," Aeronautical Engineering Review, Vol. 15, No. 10, pp. 26-41, Oct. 1956.

31. Watson, P. D. and Cary, A. M. "Transformation of Hypersonic Turbulent Boundary Layers to Incompressible Form," AIAA J, Vol. 5, No. 6, pp. 1202-1203, June, 1967.

References (continued)

32. Keener, E. R. and Hopkins, E. J. "Van Driest Generalization Applied to Turbulent Skin Friction and Velocity Profiles on the Wall of a Mach 7.4 Wind Tunnel," AIAA J, Vol. 11, No. 12, pp. 1784-1785, Dec. 1973.

33. Sommer, S. C. and Short, B. J. "Free Flight Measurements of Skin Friction of Turbulent Boundary Layers with High Rate of Heat Transfer at High Hypersonic Speeds," J. of Aero. Sci., Vol. 25, pp. 536-542, 1956.

34. Spalding, D. B. and Chi, S. W., "The Drag of Compressible Turbulent Boundary Layer on a Smooth Flat Plate with and without Heat Transfer," J. Fluid Mech., Vol. 18, Part 1, pp. 117-143, Jan. 1964.

35. Clark, F. L. and Creel, T. R. Jr. "Reference Temperature Method for Predicting Turbulent Compressible Skin Friction Coefficient," AIAA J, Vol. 11, No. 2, pp. 239-240, Feb. 1975.

36. Hebbar, K. S. and Paranjpe, P. A. "Skin Friction in Turbulent Boundary Layers," AIAA J, Vol. 7, No. 4, pp. 793-796, April 1969.

37. Tennekes, H. "Law of the Wall for Turbulent Boundary Layers in Compressible Flow," AIAA J, Vol. 5, No. 3, March 1967.

38. Hopkins, E. J., Rubesin, M. W., Inouye, M., Keener, E. R., Mateer, G. C. and Polek, T. E. "Summary and Correlation of Skin Friction and Heat-Transfer Data for a Hypersonic Turbulent Boundary Layer on Simple Shapes," NASA TN D-5089, 1969.

References (continued)

39.   Miles, J. B. and Kim, J. H.   "Evaluation of Coles' Turbulent Compressible Boundary-Layer Theory," AIAA J., Vol. 6, No. 6, pp. 1187-1189, June 1968.

40.   Hopkins, E. J. and Inouye, M.   "An Evaluation of Theories for Predicting Turbulent Skin Friction and Heat Transfer on Flat Plates at Supersonic and Hypersonic Mach Numbers," AIAA J., Vol. 9, No. 6, pp. 995-1003, June 1971.

41.   Dvorak, F. A.   "Calculation of Compressible Turbulent Boundary Layers with Roughness and Heat Transfer," AIAA J,, Vol. 10, No. 11, pp. 1447-1451, Nov. 1972.

42.   Chen, K. K.   "Compressible Turbulent Boundary Layer Heat Transfer to Rough Surfaces in Pressure Gradient," AIAA J., Vol. 10, No. 5, pp. 623-629, May 1972.

43.   Kistler, A. L.   "Fluctuation Measurements in a Supersonic Turbulent Boundary Layer," The Physics of Fluids, Vol. 2, No. 3, pp. 290-296, May-June, 1959.

44.   Owen, F. K., Horstman, C. C. and Kussoy, M. I.   "Mean and Fluctuating Flow Measurements of a Fully-Developed, Non-Adiabatic Hypersonic Boundary Layer," J. Fluid Mech., Vol. 70, Part 2, pp. 393-413, 1975.

45.   Laderman, A. J. and Demetriades, A.   "Mean and Fluctuating Flow Measurements in the Hypersonic Boundary Layer Over a Cooled Wall," J. Fluid Mech., Vol. 63, Part 1, pp. 121-144, 1974.

References (continued)

46. Laderman, A. J. and Demetriades, A. "Turbulent Fluctuations in the Hypersonic Boundary Layer Over an Adiabatic Slender Cone," The Physics of Fluids, Vol. 19, No. 3, pp. 359-361, March 1976.

47. Behrens, W. "Total Temperature Thermocouple Probe Based on Recovery Temperature of a Circular Cylinder," Int. J. Heat Mass Transfer, Vol. 14, pp. 1621-1630, 1971.

48. Coles, D. "Measurements in the Boundary Layer Flow," Ph.D. Thesis, California Institute of Technology, 1953.

49. Gran, R. L. "Step Induced Separation of a Turbulent Boundary Layer," Ph.D. Thesis, California Institute of Technology, 1970.

50. Ramaswamy, M. A. "Experimental Investigation of the Effect of Cooling on the Near Wake of Circular Cylinders at Mach Number Six," Ph.D. Thesis, California Institute of Technology, 1971.

51. Kovasznay, L.S.G. "Turbulence in Supersonic Flow," Jour. Aero. Sci., Vol. 20, No. 10, pp. 657-674, October 1953.

52. Morkovin, M. V. "Fluctuations and Hot-Wire Anemometry in Compressible Flows," AGARDograph No. 74, November 1956.

53. Laufer, J. "Some Statistical Properties of the Pressure Field Radiated by a Turbulent Boundary Layer," The Physics of Fluids, Vol. 7, No. 8, pp. 1191-1197, August 1964.

54. Jacobs, W. "Variation in Velocity Profile with Change in Surface Roughness of Boundary," Translated as NACA TM 951.

References (continued)

55. Antonia, R. A. and Luxton, R. E. "The Response of a Turbulent Boundary Layer to a Step Change in Surface Roughness. Part 2. Rough-to-Smooth," J. Fluid Mech., Vol. 53, Part 4, pp. 737-757, 1972.

56. Rotta, J. C. "Heat Transfer and Temperature Distribution in Turbulent Boundary Layers at Supersonic and Hypersonic Flow," AGARDograph 97, Part I, pp. 41-63, May 1965.

57. Bertram, M. H., and Neal, L., Jr. "Recent Experiments in Hypersonic Turbulent Boundary Layers," paper presented at the AGARD Specialists Meeting on Recent Developments in Boundary Layer Research, Naples, Italy, May 10-14, 1965.

58. Feller, W. V. "Effects of Upstream Wall Temperatures in Hypersonic Tunnel Wall Boundary Layer Profile Measurements," AIAA J., Vol. 11, No. 4, pp. 556-558, April 1973.

59. Voisinet, R. L. P., Lee, R. E. and Yanta, W. J. "An Experimental Study of the Compressible Turbulent Boundary Layer with an Adverse Pressure Gradient," AGARD CP-93 Turbulent Shear Flows, Fluid Dynamics Panel Specialists. Meeting in London, September 1971.

60. Sturek, W. B. "Wall Heat Transfer Effects on Supersonic Nozzle Wall Boundary-Layer Temperature Profiles," BRL Mem. Rept. No. 2328, Sept. 1973.

References (continued)

61. Bushnell, D. M., Johnson, C. B., Harvey, W. D., and Feller, W. V., "Comparison of Prediction Methods and Studies of Relaxation in Hypersonic Turbulent Nozzle-Wall Boundary Layers," NASA TN D-5433, 1969.

62. Lewis, J. E., Gran, R. L. and Kubota, T. "An Experiment on the Adiabatic Compressible Boundary Layer in Adverse and Favorable Pressure Gradient," J. Fluid Mech., Vol. 51, part 4, pp. 657-672, 1972.

63. Kemp, J. H. Jr., and Owen, F. K. "Nozzle Wall Boundary Layers at Mach Number 20 to 47," AIAA J., Vol. 10, No. 7, pp. 872-879, July 1972.

64. Coles, D. "The Young Person's Guide to the Data," 1968 AFOSR-IFP-Stanford Conference on Computation of Turbulent Boundary Layers.

65. Clauser, F. H. "The Turbulent Boundary Layer," Advances in Applied Mechanics, Vol. 4, Academic Press, pp. 1-51, 1956.

66. Walz, A. Boundary Layers of Flow and Temperature, MIT Press, p. 69, 1969.

67. Reda, D. C., Ketter, F. C., Jr., and Fon, C. "Compressible Turbulent Skin Friction on Rough and Rough/Wavy Walls in Adiabatic Flow," AIAA Paper No. 74-574, presented at the AIAA 7th Fluid and Plasma Dynamics Conference, Palo Alto, Calif., June 17-19, 1974.

References (continued)

68. Schlichting, H. Boundary Layer Theory, Sixth Ed., translated by J. Kestin, McGraw-Hill, p. 582, 1968.

69. Simpson, R. L. "A Generalized Correlation of Roughness Density Effects on the Turbulent Boundary Layer," AIAA J., Vol. 11, No. 2, pp. 242-244, Feb. 1973.

70. Dirling, R. B., Jr. "A Method for Computing Rough Wall Heat Transfer Rates on Reentry Nosetips," AIAA Paper No. 73-763, presented at the AIAA 8th Thermophysics Conference, Palm Springs, 1973.

71. Mills, A. F., and Courtney, J. F. "Turbulent Boundary Layers on Rough Walls," SDL No. 76-6044, Spectron Development Laboratories, Inc., Costa Mesa, Calif., March 1976.

72. Charwat, A. F., Roos, J. N., Dewey, F. C., Jr., and Hitz, J. A. "An Investigation of Separated Flows. Part I: The Pressure Field," J. Aero. Sci., Vol. 28, No. 6, pp. 457-470, 1961.

73. Rose, W. C. "Turbulence Measurements in a Compressible Boundary Layer," AIAA J., Vol. 12, No. 8, pp. 1060-1064, August, 1974.

74. Demetriades, A. "Turbulence Measurements in an Axisymmetric Compressible Wake," J. Fluid Mech., Vol. 34, part 3, pp. 465-480, 1968.

75. Laderman, A. J., and Demetriades, A. "Advanced Penetration Problem Program. Turbulence Measurements in the Hypersonic Turbulent Boundary Layer Over a Cooled Wall," Philco Ford Publication, No. U-5079, Newport Beach, Calif., 1972.

76. Owen, F. K., Hartman, C. C., and Kussoy, M. I. "Mean and Fluctuating Flow Measurements of a Fully-Developed, Non-Adiabatic Hypersonic Boundary Layer," J. Fluid Mech., Vol. 70, part 2, pp. 393-413, 1975.

77. Berg, Dale E. "Surface Roughness Effects on the Hypersonic Turbulent Boundary Layer." Ph.D. Thesis, California Institute of Technology, 1977.

TABLE I

Summary of Run Conditions and Inverse Parameters

Configuration	x (in.)	M_e	T_t (°R)	u_e (ft/sec)	ρ_e (slug/ft³)	δ^* (in.)	θ (in.)	H	$\dot{H}$
Smooth Plate									
Smooth-to-Rough k = 0.0125 in.									
Smooth-to-Rough k = 0.025 in.									

-60-

TABLE I (Cont'd)

Configuration	x (in.)	M_e	T_t (°R)	u_e (ft/sec)	ρ_e (slug/ft³)	δ^* (in.)	θ (in.)	H	$\dot{H}$
Smooth-to-Rough $x = 0.050$ in.	47.4	6.00	765.	2827.	.0001344	0.565	0.0408	14.7	-2.52
	45.4	6.03	765.	2828.	.0001236	0.547	0.0386	14.2	-2.7
	43.4	6.03	765.	2827.	.0001255	0.522	0.0370	14.1	-2.60
	41.4	6.03	765.	2827.	.0001267	0.499	0.0354	14.1	-2.89
	39.4	6.04	765.	2828.	.0001266	0.479	0.0350	13.7	-3.22
	37.4	6.05	765.	2830.	.0001275	0.460	0.0349	13.4	-3.52
	35.4	6.04	765.	2830.	.0001264	0.473	0.0354	13.4	-3.54
	33.4	6.03	765.	2829.	.0001251	0.452	0.0343	13.2	-3.65
	31.4	6.03	765.	2827.	.0001322	0.438	0.0334	12.9	-3.59
	29.4	6.06	765.	2826.	.0001244	0.402	0.0323	12.4	-4.57
	27.4	6.06	765.	2835.	.0001253	0.390	0.0321	12.5	-4.92
	47.4	6.07	745.	2826.	.0001253	0.395	0.0321	12.1	-4.60
	25.4	6.00	765.	2833.	.0001311	0.411	0.0351	11.7	-5.13
	24.4	5.99	765.	2837.	.0001311	0.361	0.0343	11.4	-5.54
Rough-to-Smooth $x = 0.050$ in.	47.4	6.01	765.	2843.	.0001246	0.555	0.0405	13.3	-3.31
	45.4	6.02	765.	2844.	.0001248	0.528	0.0392	13.4	-3.19
	43.4	6.01	765.	2841.	.0001252	0.514	0.0375	13.3	-3.56
	41.4	6.03	765.	2841.	.0001309	0.494	0.0363	13.2	-3.36
	39.4	6.08	765.	2842.	.0001281	0.478	0.0359	13.2	-3.50
	37.4	6.07	765.	2845.	.0001235	0.474	0.0373	13.4	-3.87
	35.4	5.99	765.	2840.	.0001315	0.497	0.0400	13.1	-3.85
	33.4	6.02	765.	2842.	.0001450	0.516	0.0367	12.0	-3.57
	31.4	6.02	765.	2842.	.0001450	0.507	0.0402	10.8	-4.13
	29.4	6.05	765.	2847.	.0001259	0.460	0.0356	12.2	-4.90
	27.4	6.04	765.	2847.	.0001259	0.477	0.0336	12.0	-5.19
	27.4	6.00	765.	2842.	.0001307	0.448	0.0391	12.1	-5.01
	26.4	6.02	765.	2838.	.0001354	0.404	0.0379	12.1	-4.52
	24.4	5.96	765.	2836.	.0001346	0.467	0.0375	12.2	-4.77
								12.5	-4.3

TABLE II

Results of Velocity Profile Correlation

Conf.	x	y_o	$\bar{\pi}$	δ	u_τ	$\tau_w \times 100$	$\frac{\Delta u}{u_\tau}$	$\tau_w \times 100$ (meas'd[*])
Smooth	47.4	0.0	1.46	1.02	134	.25	0.0	.25
	45.4		1.36	0.98	138	.25		
	43.4		1.34	0.94	139	.25		
	41.4		1.29	0.91	141	.25		
	39.4		1.25	0.91	143	.26		
	37.4		1.28	0.92	142	.26		
	35.4		1.45	0.93	136	.25		
	33.4		1.42	0.90	137	.27		
	31.4		1.39	0.87	139	.27		
	29.4		1.26	0.83	144	.27		
	27.4		1.12	0.83	149	.28		
	25.4		1.12	0.86	147	.29		
S → R k=0.0125	47.4	0.0063	1.34	1.01	148	.31	2.69	
	45.4		1.30	0.93	150	.30	2.40	
	43.4		1.24	0.91	151	.30	2.15	
	41.4		1.30	0.90	148	.28	1.77	
	39.4		1.23	0.90	151	.30	1.96	
	37.4		1.23	0.87	149	.28	1.50	
	35.4	0.0050	1.40	0.88	140	.26	0.51	
	33.4	0.0038	1.35	0.86	143	.27	0.82	
	31.4	0.0038	1.35	0.84	145	.29	1.35	
	29.4	0.0025	1.30	0.79	142	.26	0.07	
	28.4	0.0012	1.30	0.80	142	.26	-0.15	
	27.4	0.0	1.30	0.80	138	.25	-0.80	
	26.4		1.29	0.81	110	.26	-0.27	
	25.4		1.27	0.83	141	.28	-0.07	
	24.4		1.14	0.83	146	.30	0.29	
S → R k=0.025	47.4	0.0125	1.34	1.01	155	.34	3.76	.34
	45.4		1.30	0.94	157	.35	3.73	
	43.4		1.24	0.90	160	.35	3.67	
	41.4		1.30	0.84	160	.35	3.77	
	39.4		1.23	0.85	163	.35	3.75	
	37.4		1.23	0.84	163	.35	3.74	
	35.4	0.010	1.40	0.84	153	.32	3.07	
	33.4	0.005	1.35	0.82	155	.34	3.21	
	31.4	0.0025	1.35	0.79	153	.33	2.66	
	29.4	0.0025	1.30	0.75	153	.31	2.01	
	28.4	0.0025	1.30	0.74	150	.30	1.44	
	27.4	0.0	1.30	0.74	145	.27	0.44	.28
	26.4		1.29	0.76	146	.29	0.85	
	25.4		1.27	0.76	142	.28	0.06	
	24.4		1.14	0.75	145	.29	-0.12	

TABLE II (continued)

Conf.	x	y_o	$\overline{\pi}$	δ	u_τ	$\tau_w \times 100$	$\dfrac{\Delta u}{u_\tau}$	$\tau_w \times 100$ (meas'd*)
S → R	47.4	0.025	1.23	1.08	176	.43	6.55	
k=0.050	45.4		1.18	1.01	178	.42	6.25	.43
	43.4		1.15	0.98	180	.43	6.22	
	41.4		1.10	0.93	188	.47	6.78	
	39.4		1.10	0.90	186	.45	6.36	
	37.4		1.10	0.89	183	.43	5.87	
	35.4		1.25	0.89	174	.40	5.45	
	33.4		1.35	0.84	168	.38	5.06	
	31.4	0.010	1.35	0.84	155	.33	3.16	
	29.4	0.0	1.30	0.79	150	.29	1.46	
	28.4		1.30	0.77	146	.26	0.52	
	27.4		1.30	0.79	140	.25	-0.48	.34
	26.4		1.29	0.81	139	.24	-0.79	
	25.4		1.28	0.84	141	.27	-0.01	
	24.4		1.20	0.82	143	.28	0.15	
R → S	47.4	0.0	1.50	1.07	132	.23	-0.06	
k=0.050	45.4		1.45	1.03	134	.24	-0.07	
	43.4		1.45	0.99	139	.26	1.02	
	41.4		1.43	0.96	141	.27	1.15	
	39.4		1.40	0.93	143	.27	1.22	
	37.4	0.005	1.45	0.93	142	.25	0.96	
	35.4	0.005	1.60	0.95	136	.25	0.67	
	33.4	0.010	1.55	1.00	143	.28	2.25	
	31.4	0.015	1.50	0.99	152	.31	3.37	
	29.4	0.015	1.40	0.95	158	.33	3.73	
	28.4	0.005	1.35	0.93	162	.34	3.94	
	27.4	0.015	1.30	0.92	167	.37	4.52	
	26.4	0.005	1.28	0.91	171	.40	5.14	
	25.4	0.020	1.25	0.91	177	.42	5.73	
	24.4	0.020	1.20	0.89	181	.46	6.19	

*Measurements were made only where these values are indicated.
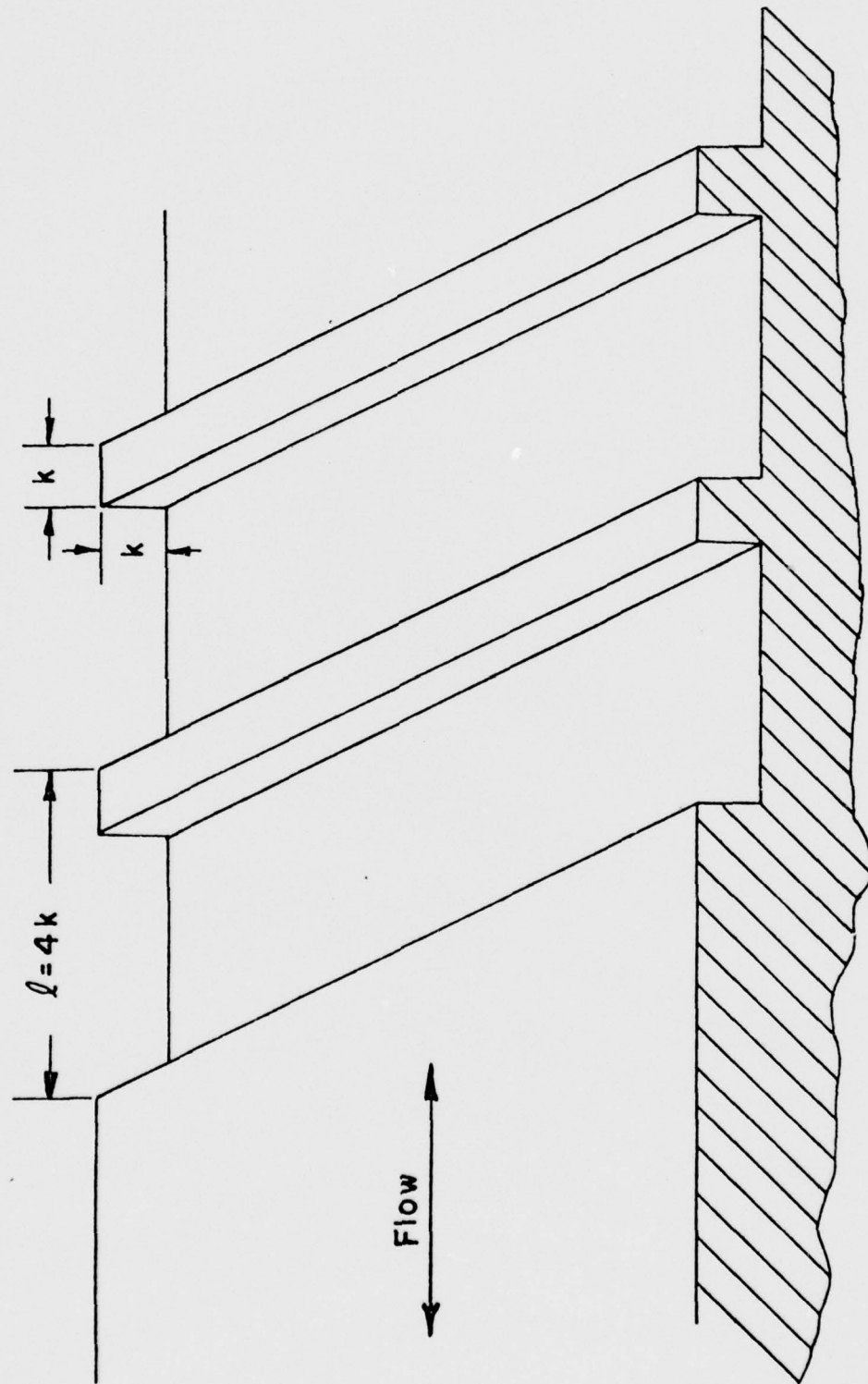
FIG. I SURFACE ROUGHNESS CONFIGURATION
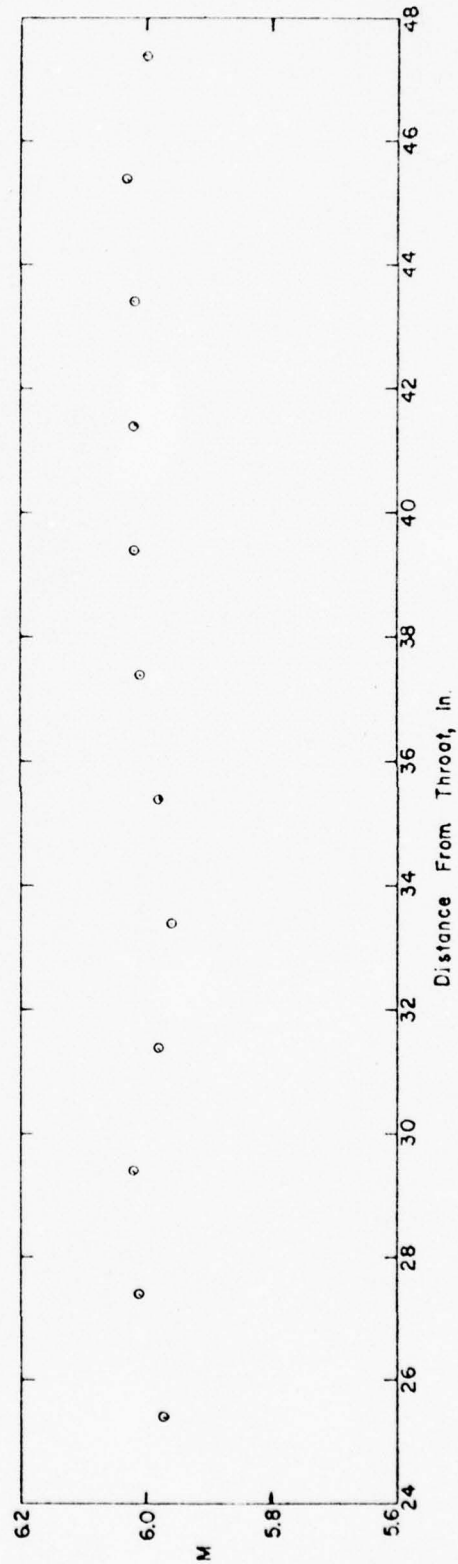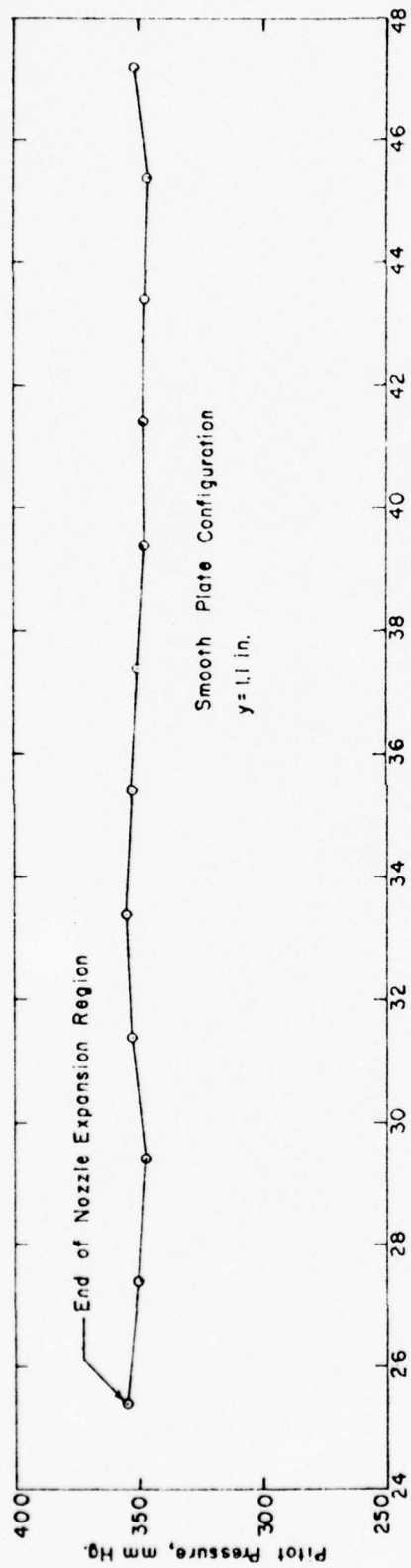
FIG. 2 AXIAL DISTRIBUTION OF FREESTREAM MACH NUMBER AND PITOT PRESSURE
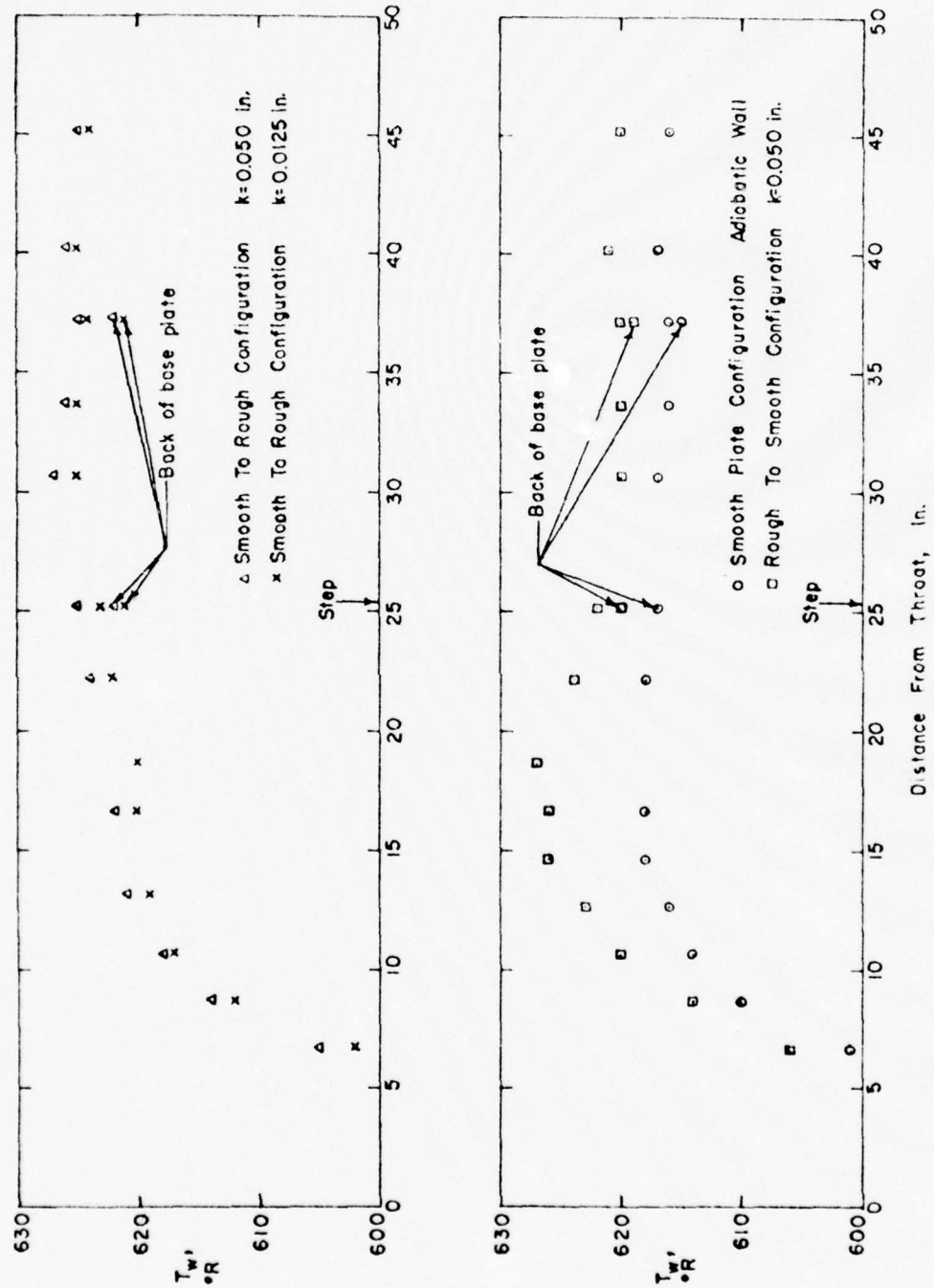
FIG. 3 AXIAL DISTRIBUTION OF WALL TEMPERATURE
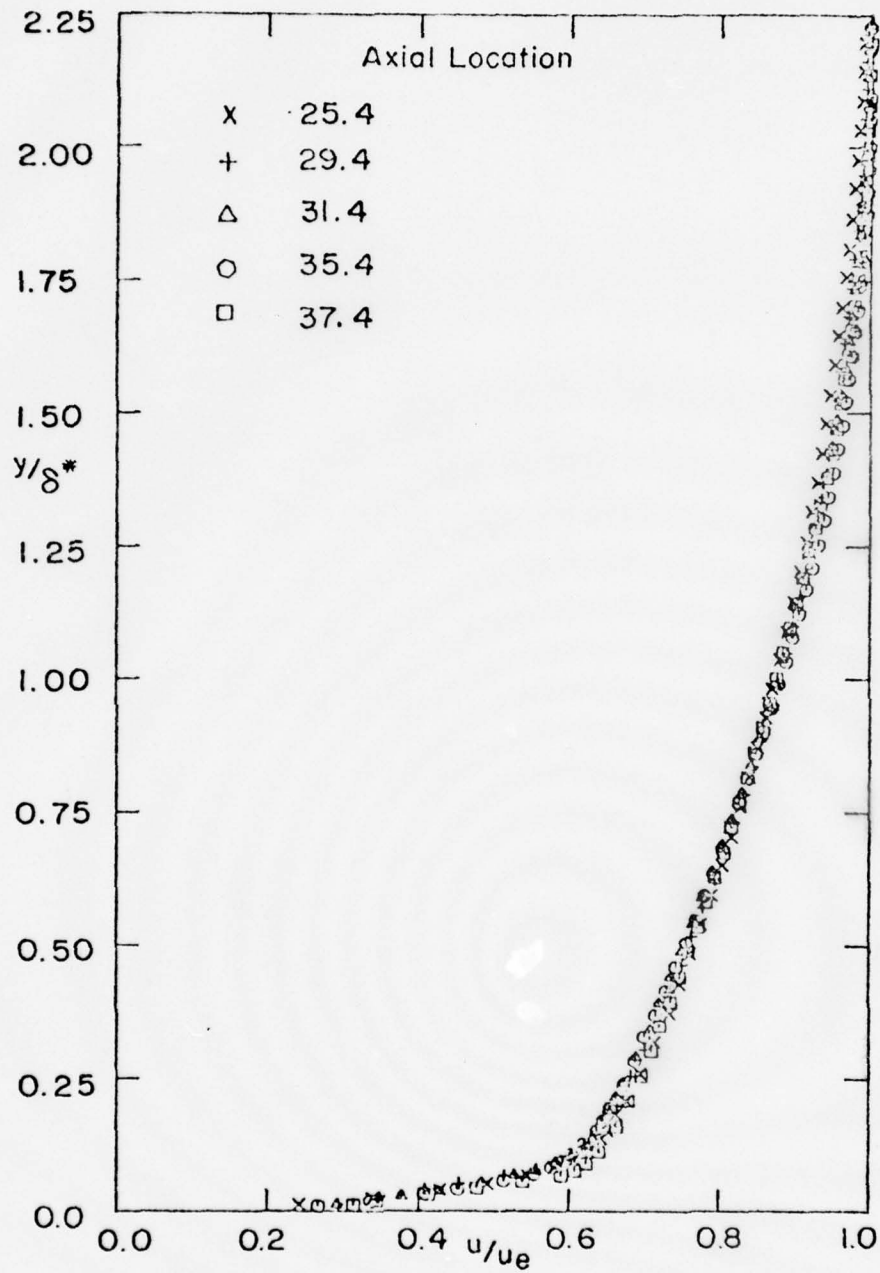
FIG 4 SMOOTH PLATE VELOCITY PROFILES
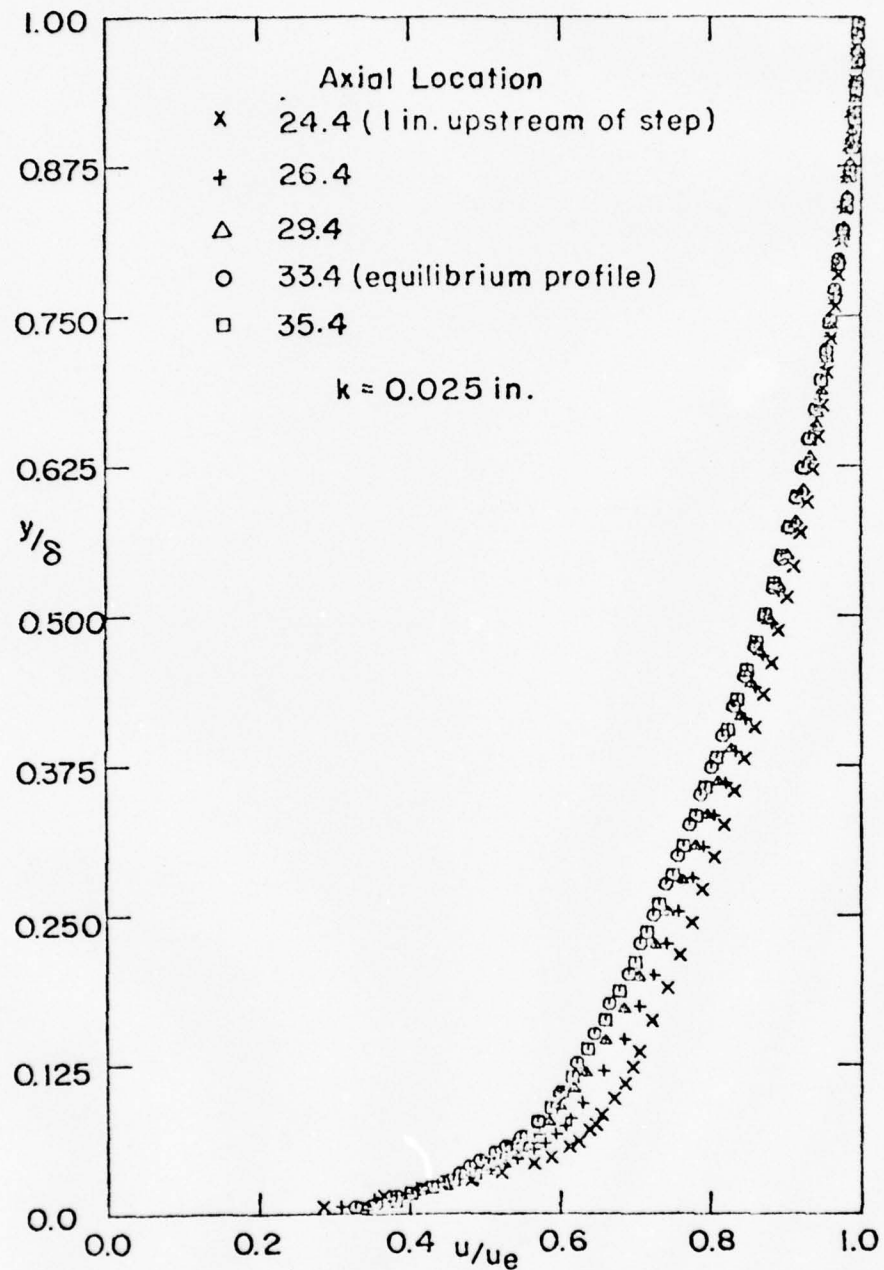
FIG.5 RESPONSE OF SMOOTH WALL BOUNDARY LAYER TO
ROUGH WALL CONDITIONS (a) VELOCITY PROFILES
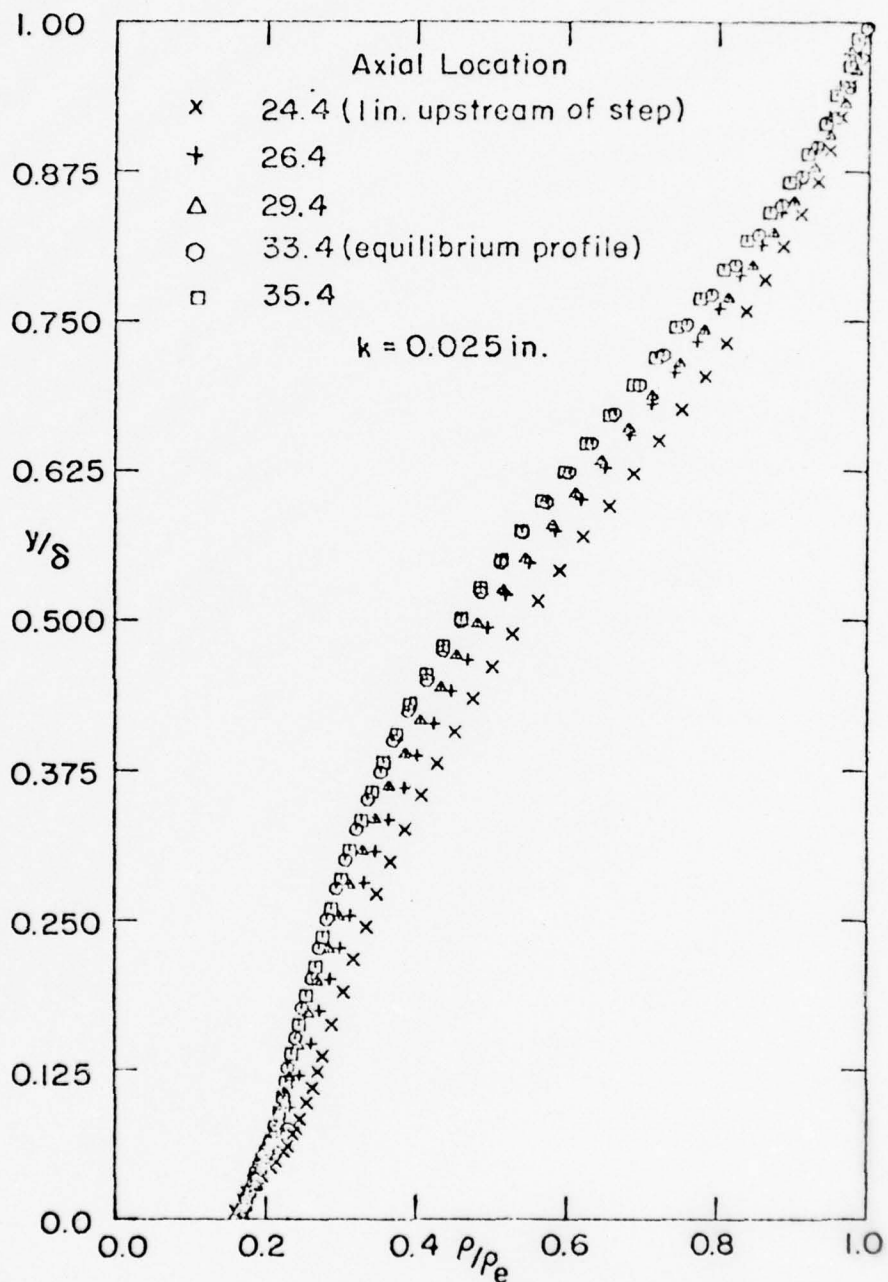
FIG. 5 RESPONSE OF SMOOTH WALL BOUNDARY LAYER
TO ROUGH WALL CONDITIONS (b) DENSITY PROFILES
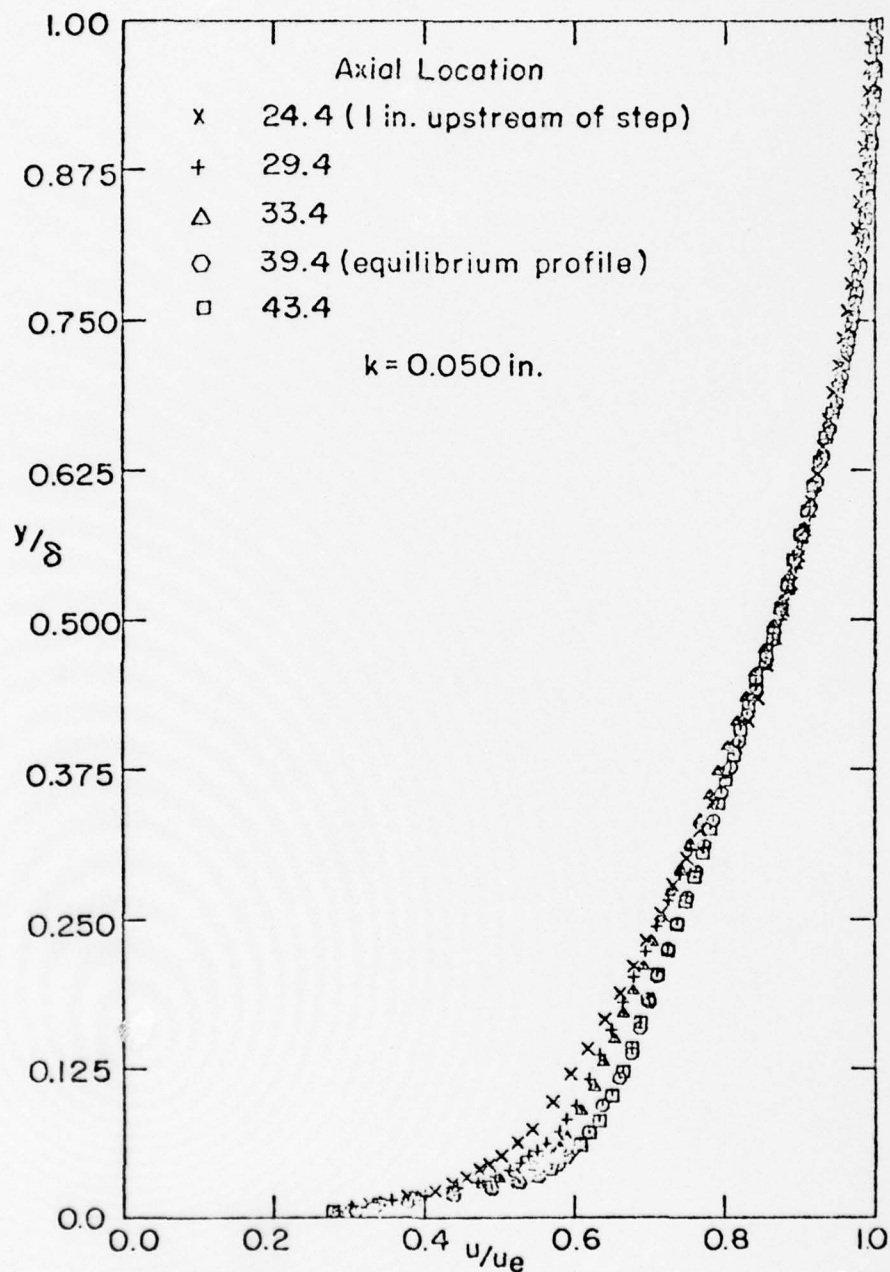
FIG. 6 RESPONSE OF ROUGH WALL BOUNDARY LAYER
TO SMOOTH WALL CONDITIONS (a) VELOCITY PROFILES
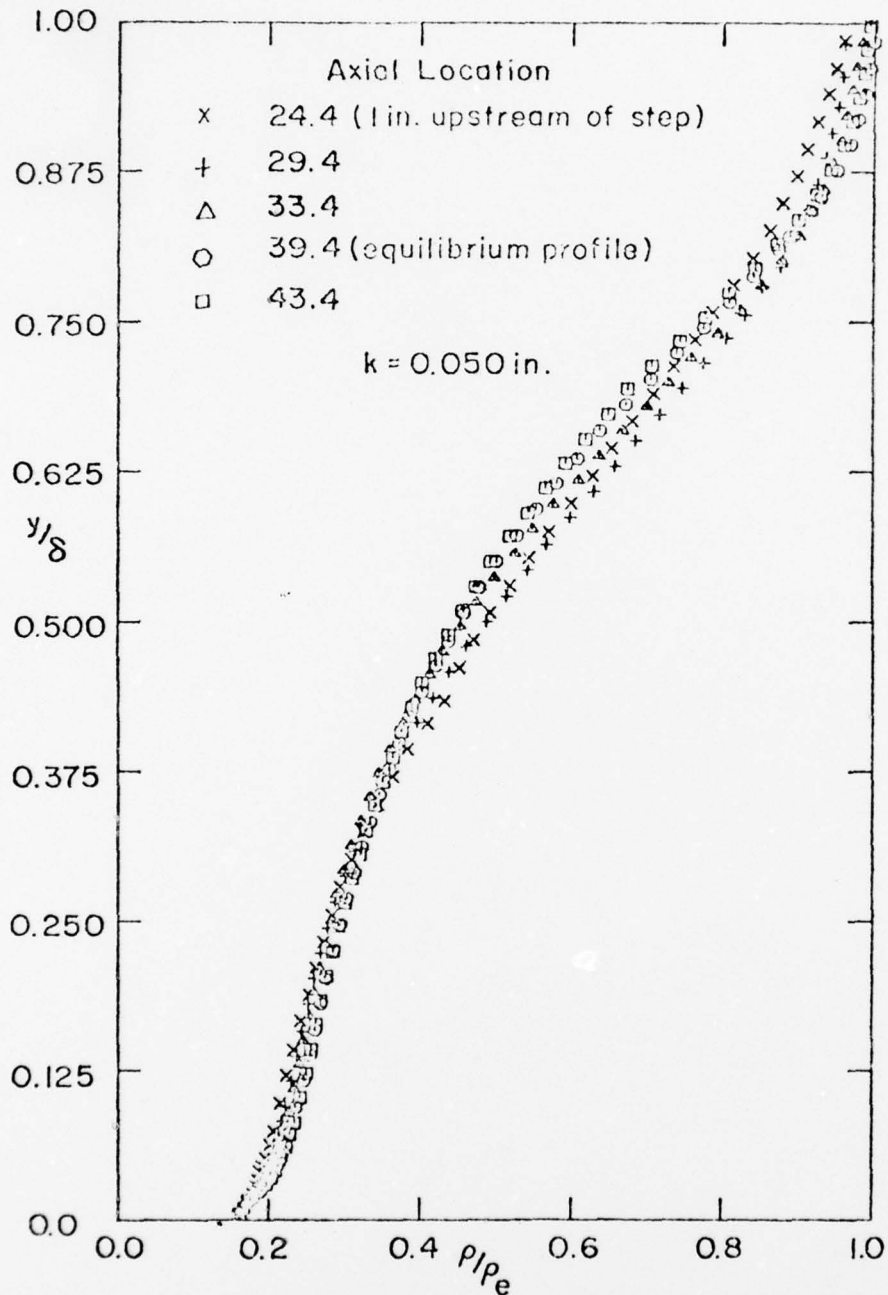
FIG. 6 RESPONSE OF ROUGH WALL BOUNDARY LAYER TO SMOOTH WALL CONDITIONS (b) DENSITY PROFILES
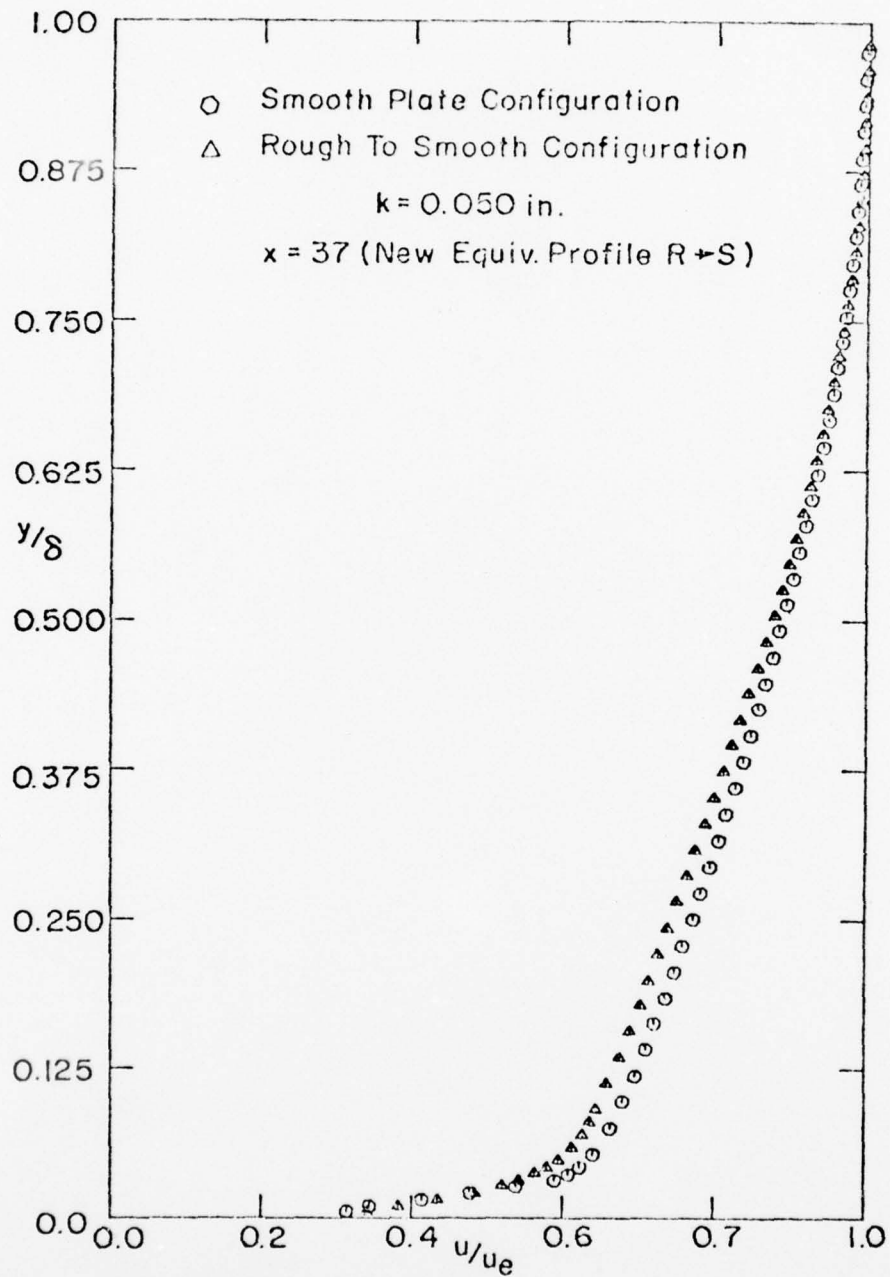
FIG. 7 EQUILIBRIUM SMOOTH WALL PROFILE DATA
(a) VELOCITY PROFILES
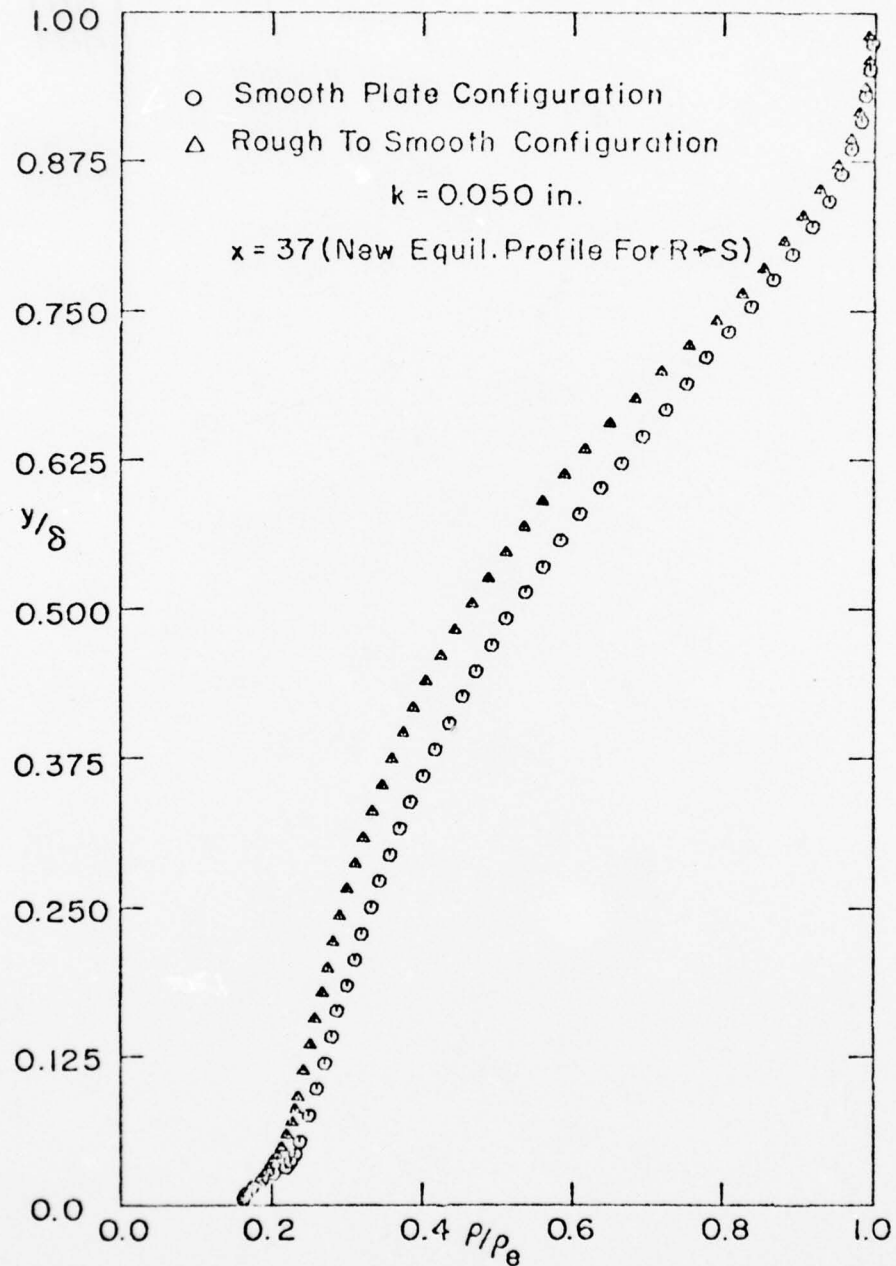
FIG. 7 EQUILIBRIUM SMOOTH WALL PROFILE DATA
(b) DENSITY PROFILES
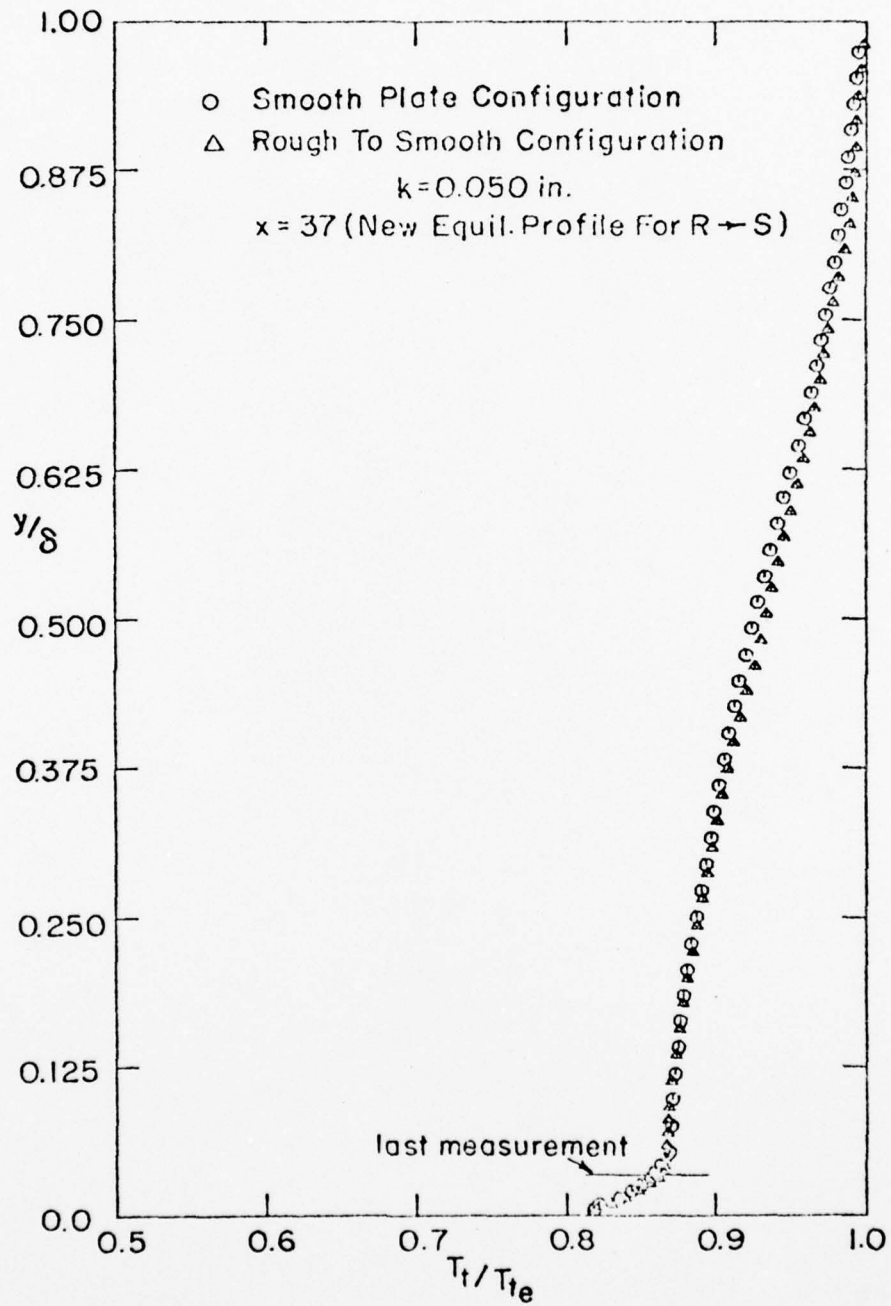
FIG. 7 EQUILIBRIUM SMOOTH WALL PROFILE DATA
(c) TOTAL TEMPERATURE PROFILES

-74-
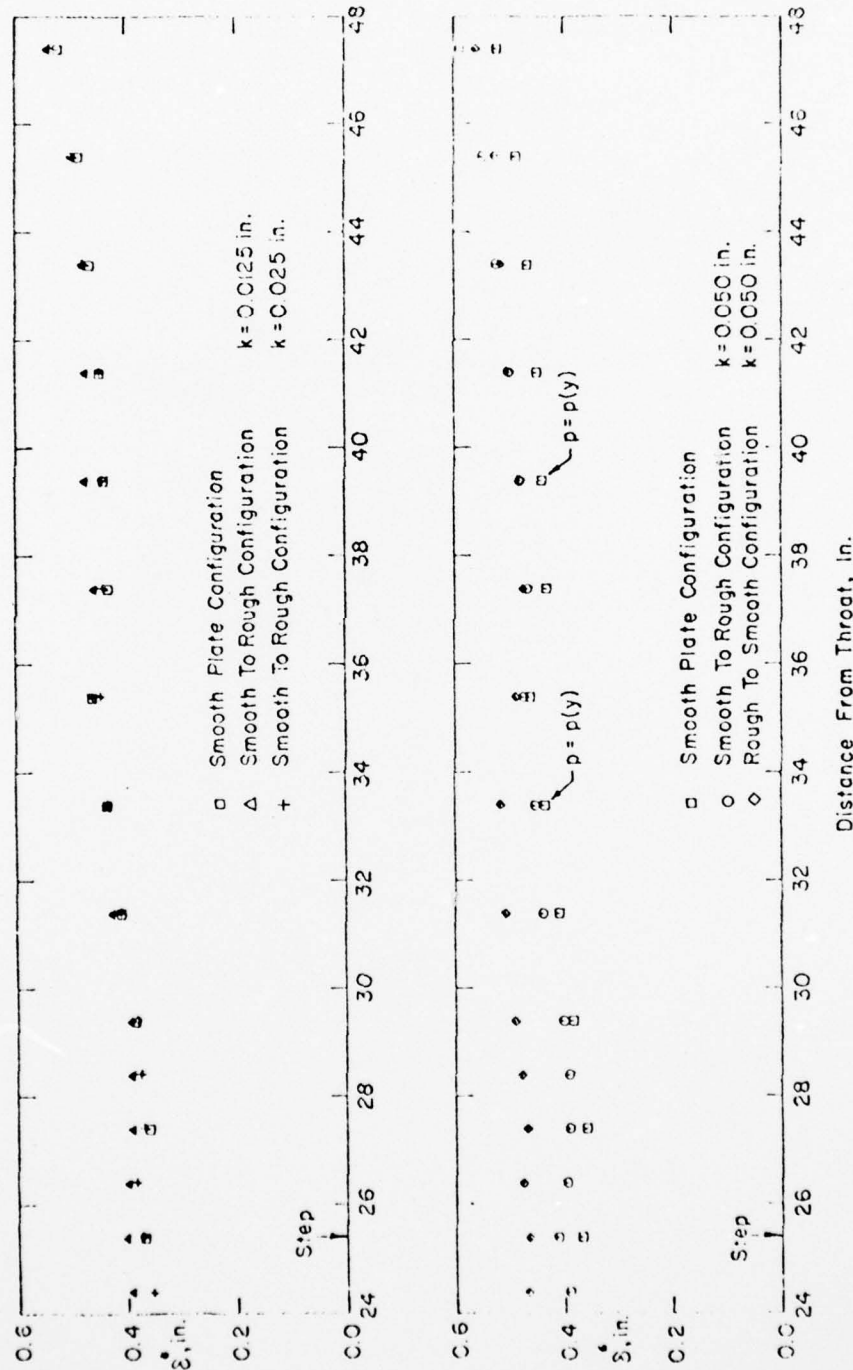
FIG. 8 AXIAL DISTRIBUTION OF DISPLACEMENT THICKNESS

-75-
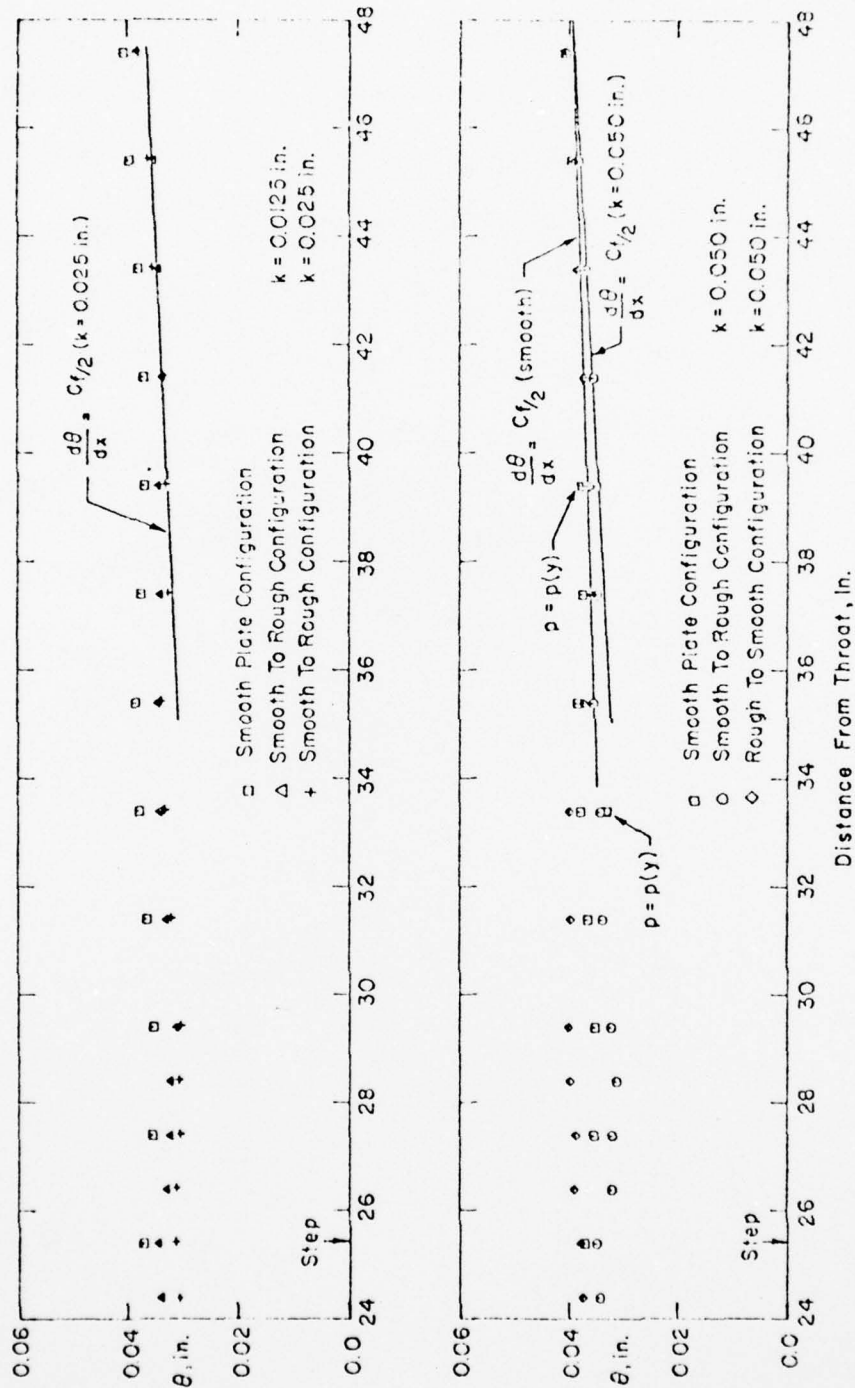
FIG 9   AXIAL DISTRIBUTION OF MOMENTUM THICKNESS
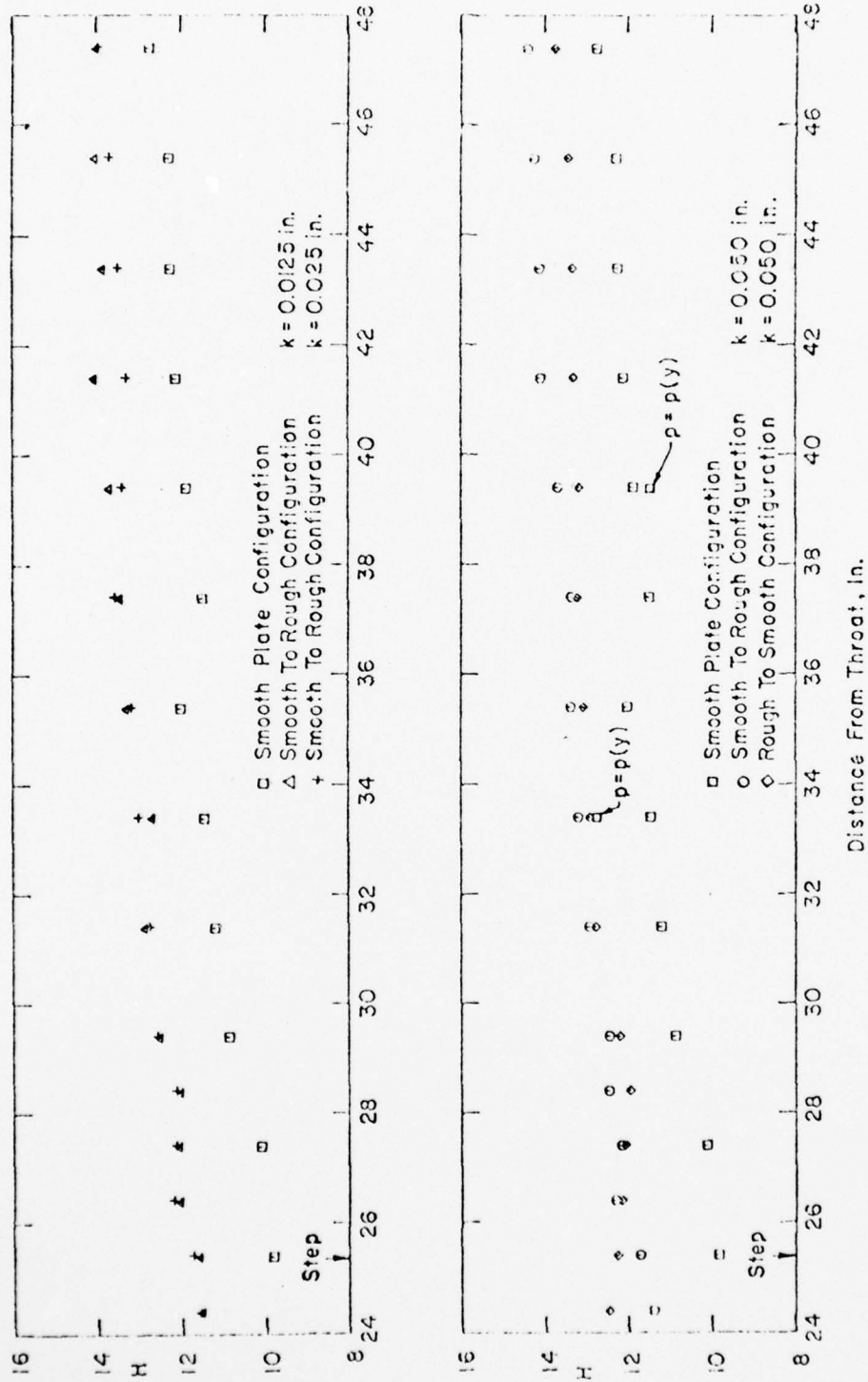
FIG. 10 AXIAL DISTRIBUTION OF SHAPE FACTOR
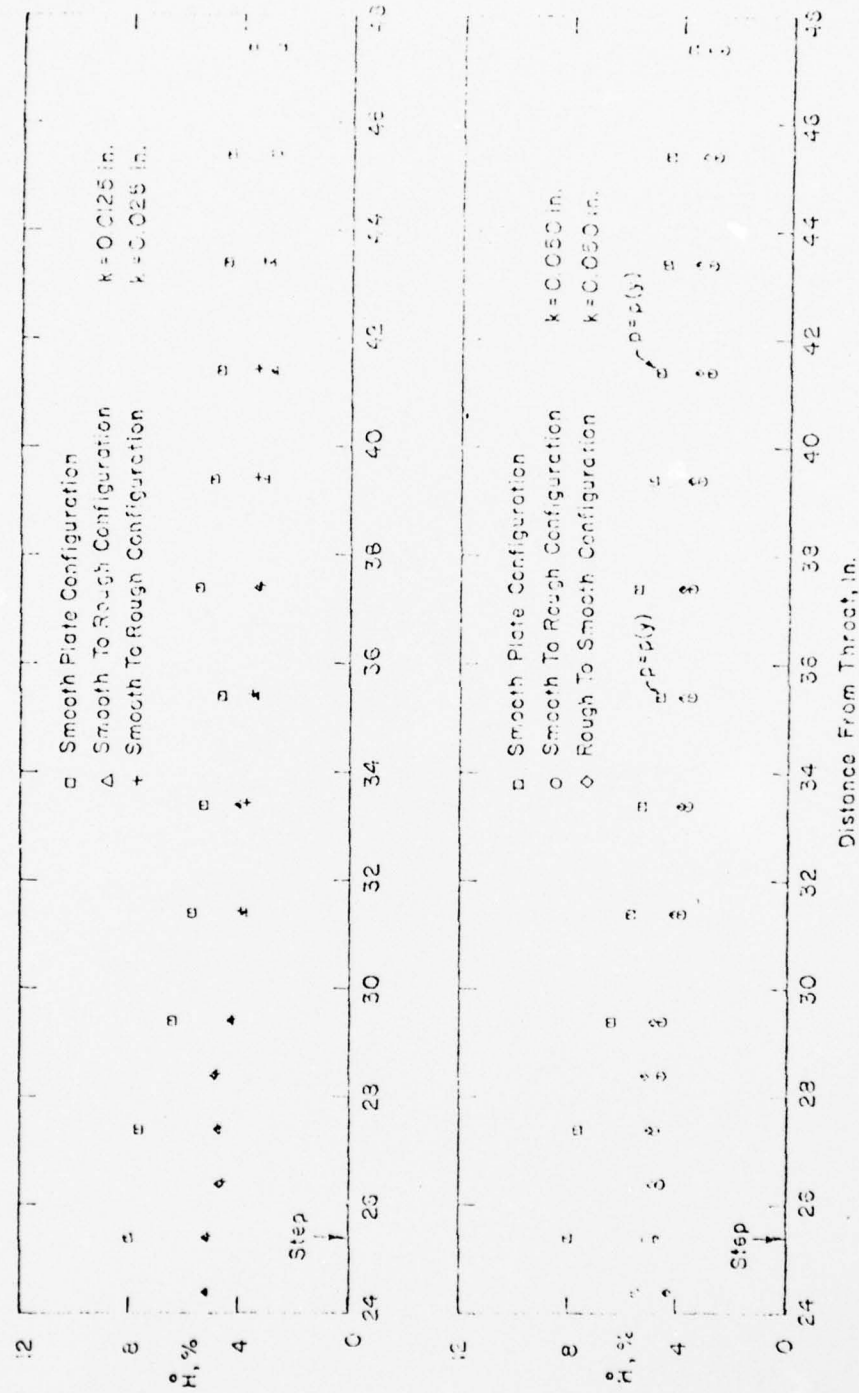
FIG. 11 AXIAL DISTRIBUTION OF ENTHALPHY FLUX
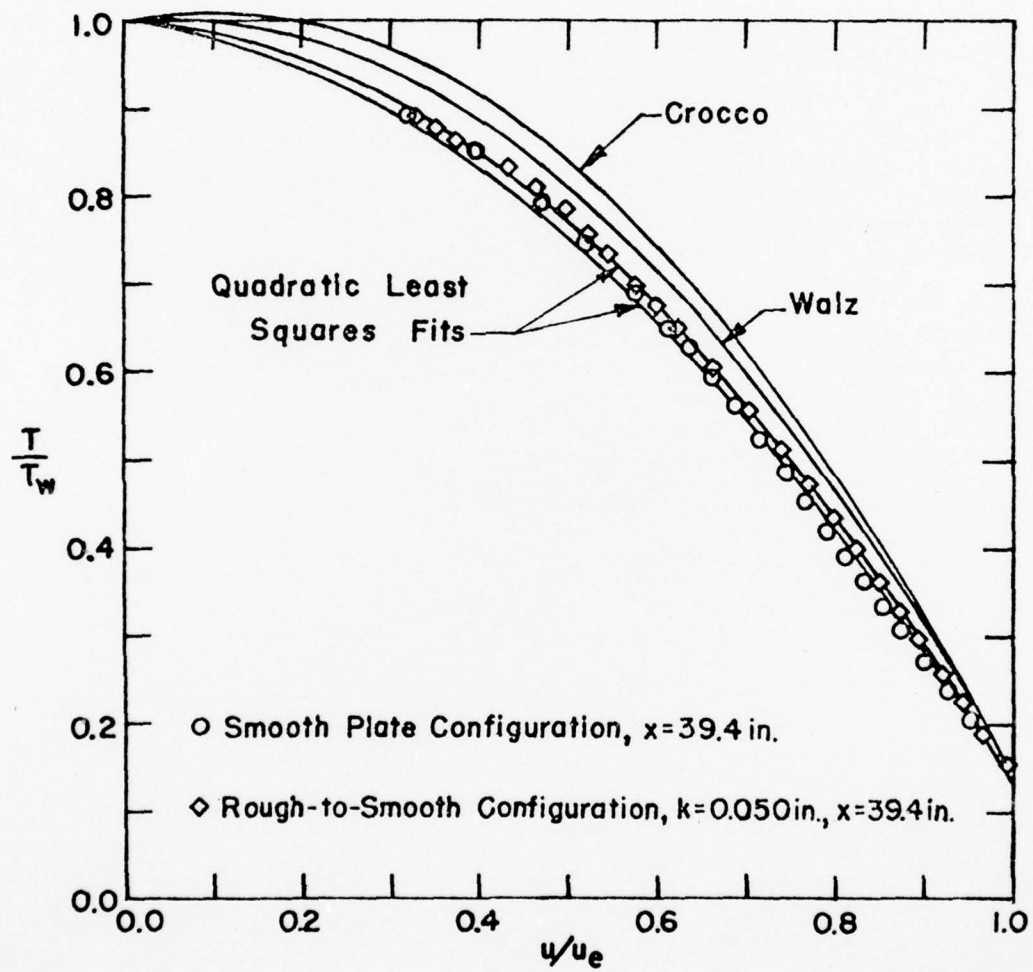
FIG. 12 TEMPERATURE-VELOCITY RELATIONSHIP
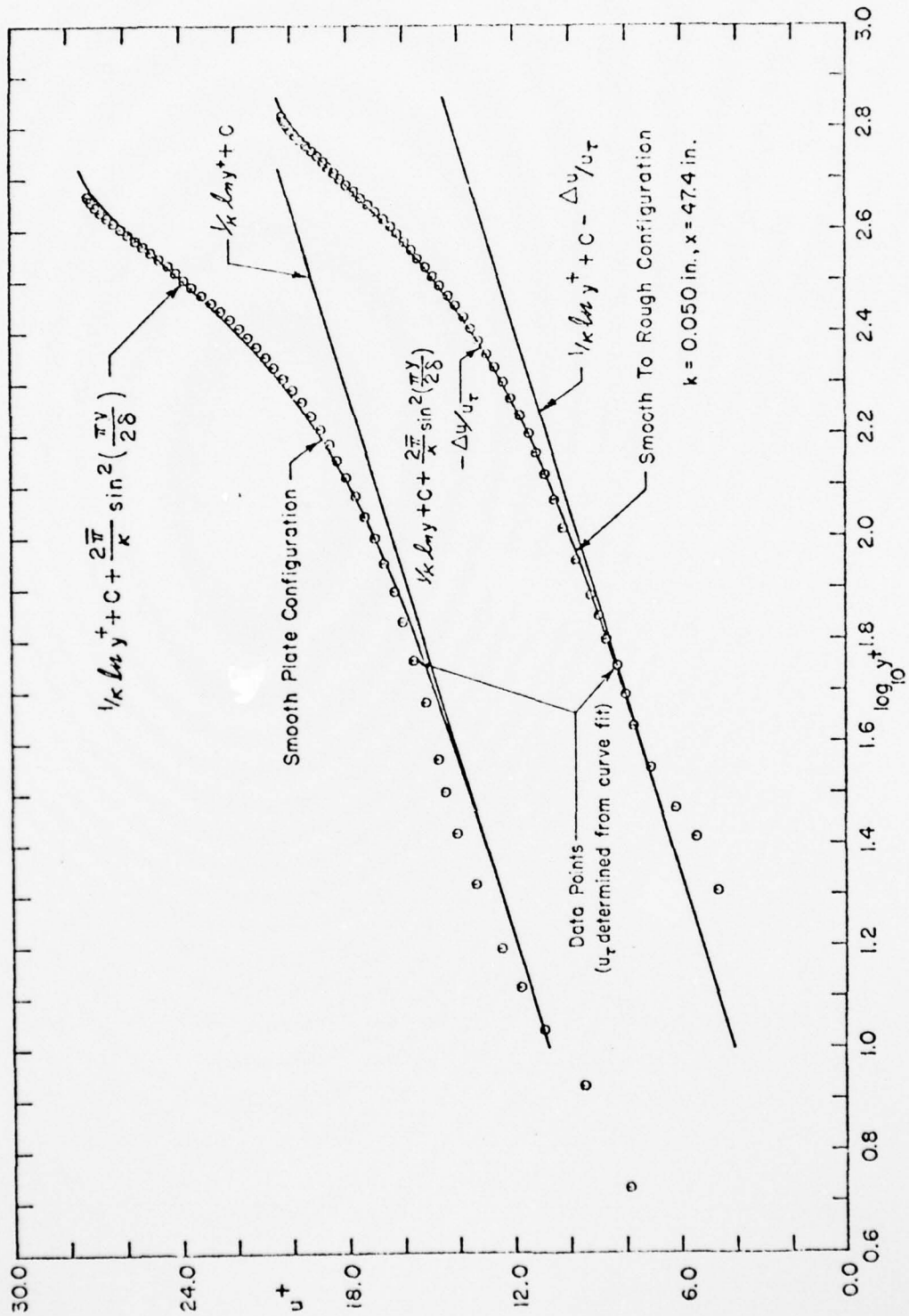
FIG. 13 FIT OF TRANSFORMED VELOCITY DATA TO THE LAW OF THE WALL
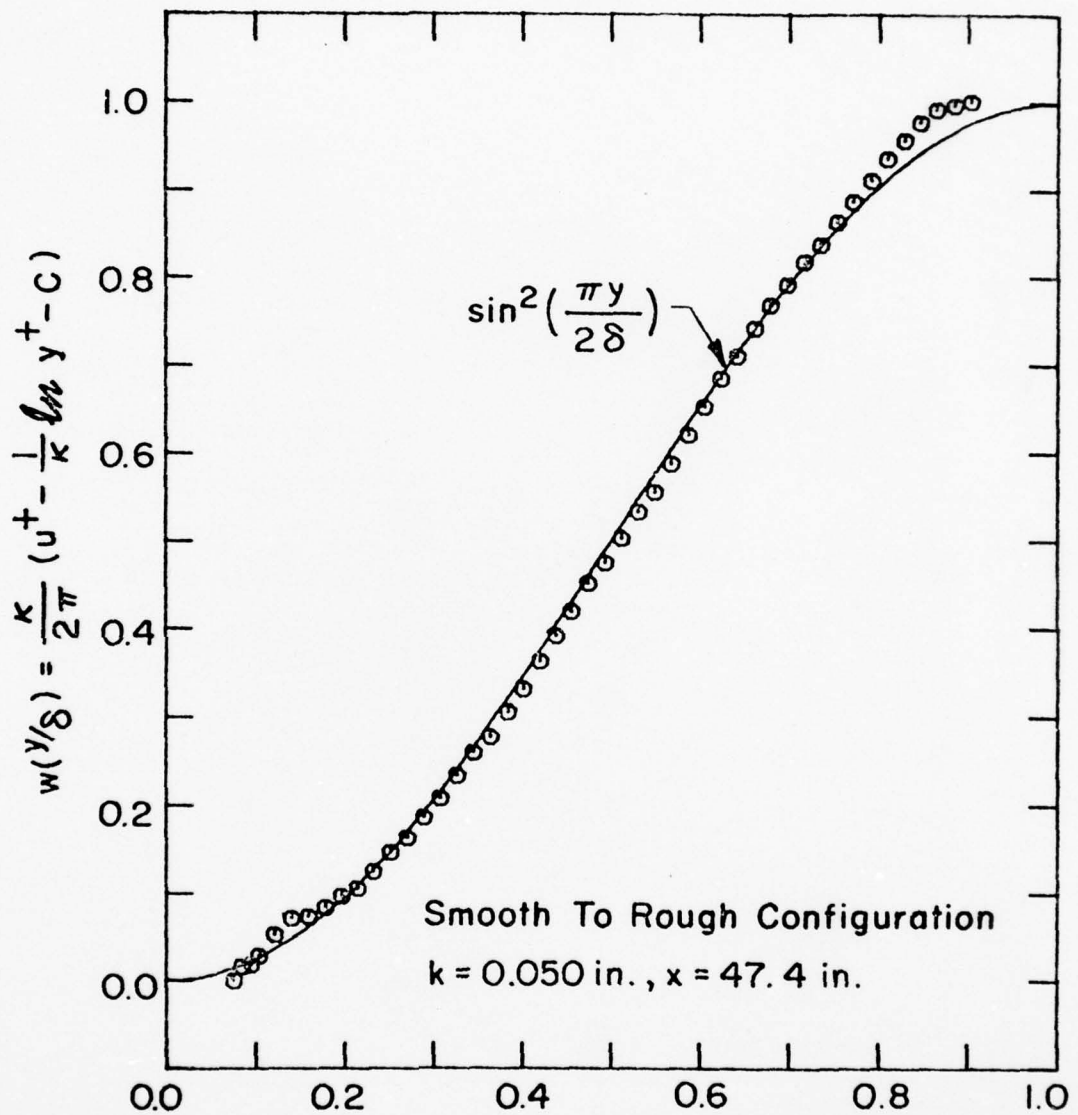
FIG. 14 FIT OF COLES' WAKE FUNCTION TO THE TRANSFORMED VELOCITY WAKE DATA

Distance From Throat, In.
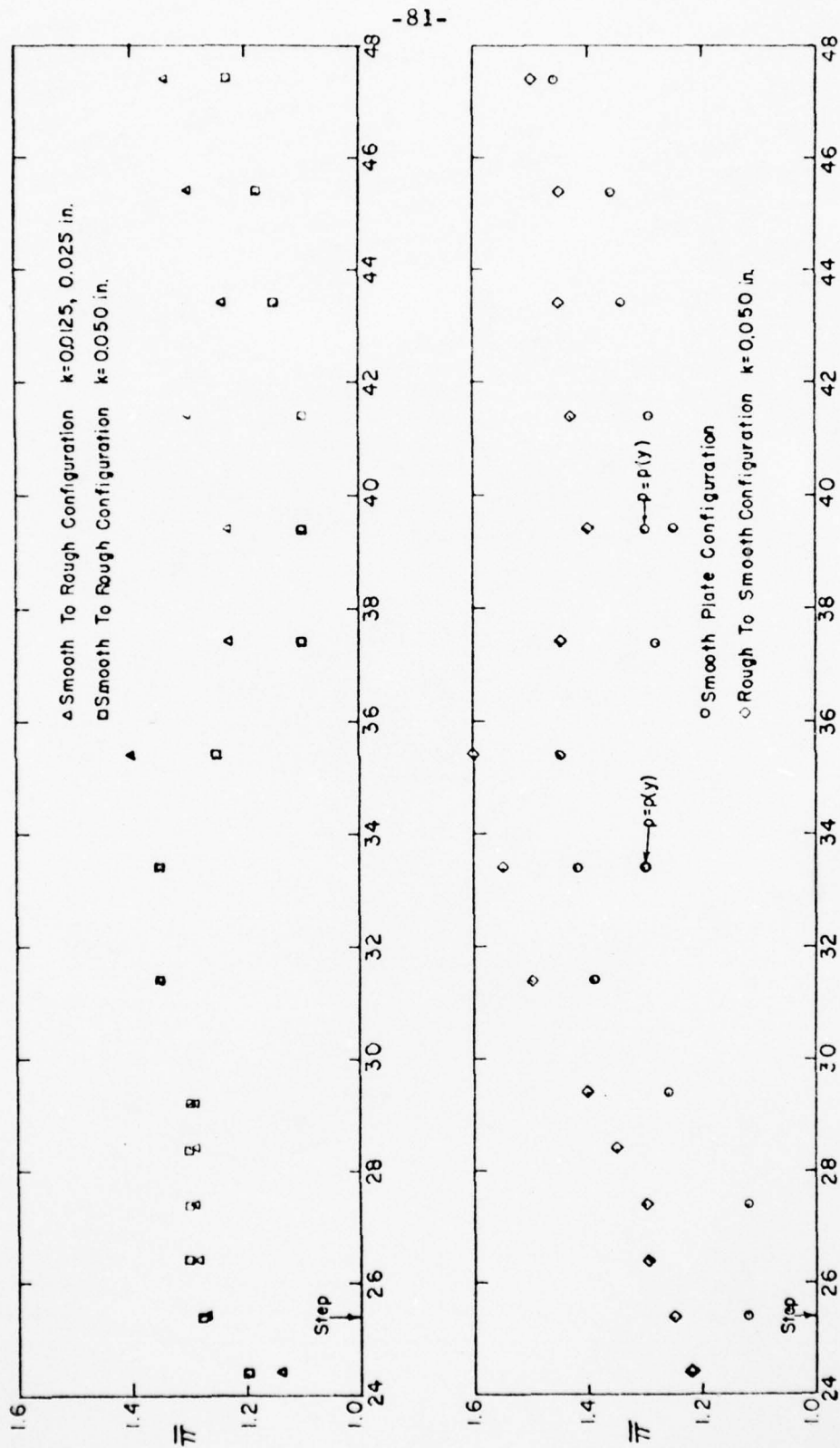
FIG. 15 AXIAL DISTRIBUTION OF WAKE STRENGTH PARAMETER
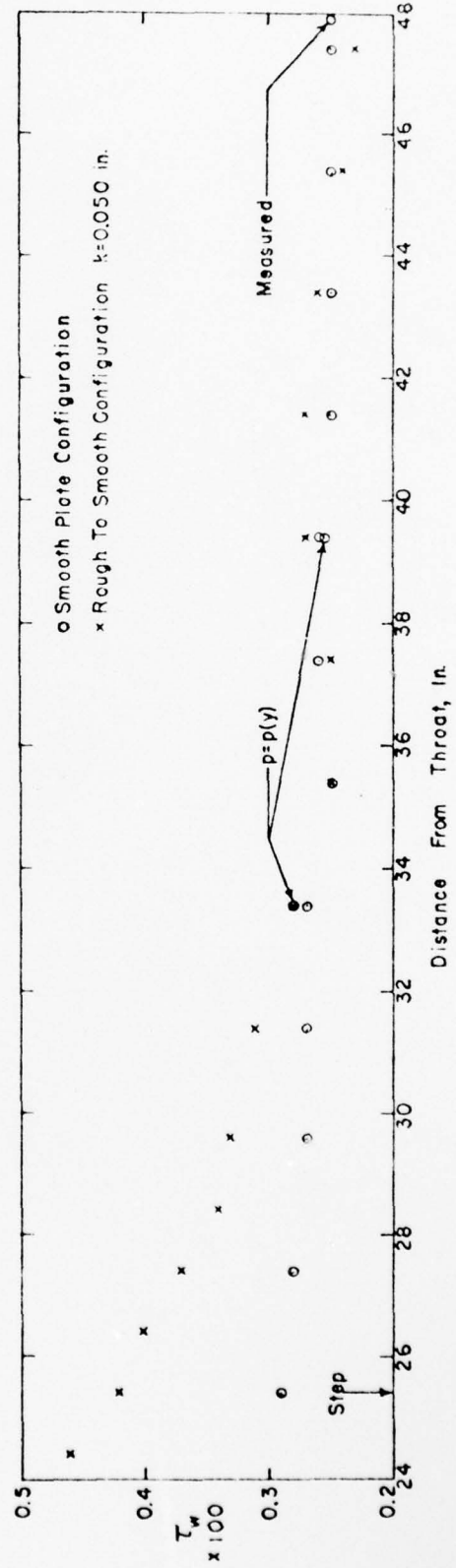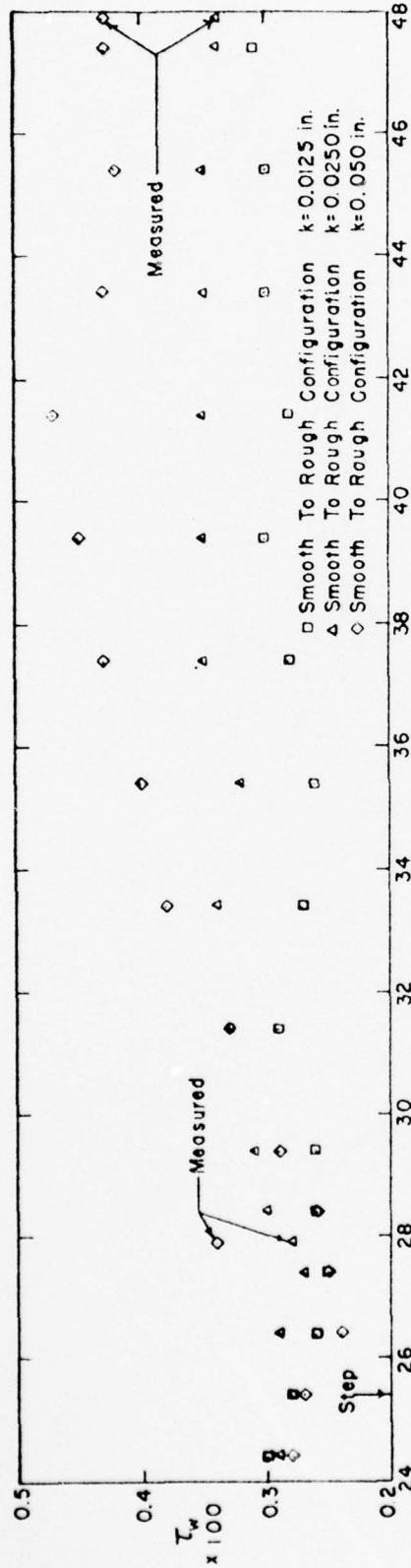
FIG.16 AXIAL DISTRIBUTION OF SKIN FRICTION
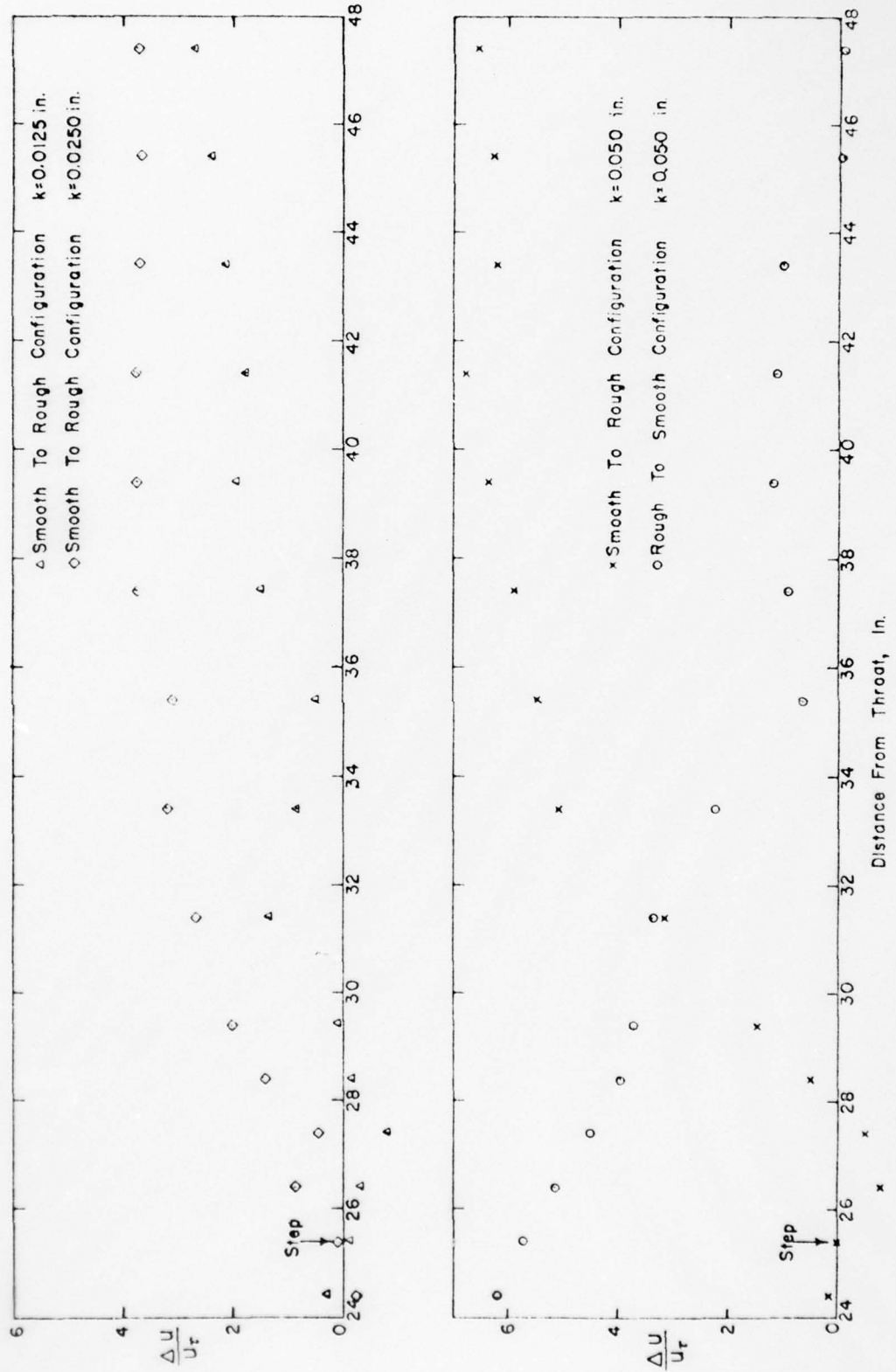
FIG.17 AXIAL DEVELOPMENT OF ROUGH WALL VELOCITY DEFECT
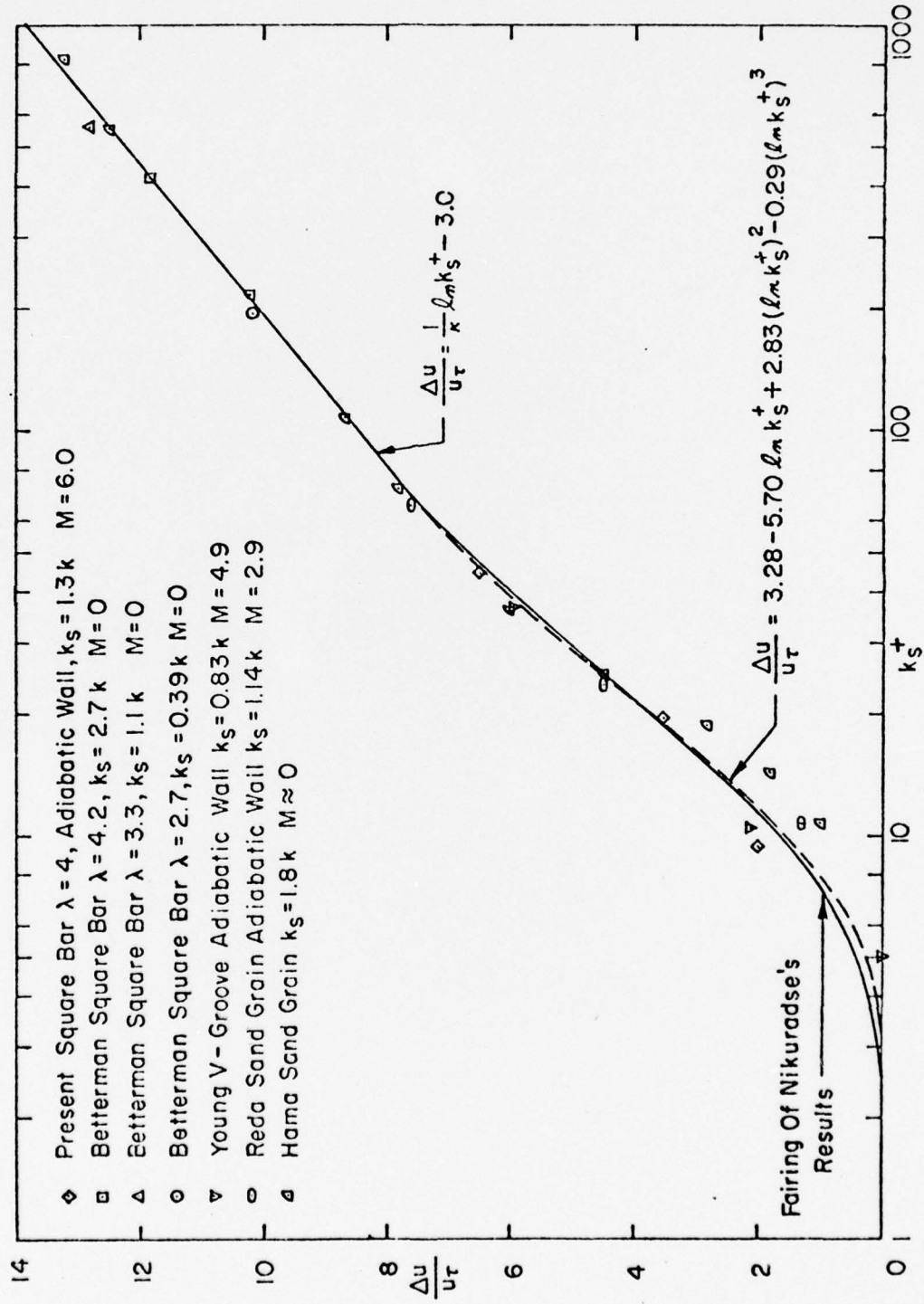
FIG. 18 ROUGH WALL VELOCITY DEFECT CORRELATION

◇ Present Sq. Bar λ = 4 Adiabatic Wall $k_s = 1.3 k$ M = 6.0
▽ Young V-Groove Adiabatic Wall $k_s = 0.83 k$ M = 4.9
θ Reda-Sand Grain Adiabatic Wall $k_s = 1.14 k$ M = 2.9

$$C_f / C_{f_0} = 0.39 (\ln k_s^+ - 2.3) + 1.0$$

Results Of Goddard [19]
0.7 < M < 4.6
Sand Grain Roughness
$k_s = k$
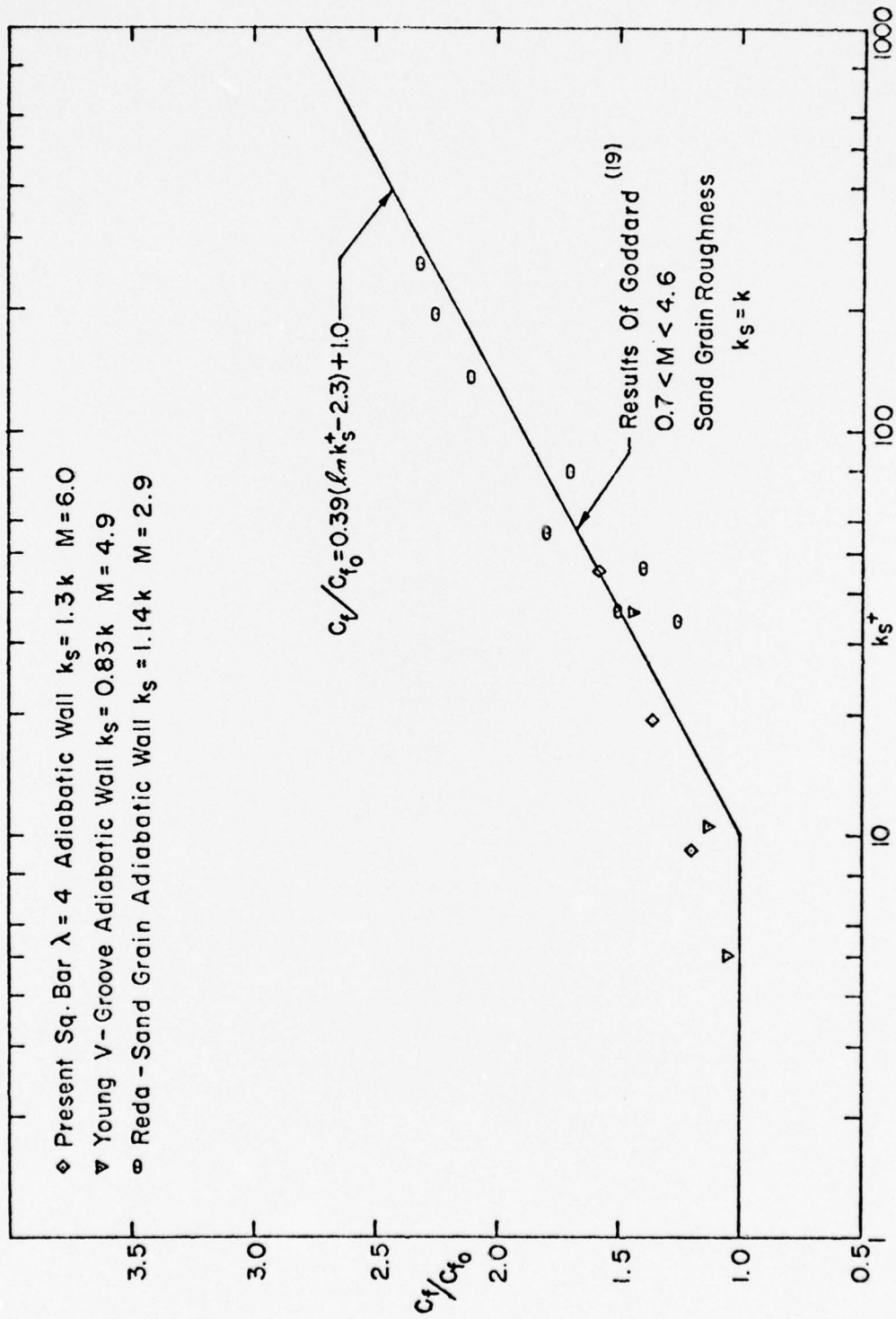
FIG. 19 ROUGH WALL SKIN FRICTION CORRELATION
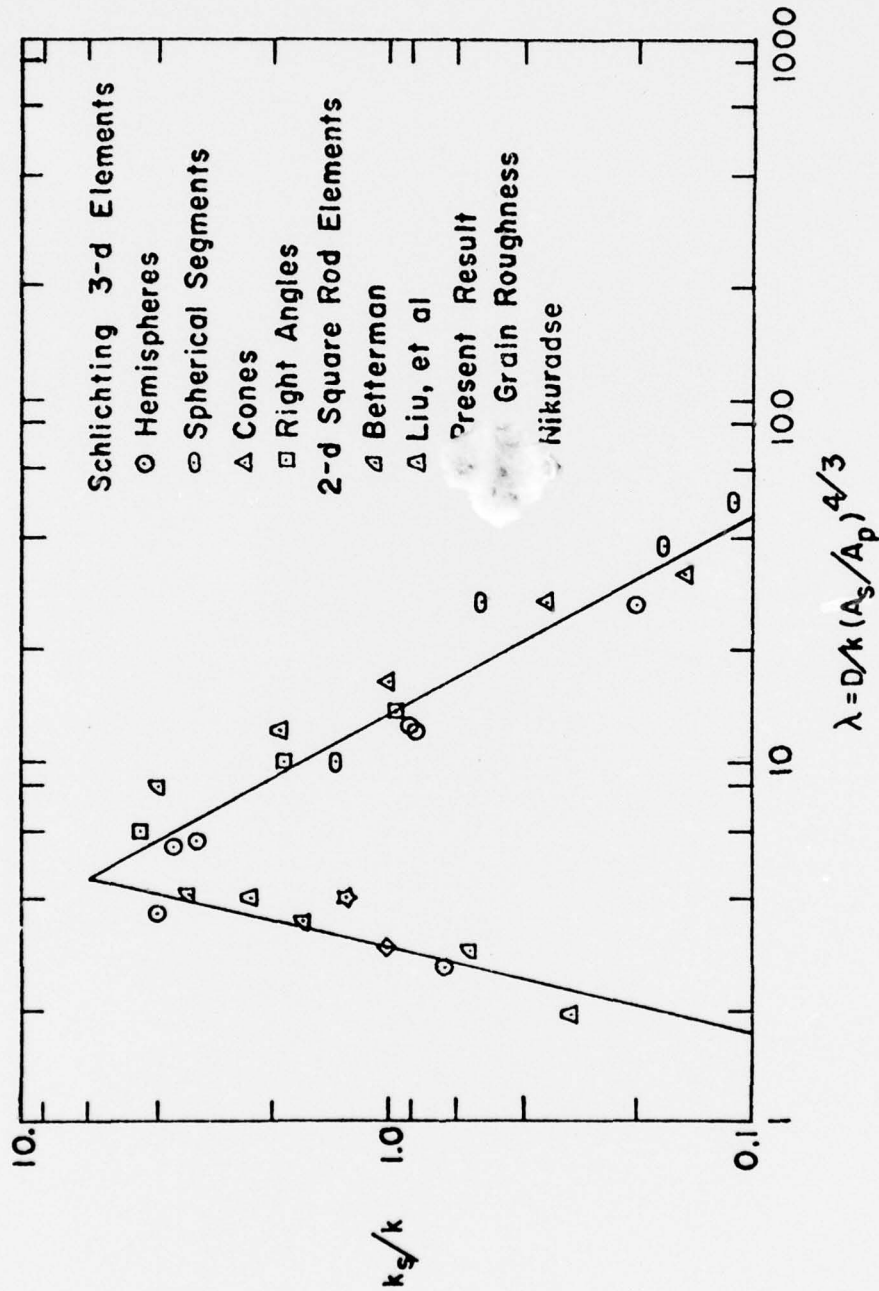
FIG. 20 COMPARISON OF PRESENT RESULTS WITH LOW SPEED
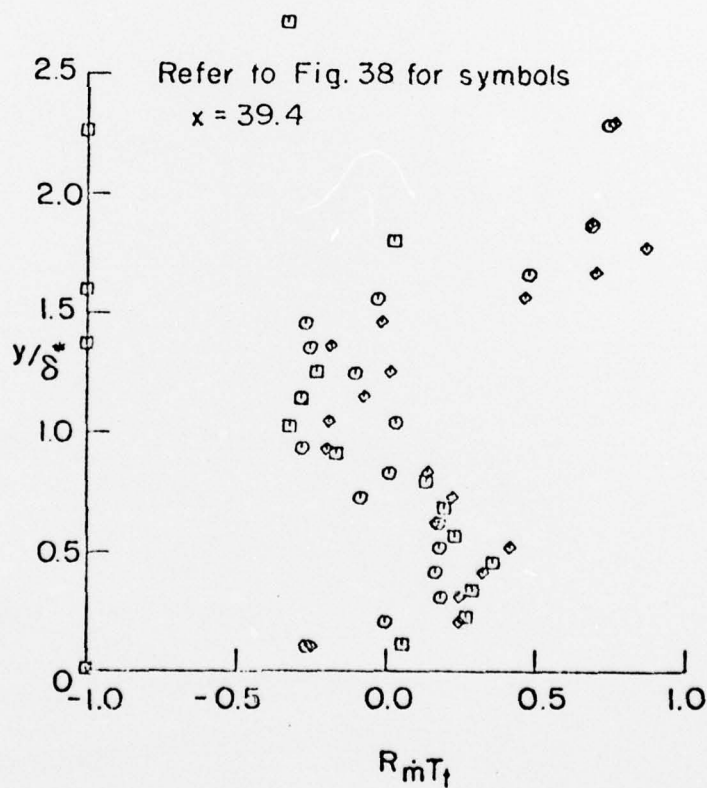EFFECTIVE ROUGHNESS CORRELATION (From Dirling)
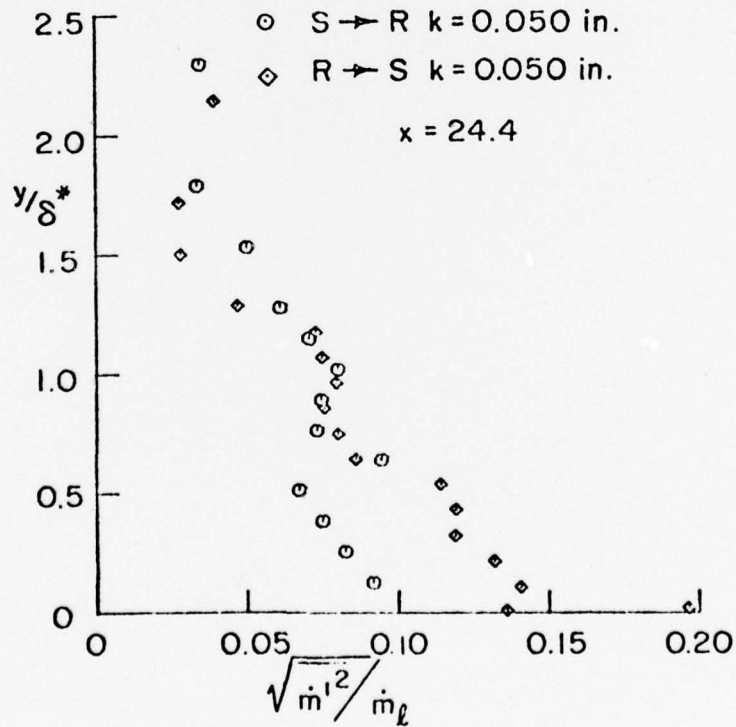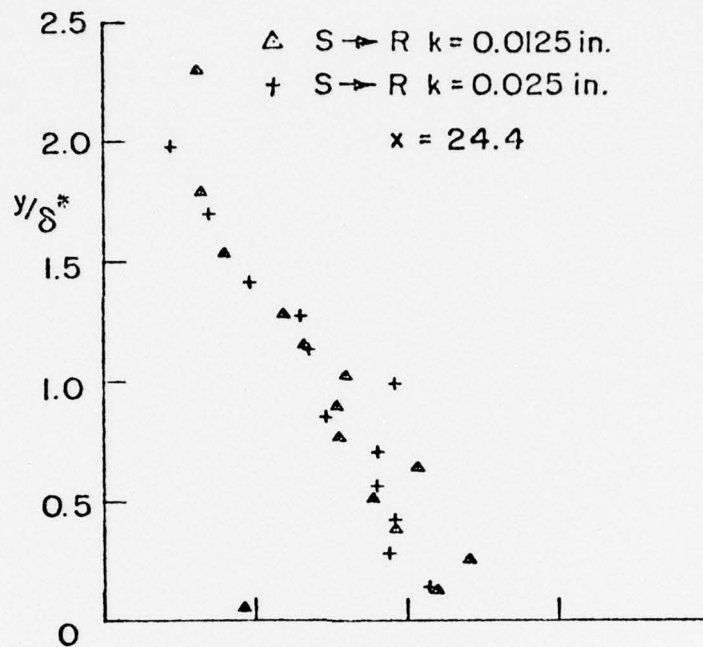
FIG. 21 MASS FLUX FLUCTUATIONS
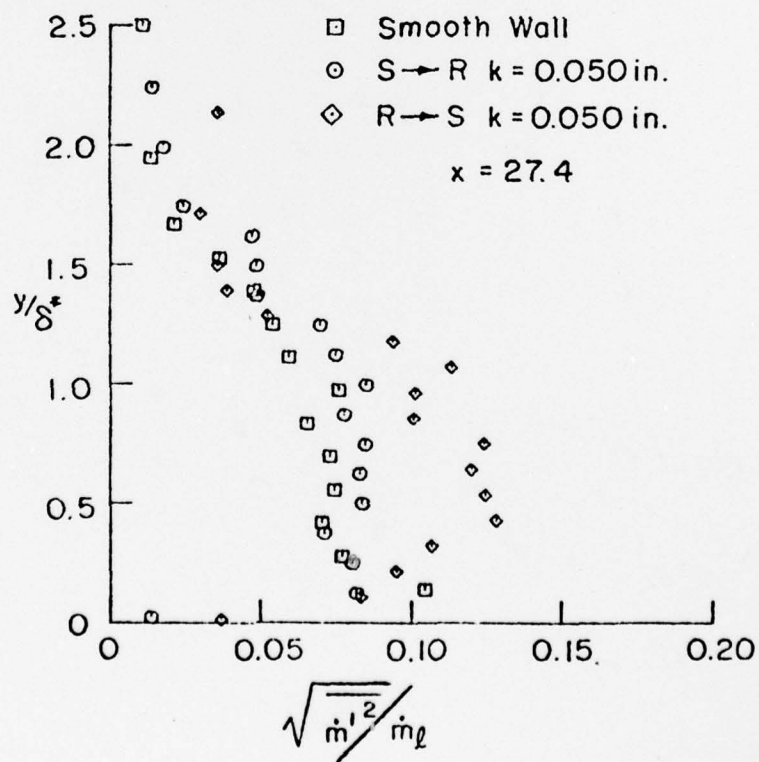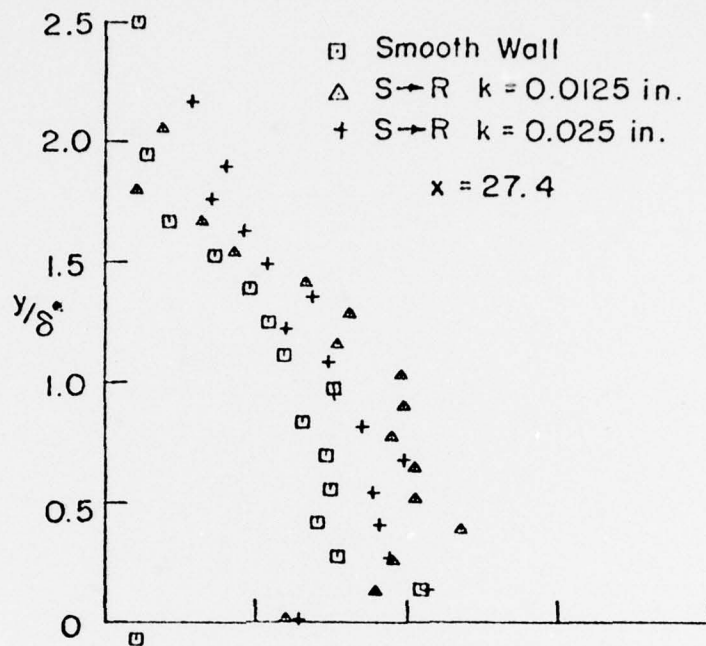
FIG.21 (CONTINUED)
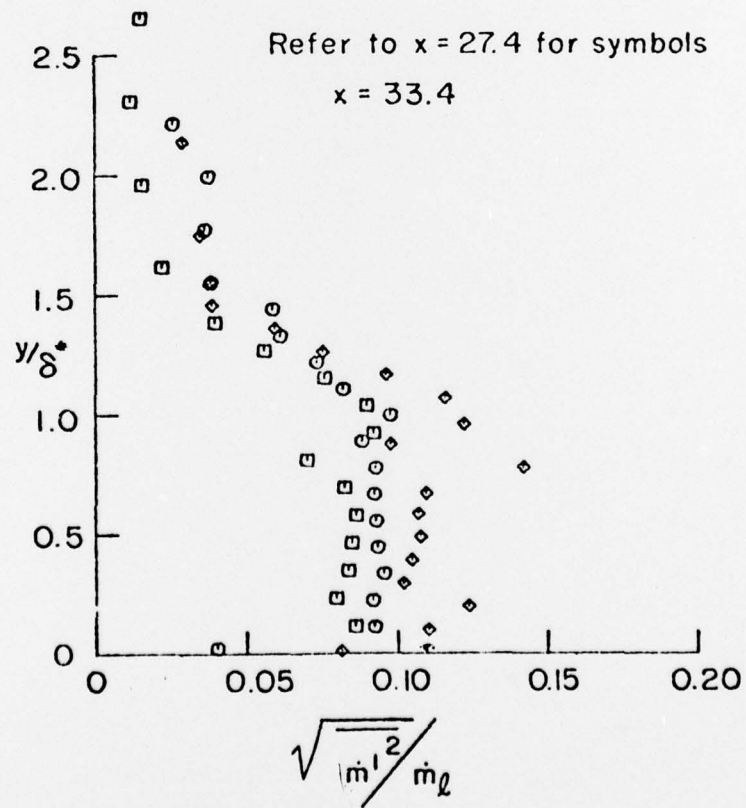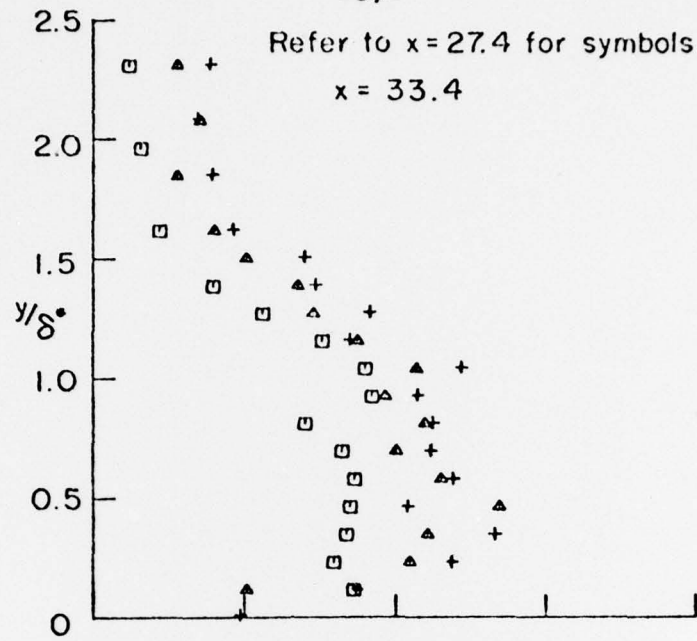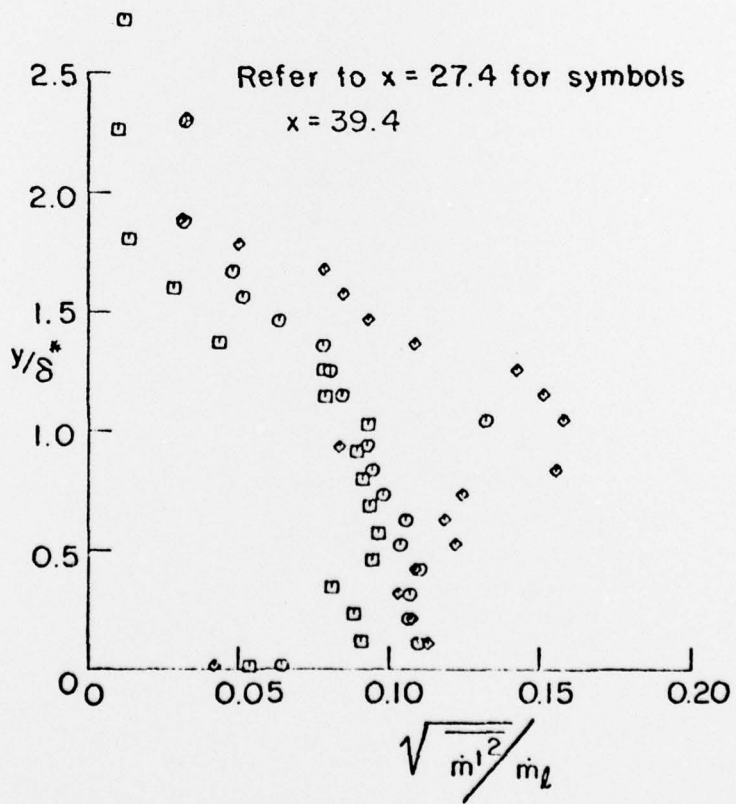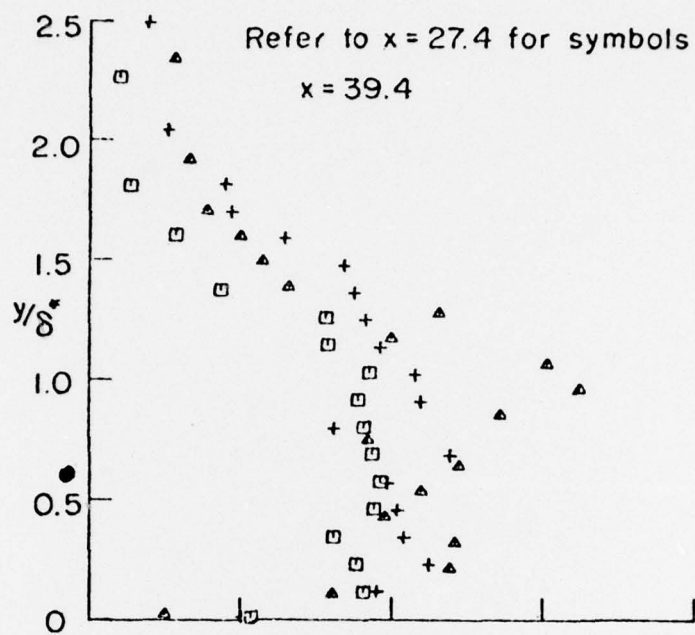
FIG. 21 (CONTINUED)
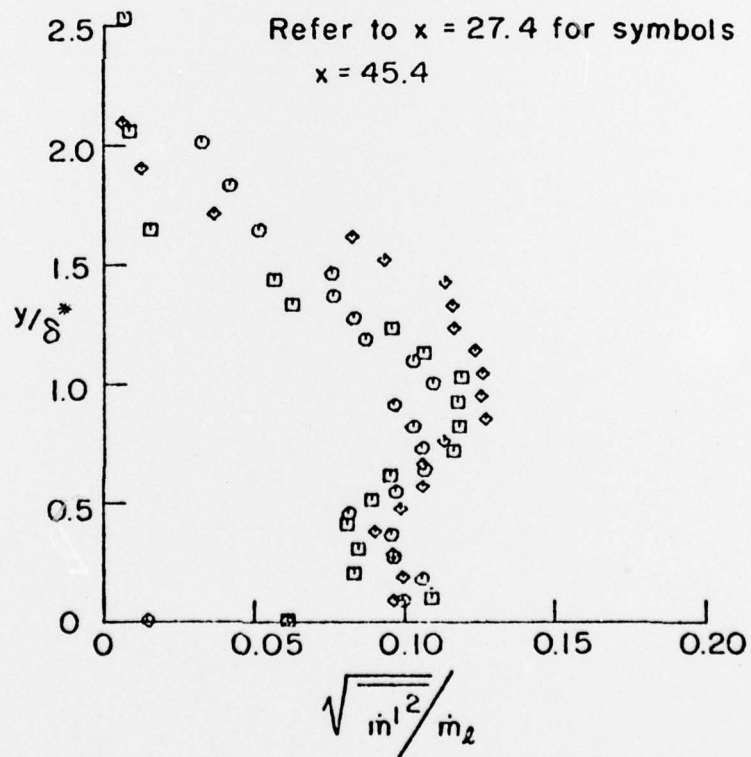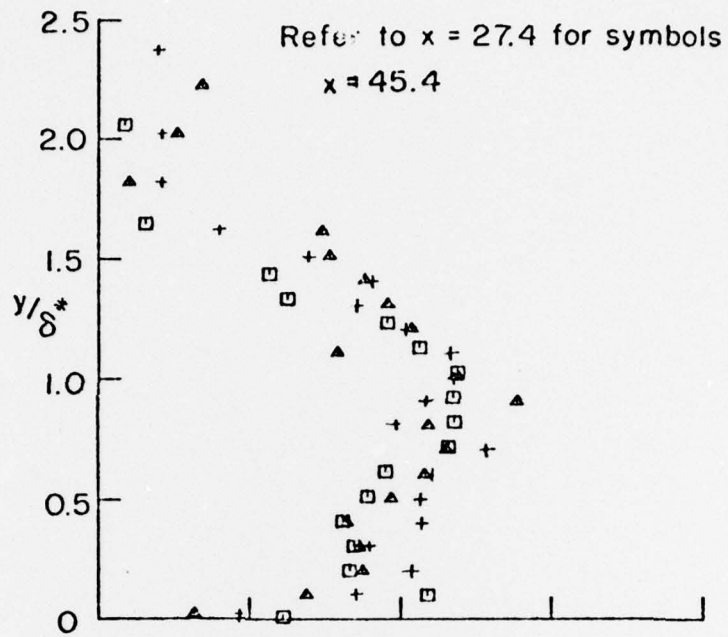
FIG. 21 (CONTINUED)
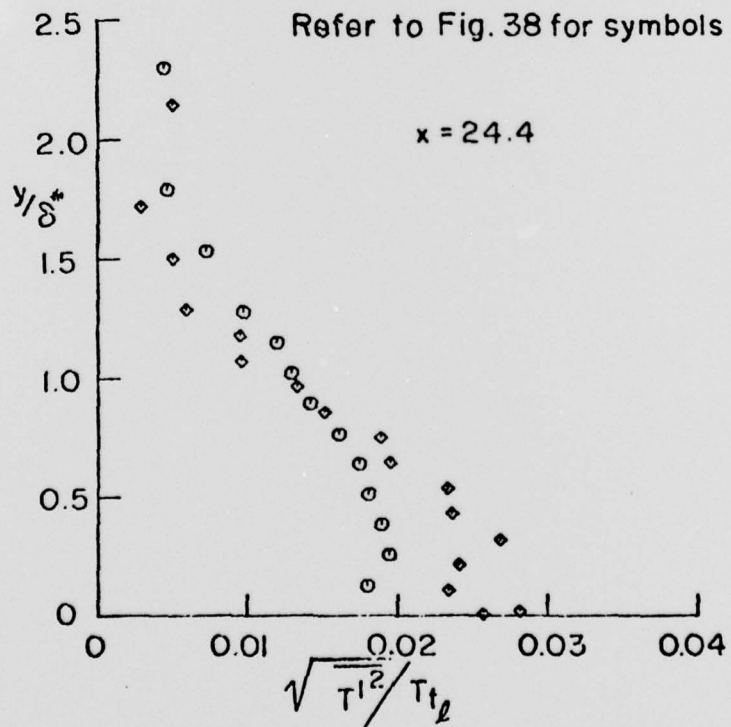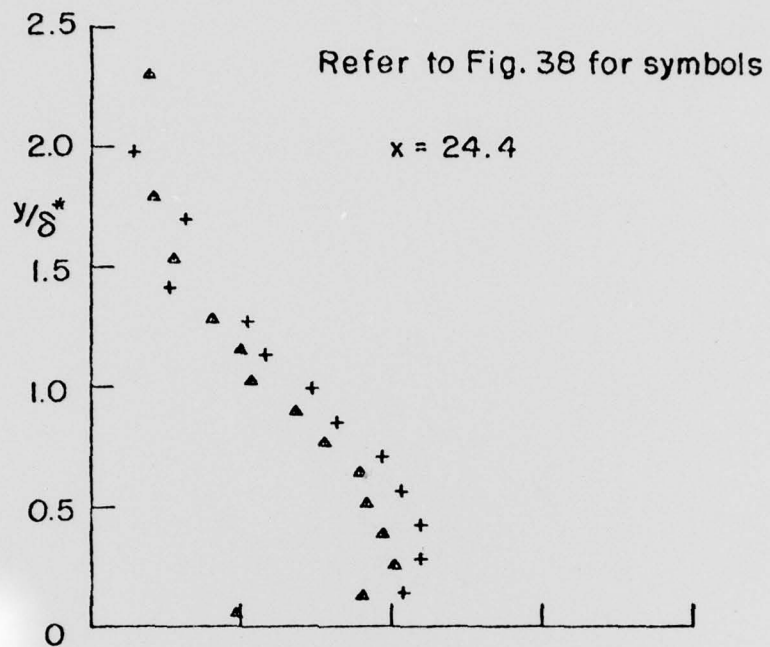
FIG 21 (CONTINUED)

FIG. 22 TOTAL TEMPERATURE
FLUCTUATIONS
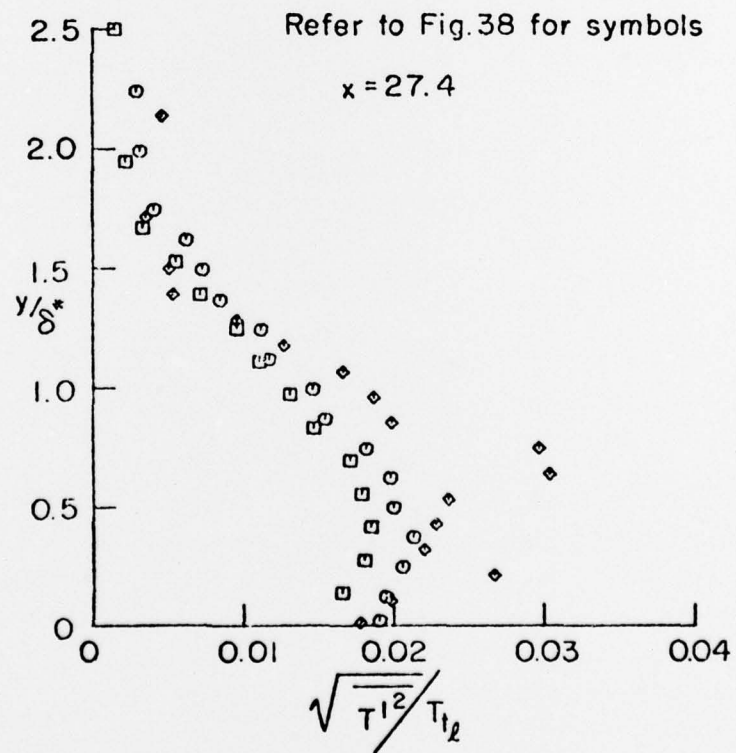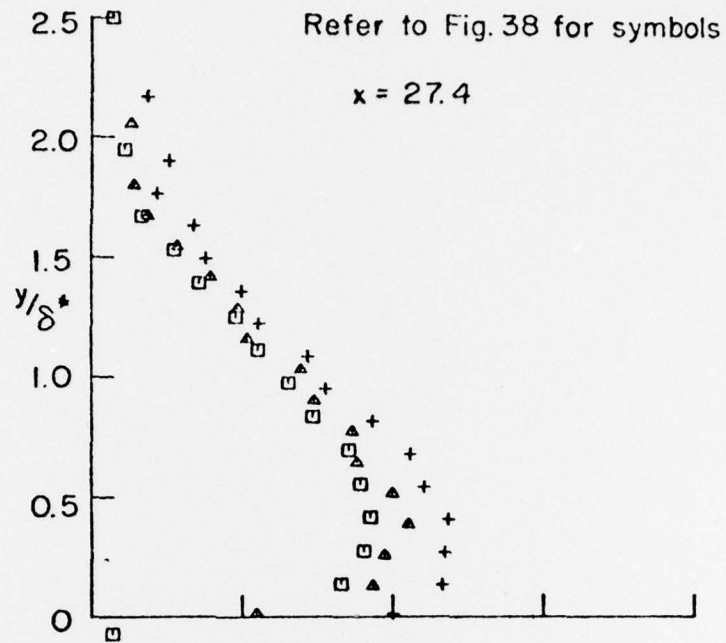
FIG. 22 (CONTINUED)
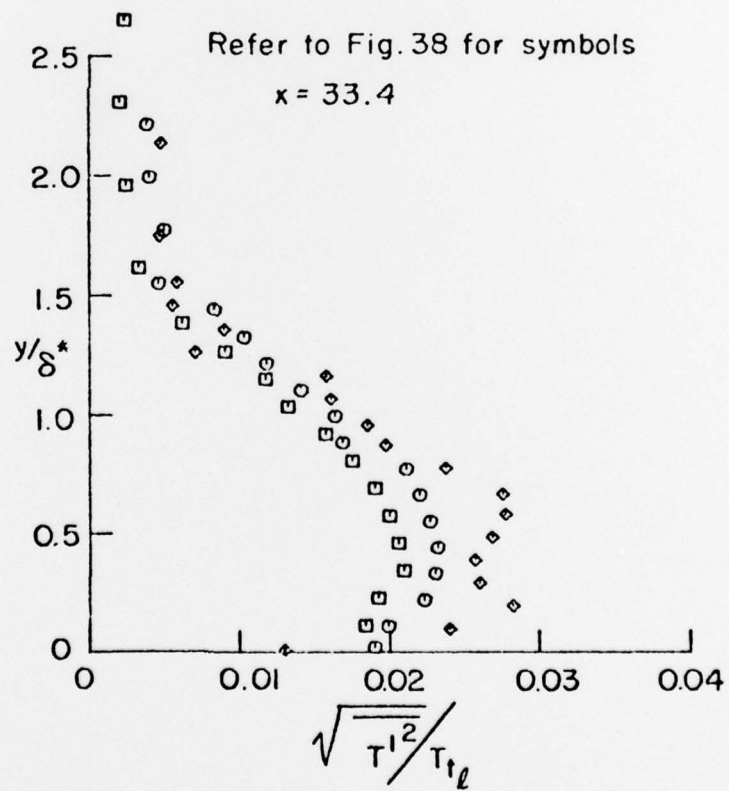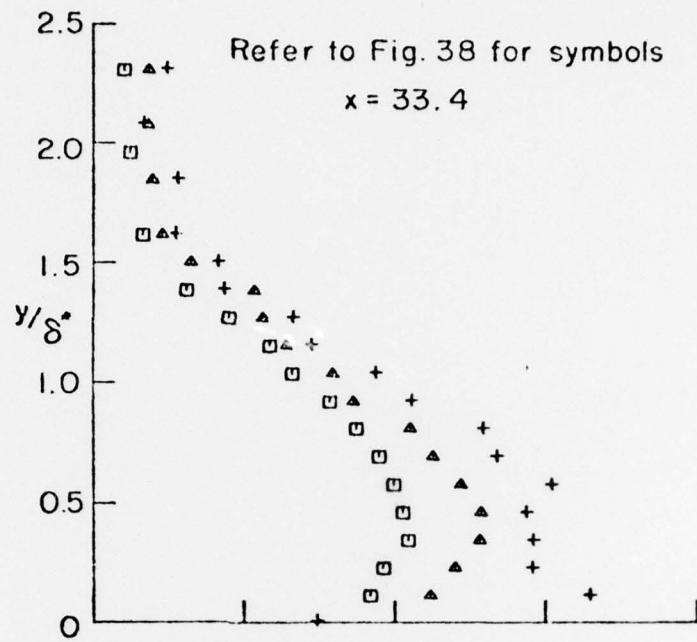
FIG. 22 (CONTINUED)
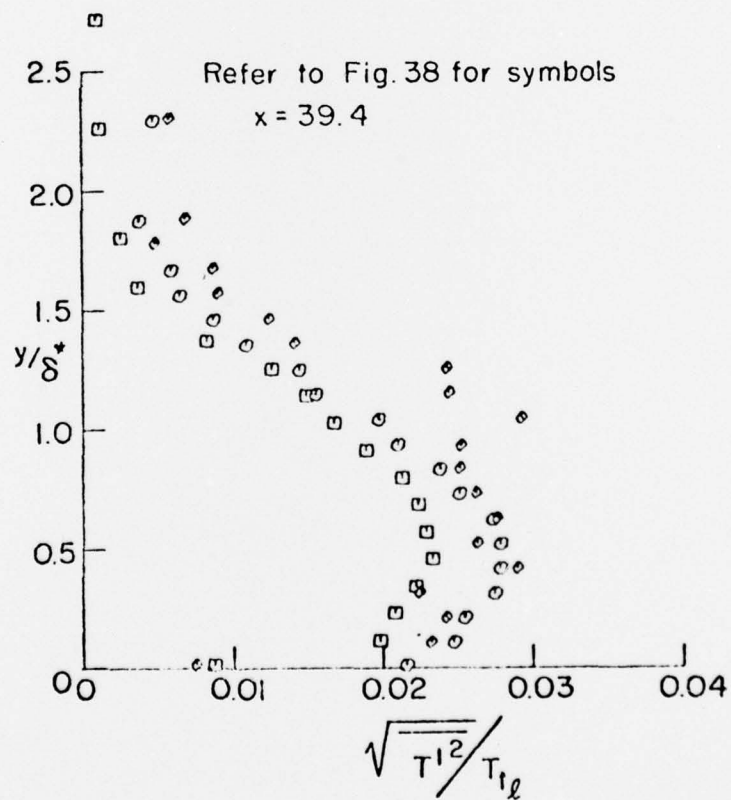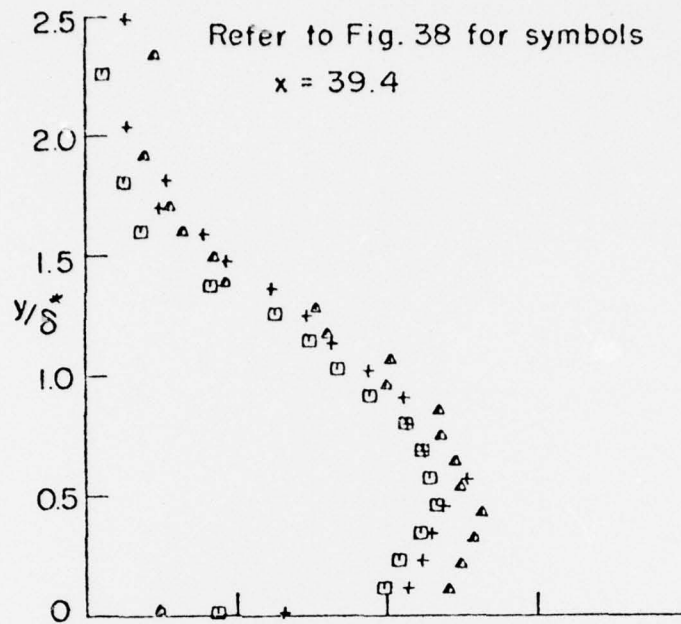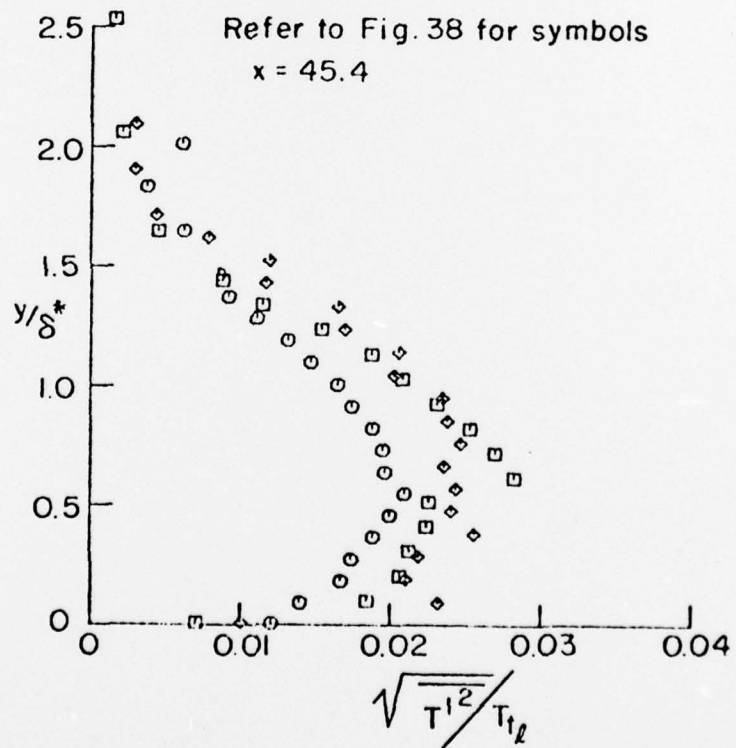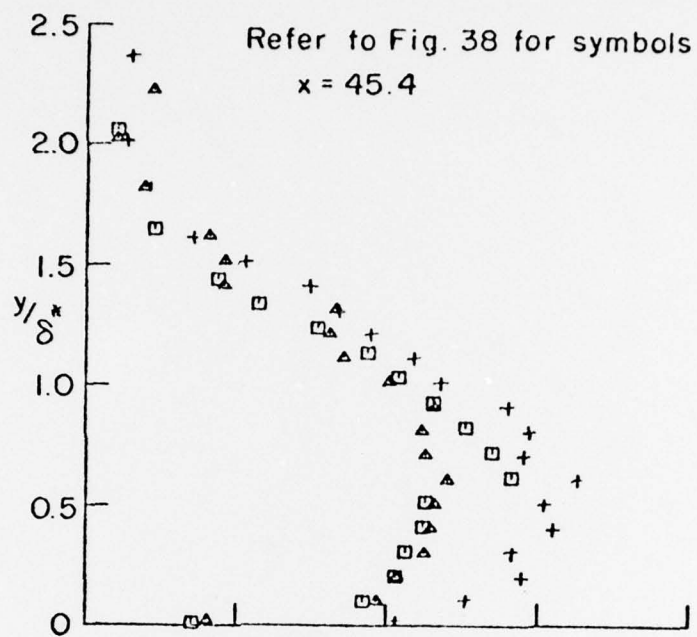
FIG. 22 (CONTINUED)
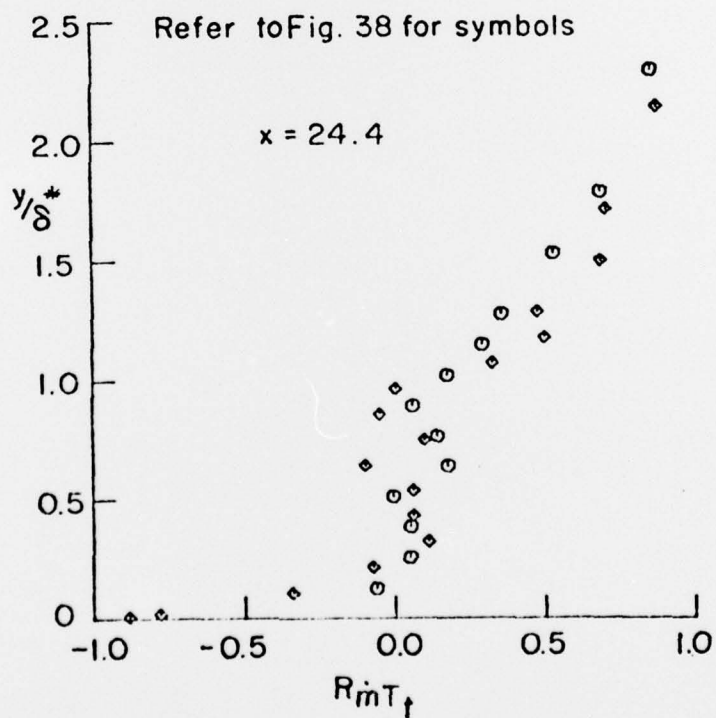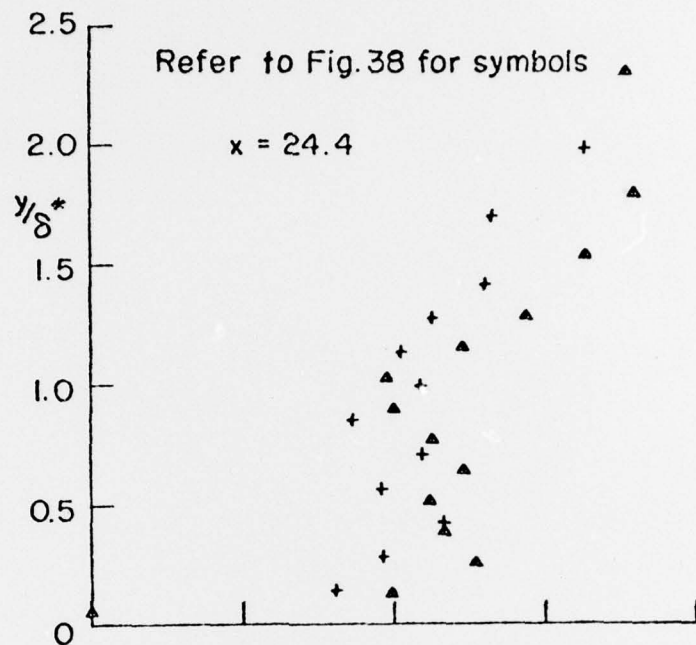
FIG. 22 (CONTINUED)

FIG. 23 MASS FLUX-TOTAL TEMPERATURE
CORRELATION COEFFICIENT
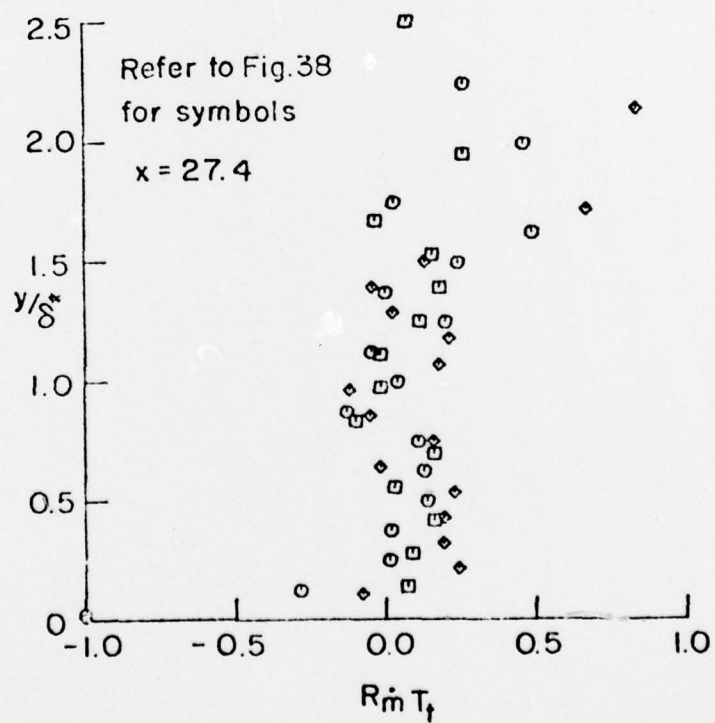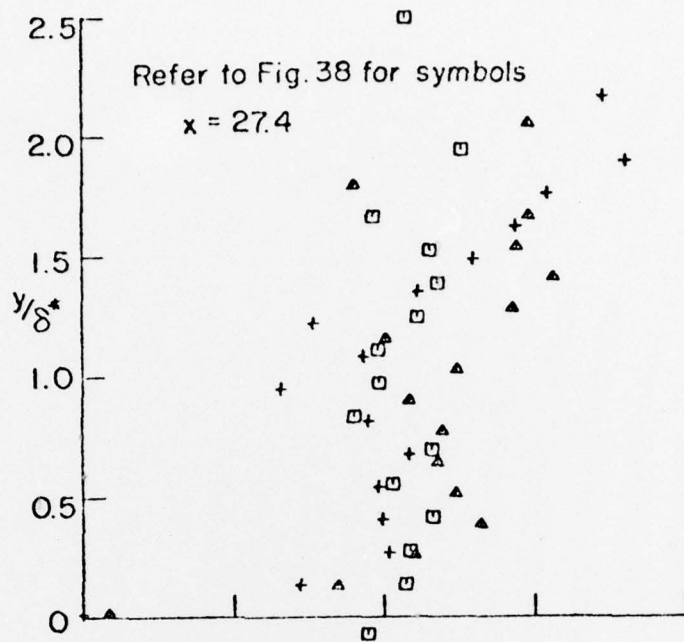
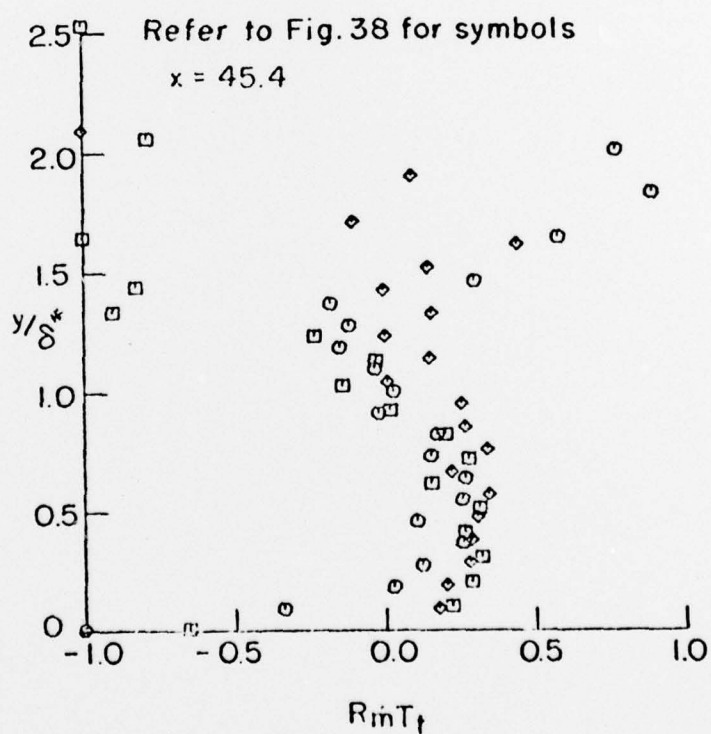FIG. 23 (CONTINUED)
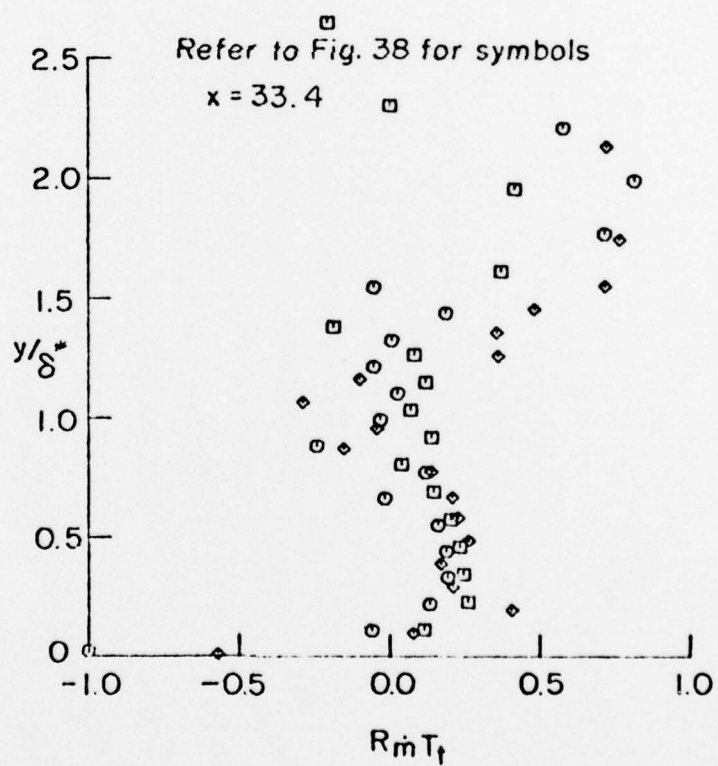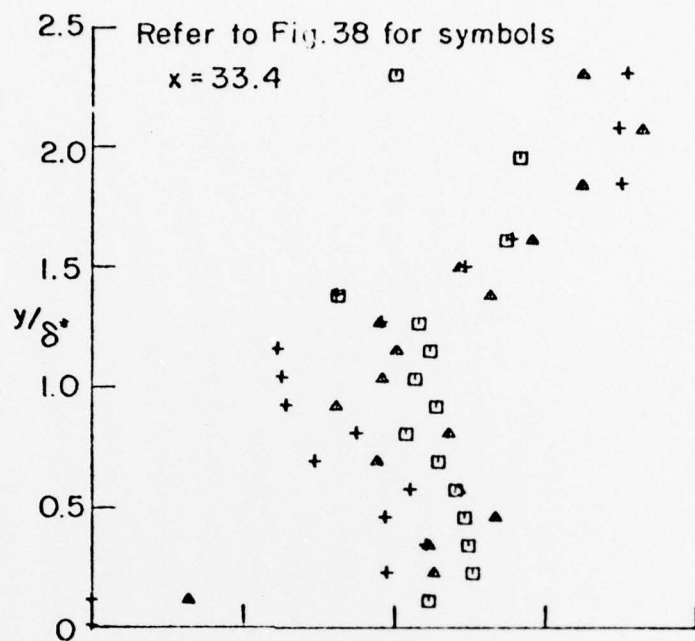
FIG. 23. (CONTINUED)
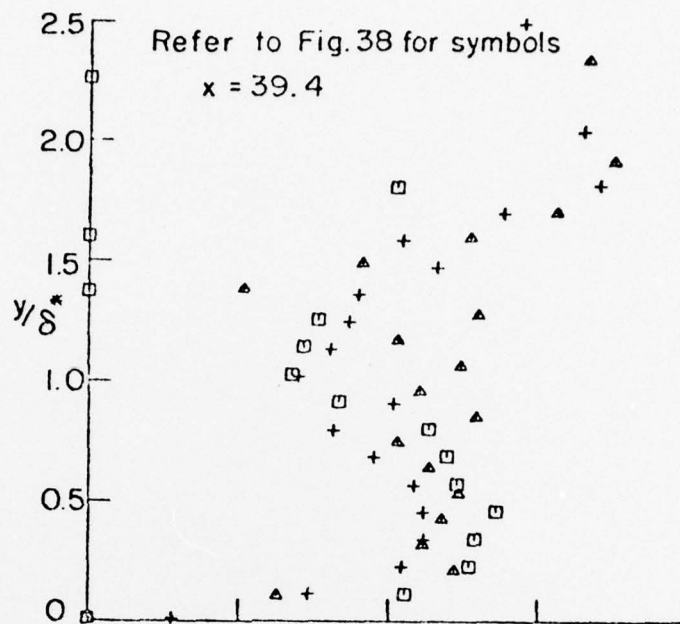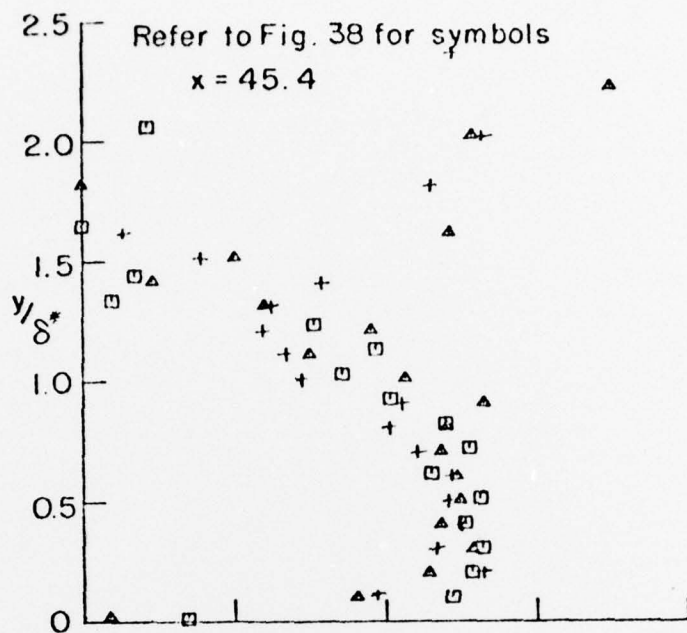
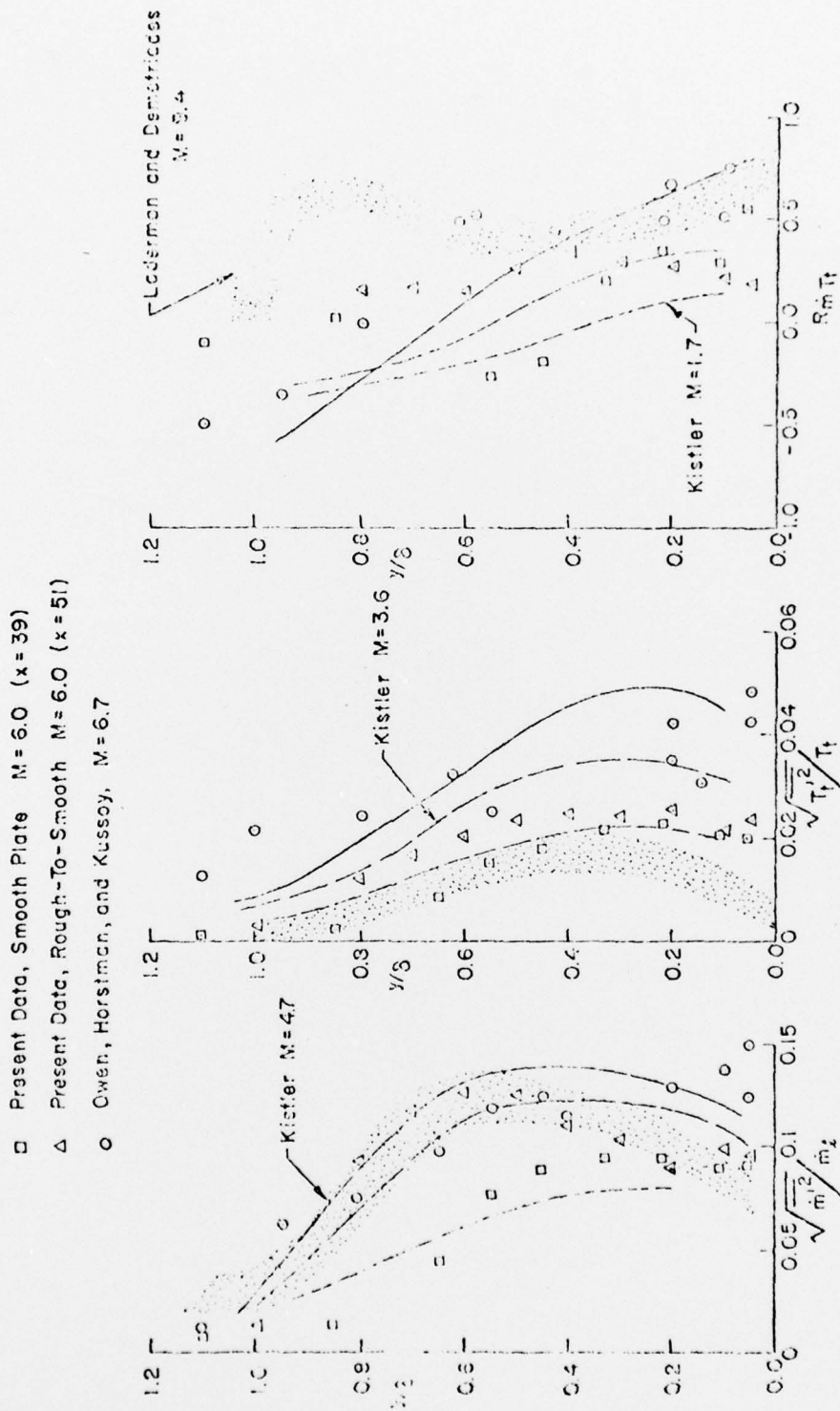FIG. 23 (CONTINUED)

FIG. 23 (CONTINUED)

FIG. 24 COMPARISON OF EQUILIBRIUM SMOOTH WALL FLUCTUATION DATA WITH PREVIOUSLY PUBLISHED RESULTS